/ 21886

National Library of Canada
Bibliothèque nationale du Canada

CANADIAN THESES ON MICROFICHE

THÈSES CANADIENNES SUR MICROFICHE

NAME OF AUTHOR/*NOM DE L'AUTEUR*	ARTHUR EUGENE LIVINGSTON
TITLE OF THESIS/*TITRE DE LA THÈSE*	BEAM-FOIL INVESTIGATIONS OF ATOMIC OSCILLATOR STRENGTHS
UNIVERSITY/*UNIVERSITÉ*	UNIVERSITY OF ALBERTA
DEGREE FOR WHICH THESIS WAS PRESENTED/ *GRADE POUR LEQUEL CETTE THÈSE FUT PRÉSENTÉE*	Ph. D.
YEAR THIS DEGREE CONFERRED/*ANNÉE D'OBTENTION DE CE DEGRÉ*	1974
NAME OF SUPERVISOR/*NOM DU DIRECTEUR DE THÈSE*	DR. E.H. PINNINGTON

Permission is hereby granted to the NATIONAL LIBRARY OF CANADA to microfilm this thesis and to lend or sell copies of the film.

The author reserves other publication rights, and neither the thesis nor extensive extracts from it may be printed or otherwise reproduced without the author's written permission.

L'autorisation est, par la présente, accordée à la BIBLIOTHÈQUE NATIONALE DU CANADA de microfilmer cette thèse et de prêter ou de vendre des exemplaires du film.

L'auteur se réserve les autres droits de publication; ni la thèse ni de longs extraits de celle-ci ne doivent être imprimés ou autrement reproduits sans l'autorisation écrite de l'auteur.

DATED/*DATÉ* Sept 4, 1974 SIGNED/*SIGNÉ* A. E. Gene Livingston

PERMANENT ADDRESS/*RÉSIDENCE FIXE*
Institut de Physique Nucléaire
Université de Liège
Liège, Belgique

NL-91 (11-73)

THE UNIVERSITY OF ALBERTA

BEAM-FOIL INVESTIGATIONS OF ATOMIC OSCILLATOR STRENGTHS

by

Ⓒ ARTHUR EUGENE LIVINGSTON

A THESIS
SUBMITTED TO THE FACULTY OF GRADUATE STUDIES AND RESEARCH
IN PARTIAL FULFILLMENT OF THE REQUIREMENTS FOR THE DEGREE
OF DOCTOR OF PHILOSOPHY

DEPARTMENT OF PHYSICS

EDMONTON, ALBERTA

FALL, 1974

THE UNIVERSITY OF ALBERTA

FACULTY OF GRADUATE STUDIES AND RESEARCH

The undersigned certify that they have read, and recommend to the Faculty of Graduate Studies and Research, for acceptance, a thesis entitled BEAM-FOIL INVESTIGATIONS OF ATOMIC OSCILLATOR STRENGTHS submitted by Arthur Eugene Livingston in partial fulfilment of the requirements for the degree of Doctor of Philosophy.

E. H. Pinnington
Supervisor

Douglas M Sheppard

A. Kernahan

Pete Ams

H. G. Berry
External Examiner

Date: May 23rd, 1974

ABSTRACT

Atomic spectra and radiative mean lives for 52 ions of the elements B, N, O, F, Ne, Si, P, S, Ar, and Kr have been investigated by the method of beam-foil spectroscopy. Experimental and analytic techniques have been developed to produce reliable mean-life results for transitions in the vacuum ultraviolet region. Mean lives of about 300 terms have been measured, involving transitions in the wavelength range 250-2000 Å. The recognition of systematic trends in atomic properties has led to proposed classifications of several previously unassigned transitions and has enabled extensive correlations to be made among derived oscillator strengths for transitions within isoelectronic sequences. Over 40 oscillator-strength trends are discussed. Detailed comparison is made with previous experimental and theoretical work, and several new trends are established. Many of the atomic transitions studied are prominent in the spectra of astrophysical sources.

FOREWORD

The beam-foil spectroscopy program at the University of Alberta was initiated by Dr. E.H. Pinnington in 1967. In association with Dr. J.A. Kernahan and Mr. C.C. Lin, equipment was developed and experiments were performed from 1968 to 1970 to study spectra and lifetimes of several elements in the visible and ultraviolet wavelength regions. In 1970, a vacuum ultraviolet spectrometer was purchased, and Dr. D.J.G. Irwin and the author joined the beam-foil group. Since that time, improvement of the experimental system and techniques has continued, with emphasis being placed on studies in the vacuum ultraviolet region for numerous elements. Mr. Lin obtained his Ph. D. degree and left the group in 1971; Dr. Pinnington enjoyed a sabbatical leave of absence from mid-1971 to mid-1972; Dr. Irwin completed his postdoctoral research with the group in 1973.

The nature of beam-foil spectroscopy experiments normally demands a group effort, particularly for the efficient acquisition of large quantities of data, although individual contributions to certain aspects of the program may differ. In this thesis, the term "our project" is used in various ways throughout the text in recognition of the collective effort that has been involved in obtaining the basic results that are being presented. The data for these results were obtained during a series of 4- to 8-week experiments in May 1971, July and August 1972, February 1973, and August 1973.

The author has made extensive contributions to all stages of the program: the preparations for experiments, the directing of experiments and the acquisition of data, the computer reduction of data, and the analysis and interpretation of results. The main emphasis of the author's research initially lay in the development of experimental and analytic techniques for the generation of reliable beam-foil results. This led to concentration upon the detailed interpretation of these results, enabling comparison and significant criticism to be made regarding earlier work in the field, as well as extending the knowledge of atomic properties by the utilization of systematic trends in the analysis. In particular, all interpretations and discussions involving new spectroscopic classifications and homologous and isoelectronic correlations among related ions in Chapters V and VI represent individual work by the author.

ACKNOWLEDGMENTS

I am grateful to Dr. E.H. Pinnington for having stimulated my interest in beam-foil spectroscopy and for providing valuable assistance and advice throughout his supervision of my research program. I appreciate having been able to attend two international spectroscopy conferences with his support.

Dr. D.J.G. Irwin has been responsible for conceiving and designing most of the modifications of equipment during this project, and I gratefully acknowledge his contributions to the improvement of the efficiency and reliability of the experimental system. Our collaboration on the development of experimental and analytic techniques has been most rewarding for me.

I wish to thank Dr. J.A. Kernahan for his assistance during the experiments and during the analysis of data. The large quantities of beam-foil data and results that have been accumulated during this project represent many hours of collective effort on the part of all members of the group.

Mr. E.A. Foster has provided expert technical assistance in the design and construction of numerous pieces of equipment, particularly the detector housings and the target chambers with their accessories.

I am especially grateful to the personnel of the Radiation Research Laboratory at the University of Alberta for their help in assembling equipment and operating the Van de Graaff accelerator, and for their patient tolerance of our beam-foil sessions. Mr. R.J. Gardner designed and assembled the stepping-motor control-circuit that has been used for collecting nearly all the lifetime data.

I thank the University of Alberta for the financial support that has enabled me to pursue my doctoral program during the past four years.

Finally, I wish to express my gratitude to my wife, Sibylle, for her many contributions during my research program. As a laboratory technician with our group, she has prepared nearly all our foil targets and has assisted in both the acquisition and the computer analysis of beam-foil data. In addition, she provided all of the drawings for this thesis, for which I am particularly grateful. Most of all, I deeply appreciate her continuous support throughout my doctoral studies and research, and her understanding during the many evenings and weekends that I have devoted to this work.

TABLE OF CONTENTS

Page

CHAPTER I INTRODUCTION 1

CHAPTER II EQUIPMENT 7

CHAPTER III EXPERIMENTAL TECHNIQUES 16

3.1 Source Gases 16

3.2 Foil Ionization 19

3.3 Spectra 22

3.4 Ion-velocity Measurements 30

3.5 Decay Measurements 33

CHAPTER IV ANALYTIC TECHNIQUES 43

4.1 Preparation of Data 43

4.2 Preliminary Numerical Analysis 44

4.3 Final Analysis and Interpretation 47

4.4 Final Results 53

CHAPTER V SPECTRUM AND MEAN-LIFE RESULTS 55

5.1 Spectra 56

5.2 Mean Lives 78

CHAPTER VI REGULARITIES AND SYSTEMATIC TRENDS AMONG OSCILLATOR STRENGTHS ALONG ISOELECTRONIC SEQUENCES 86

6.1 Uniform Trends Along Second-Period Sequences 90

6.2 Uniform Trends Along Third-Period Sequences 104

CHAPTER VI (cont'd) Page

6.3 Anomalous Trends 116

6.3.1 Penetrating Series Interaction 118

6.3.2 Nonpenetrating Series Interaction 125

6.3.3 Competing Interactions 134

6.3.4 Third-Period Nonpenetrating Series 148

6.4 Fourth-Period Sequences 167

CHAPTER VII SUMMARY 171

BIBLIOGRAPHY 174

APPENDIX I REPORTS AND PUBLICATIONS OF RESULTS OBTAINED DURING THIS RESEARCH PROJECT 184

APPENDIX II MEAN-LIFE VALUES OBTAINED DURING THIS PROJECT 188

LIST OF TABLES

		Page
Table 5.1	Unassigned Transitions in Argon	60
Table 5.2	Proposed Classifications in Argon and Phosphorus	69
Table 5.3	Mean Lives for Homologous Transitions in Argon and Krypton	77

LIST OF FIGURES

Figure Page

1. Schematic of the experimental system 8

2. Block diagram of the electronics 8

3. Partially disassembled lifetime chamber 12

4. Lifetime chamber, mounted on the spectrometer 12

5. Panel face of stepping-motor control unit 12

6. Spectra from unresolved SF^+, SiF^+, BF_2^+ at 1.6 MeV 18

7. Spectra from unresolved SF_3^+, SiF_3^+ at 1.0 MeV 18

8. Relative contributions of silicon and phosphorus in unresolved beams 20

9. Spectra of argon at various energies 21

10. Kr^+ beam-residual gas emission 24

11. Instrumental resolution effects in the argon spectrum 24

12. Energy/intensity dependence in nitrogen 24

13. Photon-counted spectra of sulfur: beam-gas and beam-foil 29

14. Photon-counted spectrum of oxygen at 834 Å 29

15. Analog spectrum of Doppler-shifted oxygen emission 31

16. Photon-counted peaks of Doppler-shifted nitrogen transition 31

17. Schematic of geometrical limitations; experimental decay data 38

18. Decay data and computer fits for sulfur transitions 41

19. Composite spectra of oxygen (250-900 Å) 57

Figure Page

20. Argon spectra (1050-1400 Å, 1.7 and 1.2 MeV) 61

21. Argon spectra (1400-1750 Å, 1.7 and 1.2 MeV) 62

22. Argon spectra (400-750 Å, 1.8 and 1.2 MeV) 64

23. Argon spectra (400-750 Å, 0.8 and 0.4 MeV) 65

24. Argon spectra (750-1100 Å, 1.8 and 1.2 MeV) 66

25. Argon spectra (750-1100 Å, 0.8 and 0.4 MeV) 67

26. Argon spectra (660-1070 Å, 0.4 and 0.2 MeV) 68

27. Sections of phosphorus spectra 72

28. Krypton spectra (400-1100 Å, 1.5 MeV) 74

29. ANDC analysis in P IV 84

30. B I sequence $2s2p^2\ ^4P-2p^3\ ^4S^o$ 91

31. B I sequence $2s^22p\ ^2P^o-2s2p^2\ ^2P$ 92

32. N I sequence $2s^22p^3\ ^2P^o-2s2p^4\ ^2S$ 97

33. F I sequence $2p^5\ ^2P^o-2p^43s\ ^2P$ 97

34. Be I sequence $2s^2\ ^1S-2s2p\ ^1P^o$ 101

35. Na I sequence $3s\ ^2S-3p\ ^2P^o$ 106

36. Na I sequence $3p\ ^2P^o-3d\ ^2D$ 106

37. Mg I sequence $3s^2\ ^1S-3s3p\ ^1P^o$ 110

38. Mg I sequence $3s3p\ ^3P^o-3p^2\ ^3P$ 110

39. Mg I sequence $3s3p\ ^3P^o-3s3d\ ^3D$ 114

40. Al I sequence $3s3p^2\ ^4P-3p^3\ ^4S^o$ 114

Figure Page

41. B I sequence $2p\ ^2P^o-3s\ ^2S$ 119

42. B I sequence $2s^22p\ ^2P^o-2s2p^2\ ^2S$ 119

43. Mg I sequence $3s3p\ ^1P^o-3p^2\ ^1S$ and $3s3p\ ^1P^o-3s4s\ ^1S$ 123

44. Al I sequence $3s^23p\ ^2P^o-3s^24s\ ^2S$ and $3s^23p\ ^2P^o-3s3p^2\ ^2S$ 123

45. B I sequence $2s^22p\ ^2P^o-2s2p^2\ ^2D$ 128

46. C I sequence $2s^22p^2\ ^1D-2s2p^3\ ^1D^o$ 128

47. Si I sequence $3s^23p^2\ ^1D-3s3p^3\ ^1D^o$ 132

48. P I sequence $3s^23p^2\ ^4S^o-3s3p^4\ ^4P$ 132

49. N I sequence $2s^22p^3\ ^4S^o-2s2p^4\ ^4P$ 136

50. N I sequence $2p^3\ ^4S^o-2p^23s\ ^4P$ 136

51. N I sequence $2s^22p^3\ ^2D^o-2s2p^4\ ^2D$ 140

52. N I sequence $2p^3\ ^2D^o-2p^23s'\ ^2D$ 140

53. O I sequence $2s^22p^4\ ^3P-2s2p^5\ ^3P^o$ 142

54. C I sequence $2s^22p^2\ ^1D-2s2p^3\ ^1P^o$ 144

55. C I sequence $2p^2\ ^1D-2p3s\ ^1P^o$ 144

56. N I sequence $2s^22p^3\ ^2D^o-2s2p^4\ ^2P$ 147

57. N I sequence $2p^3\ ^2D^o-2p^23s\ ^2P$ 147

58. S I sequence $3s^23p^4\ ^1D-3s3p^5\ ^1P^o$ 151

59. S I sequence $3s^23p^4\ ^3P-3s3p^5\ ^3P^o$ 151

60. Energies of interacting terms along three isoelectronic sequences 154

61. Al I sequence $3s^23p\ ^2P^o-[3s3p^2]\ ^2D$ 155

62. Al I sequence $3s^23p\ ^2P^o-[3s^23d]\ ^2D$ 155

Figure Page

63. Mg I sequence $3s3p\ ^1P^o - [3p^2]\ ^1D$ 159
64. Mg I sequence $3s3p\ ^1P^o - [3s3d]\ ^1D$ 159
65. Si I sequence $3s^23p^2\ ^3P - [3s3p^3]\ ^3D^o$ 163
66. Si I sequence $3s^23p^2\ ^3P - [3s^23p3d]\ ^3D^o$ 163
67. Mg I sequence $3s3d\ ^3D - 3p3d\ ^3F^o$ 165
68. Mg I sequence $3s3d\ ^3D - 3s4f\ ^3F^o$ 165
69. Cu I, Zn I, Ga I sequences 169

CHAPTER I

INTRODUCTION

The technique of beam-foil spectroscopy was introduced a little more than ten years ago (Ka 63, Ba 64), and it has since become established as the most versatile laboratory source for the production of astrophysically interesting spectra. This relatively new method of atomic excitation utilizes ionized atoms or molecules that have been accelerated to a high speed by an ion accelerator and directed through a thin foil, usually made of carbon. The ion-foil interaction produces further ionization and electronic excitation of the beam constituents as well as dissociation in the case of a molecular beam. The resultant characteristic spontaneous emission by the atomic ions that are produced is detected on the "downstream" side of the foil. Although the idea of studying atomic properties with ion beams is not new, the use of foil excitation provides several outstanding advantages and unique features when compared with the earlier beam-gas method and with other spectroscopic emission sources.

One unique characteristic is that the very small thickness of the foil defines its position as the precise point of excitation. A typical foil thickness

($\sim 10^3$ Å = 10^{-7} m) and ion speed (~ 1 mm/ns = 10^6 m/s) yields a foil traversal-time of $\sim 10^{-13}$ seconds. The ion speed is essentially constant so that position downstream from the foil simply represents time since excitation. Hence, the emission can be studied spatially along a linear time scale possessing a precisely defined origin.

A second particular advantage of the foil excitation mechanism is its efficient production of multiply-ionized beam atoms. For example, simultaneous emission from transitions in the eight lowest ionization stages of argon can be observed in a foil-excited Ar^+ beam (see Ch.III) and, at very high incident-ion energy, hydrogen-like Ar^{17+} has been produced with the technique (Ma 72a). The implication of such widespread ionization by the beam-foil interaction is that virtually all excited electronic states within these ions should be produced. This non-selective excitation results in a spectroscopically rich emission source, allowing a wide range of ions and transitions to be studied within a single beam. The price paid for this profusion is line-blending and identification difficulties in spectra and cascading complications in intensity-decay measurements of atomic lifetimes.

The requirement of high-vacuum conditions in the accelerator beam line (and hence at the foil) proves to be another advantage. Collisional effects such as recombination of electrons and ions and collisional de-excitation of excited ions are absent. Furthermore, trapping of resonance radiation is unimportant because of the low particle densities in the beam. The spontaneous decay of excited levels is observed and level lifetimes can be measured directly. By coupling a vacuum spectrograph to the target chamber, a windowless system is available for studying even XUV radiation. Details of these and other advantages of the beam-foil technique are given in review articles by Bashkin (Ba 68) and Bickel (Bi 67a). The most comprehensive reports on results of various applications of the technique, and on related subjects, are the published proceedings of the last two international beam-foil conferences (Ma 72a, Ba 73a).

The most widely known application of the beam foil technique is in the measurement of radiative mean lives.* The method is, in principle, simple, direct, and precise. Distance measured along the beam downstream of the foil represents time elapsed after excitation. The mean life of a particular excited state of a chosen ion-beam component is found by monitoring the (exponential) intensity decay of the emission from an appropriate transition, with distance from the foil. For multiply-ionized atoms, beam-foil mean-life measurements are often the only experimental results available.

---

* The expressions "mean life" and "lifetime" are often used interchangeably. In this thesis, lifetime refers to a single energy level, whereas mean life represents a weighted average value for all the levels within a single term and is obtained from the multiplet transition probability (as defined, for example, by Wiese et al (Wi 69)). A lifetime is a mean life only when the term is actually a single level (i.e. a singlet term or an L = 0 term). The difference between the lifetime of a level within a term and the mean life of the term is small if the wavelengths of the transitions in the multiplet are nearly the same, as is usually the case.

Mean lives can perhaps be categorized as basic atomic data and their measurement justified solely on that basis. However, they are important in laser studies, where relative level populations are critical, and they are useful for verifying atomic energy level structures. Wider application arises from the many instances where mean lives can be converted into transition probabilities or oscillator strengths (f-values). Reliable determinations of these parameters serve as guidance for theoretical atomic structure calculations, particularly in heavier elements where electronic structures become increasingly complicated. Probably the most appealing application, though, is in astrophysics: absolute f-values are often needed to derive element abundances in stars. These abundances provide crucial tests of solar and stellar models and theories of nucleosynthesis. Beam-foil measurements in iron (Wh 70) and chromium (Co 71) represent two instances where the experimental results have revised previously accepted (solar) abundances.

Even when a lifetime result representing a particular ion or transition is not directly useful itself, important conclusions can often be drawn for a related ion or transition of interest by the use of well-known systematic trends in atomic properties. For experimental or physical reasons, a certain transition may be difficult to study directly, and the above indirect approach can then frequently be applied. Clearly, it is important to establish reliable trends involving a wide variety of elements, ionization stages and transitions. The beam-foil technique is ideally suited for the establishment of such trends for lifetimes and f-values along isoelectronic sequences, and it is to this problem that the major section of this thesis is devoted.

One objective of this project was to develop experimental and analytic techniques for obtaining reliable beam-foil spectra and mean lives in the vacuum ultraviolet region. Possible systematic errors associated with vacuum ultraviolet beam-foil work were recognized and eliminated or reduced by modifying equipment and data-collection methods. A multi-exponential curve-fitting program was developed to extract mean lives from experimental intensity-decay data and to assess the reliability of the results.

The second objective was to apply these techniques to the study of atomic transitions in elements of direct astrophysical interest, such as those employed for solar abundance calculations (Po 62, En 70) and those observed in low-density interstellar gas clouds (Mo 73). Extensive beam-foil studies were carried out on several ionization stages of nitrogen, oxygen, and neon in the second period; silicon, phosphorus, sulfur, and argon in the third period; and krypton in the fourth period.

The final objective involved the recognition and utilization of systematic trends in atomic properties, that have recently been shown to be especially useful for the interpretation of f-value results (Wi 68a,b). Spectra and mean lives for related ions among the above elements have been correlated for the investigation of such systematic trends, and several important classes of regularities have been confirmed or established.

CHAPTER II

EQUIPMENT

The basic experimental arrangement necessary for beam-foil spectroscopy is now fairly well-known. A schematic diagram of the system used at the University of Alberta is shown in Fig. 1. A block diagram of the electronics employed to monitor or control experimental conditions, and to acquire data, is shown in Fig. 2. Brief descriptions are given below for the individual components of this system.

The Accelerator and Ion Source

The particle accelerator is the horizontal 2 MV Model AK Van de Graaff belonging to the Radiation Research Laboratory of the University of Alberta. The ion source utilizes radio-frequency excitation of the chosen source gas, and normally produces singly-ionized atoms or molecules. The source-gas container has two storage chambers, with individual outlets to the ionization chamber and independent thermo-mechanical leak-rate controls. This allows two different gases to be available at one time. Beams of singly-charged positive ions with an energy in the range 0.2 to 1.8 MeV were utilized for the beam-foil investigations to be discussed in this thesis. Ion currents of up to

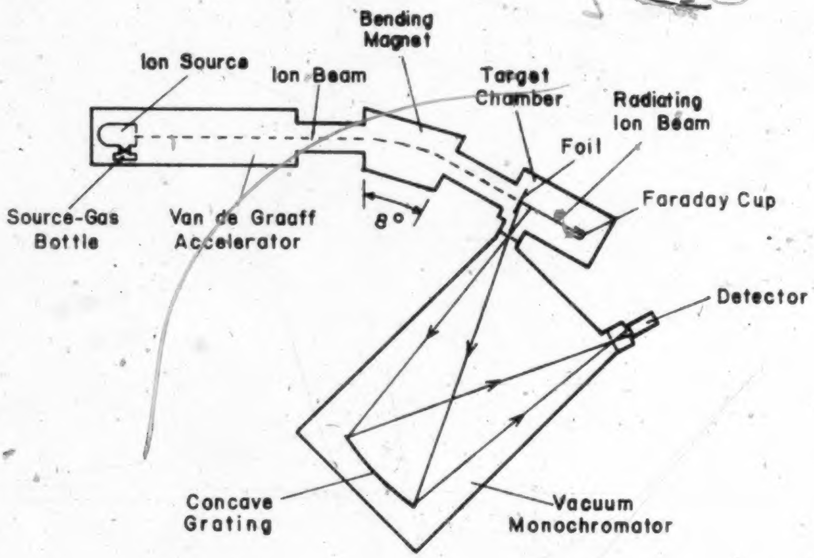
Bending Magnet
Ion Source
Ion Beam
Target Chamber
Radiating Ion Beam
Foil
Faraday Cup
Source-Gas Bottle
Van de Graaff Accelerator
8°
Detector
Concave Grating
Vacuum Monochromator

Fig.1. Schematic of the beam-foil spectroscopy experimental system (not to scale).

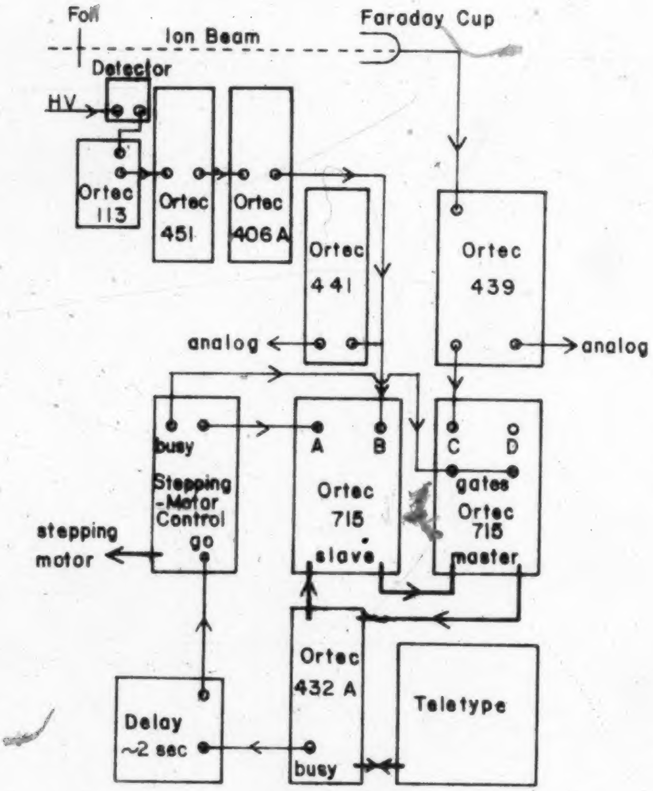
Foil
Ion Beam
Faraday Cup
Detector
HV
Ortec 113
Ortec 451
Ortec 406A
Ortec 441
Ortec 439
analog
analog
busy
Stepping-Motor Control
go
stepping motor
A
B
Ortec 715
slave
C
D
gates
Ortec 715
master
Ortec 432 A
busy
Teletype
Delay ~2 sec

Fig.2. Block diagram of the electronics.

Ortec components:

113	Preamplifier
451	Spectroscopy amplifier
406A	Single channel analyzer
441	Ratemeter
439	Current digitizer
715	Dual counter/timer
432A	Print-out control

several microamperes were available for most ions, although currents of 0.5-1.0 μA were normally used to achieve beam stability and to prevent premature foil-breakage.

The Bending Magnet

An electromagnet is employed to allow mass selection in the source beam. Field strengths of up to 5 kilogauss are applied vertically to deflect ions of up to about 200 amu through an angle of 8 degrees. The field strength is monitored directly with a gaussmeter. A drift path of 3 meters between magnet and target chamber yields a calculated mass separation at the target chamber of about (200/m) mm/amu, where m is the ion mass in amu (e.g. 10 mm/amu for Ne^+ and 2.4 mm/amu for Kr^+). In practice, sharp beam focussing was rarely obtained, owing to limitations in the available focussing controls, and neighboring mass-beams usually overlapped.

The Beam Viewers

Beam conditions can be monitored with (two) optional beam viewers that are normally placed before the magnet and before the target chamber. Each consists of a vacuum-tight housing (with viewing window on top) containing a 2 inch square quartz plate that can be manually rotated into the beam path. The quartz fluoresces under bombardment by beam ions and is a convenient indicator of such characteristics as stability, uniformity, and width of the beam. In particular, closely-spaced mass components can be observed simultaneously in the (downstream) viewer, thus allowing the identification of more than one isotope for neon and for krypton. The predicted mass separations may be roughly verified in this manner.

The Target Chambers

Two foil chambers have been used for the present beam-foil studies: the lifetime chamber for the recording of most spectra and the measuring of intensity decays; the velocity chamber for the determination of ion speed following passage through the foil.

(a) The velocity chamber

The design and operation of the velocity chamber have been reported previously (Pi 69, Pi 70). The ion speed is determined by measuring the shift in the wavelength of a spectrum line which is caused by the Doppler effect introduced by viewing the beam at an angle other than 90° to its axis. The application of this technique to the vacuum ultraviolet region is to be described in Ch. III.

(b) The lifetime chamber

The basic design of the lifetime chamber was formulated during an earlier project (Li 71). Several subsequent modifications and a more complete description of the chamber are to be reported elsewhere (Ir 74a). Fig. 3 is a photograph of the lifetime chamber with its housing removed. The foil and Faraday cup are attached with a fixed separation (84 mm) to a common base that is moved along the beam axis, past the spectrometer entrance slit, by a precision screw mechanism having a pitch of 1 mm. The screw is driven (via a vacuum feed-through) with a stepping motor (Slo-Syn TS 25-1009) which, in turn, is controlled by a stepping-control circuit (Ir 74a). Eight different foil step sizes between 0.1 mm and 8 mm are available. The chamber and stepping motor are shown in Fig. 4, secured in normal operating position on the spectrometer entrance slit housing. A detector is attached to the exit slit housing. Foils are mounted, in pairs, on slides that can be manually positioned in a guide by use of a combination slide magazine/slide remover, operated via a vacuum feed-through. In Fig. 3, a foil slide is in position and the partially-filled magazine, attached to its mounting flange, is shown separately. Also visible are a beam

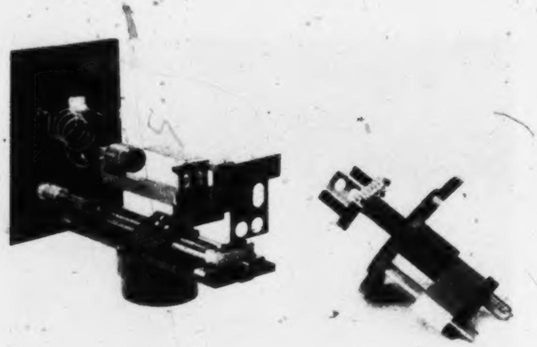

Fig.3. Partially disassembled lifetime chamber.

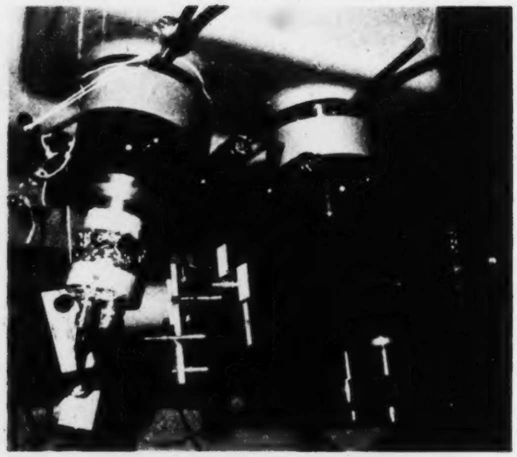

Fig.4. Lifetime chamber, with stepping motor, mounted on the spectrometer entrance slit housing.

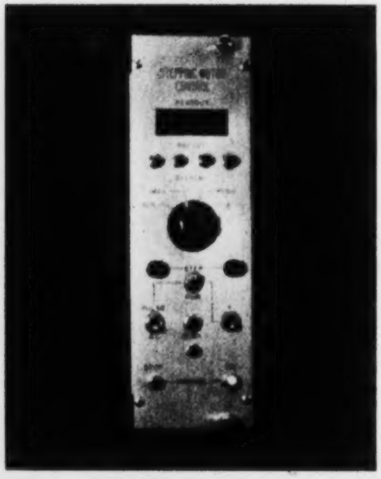
STEPPING MOTOR
CONTROL

Fig.5. Panel face of stepping-motor control unit.

collimator and an (optional) voltage plate used for sweeping electrons out of the beam.

The Spectrometer

Radiation emitted by the foil-excited ions is analyzed with a McPherson Model 225 one-meter vacuum monochromator. Two concave gratings, blazed at 1500 Å and 900 Å in first order, are used to disperse radiation emitted between 1050 Å and 2000 Å and below 1050 Å, respectively. The gratings are Bausch and Lomb aluminum replicas (600 rulings/mm) overcoated with magnesium fluoride and with platinum, respectively, to enhance optical efficiency. Each is of tripartite design having full width 96 mm and height 56 mm. A mask is normally placed over the front of the grating to decrease the horizontal acceptance angle of the system and allow intensity decay measurements to begin closer to the foil. The mask may be moved into position from outside the spectrometer without disturbing the vacuum (Ir 74a). The importance of employing grating masks for decay measurements is discussed in Ch. III.

The Detectors

An EMR 542G photomultiplier (with lithium fluoride window) [illegible] employed for the detection of radiation in the wavelength region 1050 Å to 2000 Å, while a Bendix 4219 Spiraltron electron multiplier (windowless) is used for wavelengths below 1100 Å. Typical dark count rates were observed to be about 0.4/sec for the EMR detector and less than 0.1/sec for the Spiraltron, under our normal operating conditions. A protection circuit has been designed and built for the Spiraltron to disconnect its high voltage supply if a destructively high output current should arise. This may occur, for example, when there is a sudden rise in the pressure inside the spectrometer.

Electronics

The block diagram of the data acquisition system in Fig. 2 illustrates the components employed to monitor the photon counts and beam current, as well as the stepping-motor control and the Teletype output facility. A detailed description of this system is to appear elsewhere (Ir 74a). The amplifiers, discriminator, ratemeter, and scalers represent a standard pulse-counting facility. The current digitizer allows normalization of the photon count to a pre-set quantity of integrated beam current. The print-out control transfers the contents of chosen scaler channels to a Teletype 33 ASR printer and its paper-tape punch. The stepping control circuit allows the foil to be stepped or advanced continuously in either direction between pulse-counting periods. After manual initiation of a counting sequence, data acquisition and foil advancement proceeds automatically. The step size may be altered during the sequence. This stepping facility is also adaptable to the McPherson wavelength drive for photon counting of spectra. The face of the stepping control unit is shown in Fig. 5.

CHAPTER III

EXPERIMENTAL TECHNIQUES

The development of consistent experimental procedures and the recognition of possible sources of systematic error are both necessary if reliable results are to be obtained with the beam-foil technique. Some early work in the field suffered, in particular, from a lack of attention to certain systematic effects that were revealed by subsequent investigations (see, for example, Chapter V). Experimental techniques that have been developed during this project for the measurement of reliable beam-foil spectra and mean lives in the vacuum ultraviolet region will be discussed in the present chapter.

3.1 Source Gases

The restriction to gaseous sources imposed by the method of ionization in the accelerator allowed the use of high-purity nitrogen, oxygen, neon, argon, and krypton. The third-period elements silicon, phosphorus, and sulfur are not gases in nature, and suitable gaseous compounds were needed to allow beam-foil studies of these elements. Following Berry et al (Be 70b), we used SF_6 gas to investigate sulfur, and the success with this source led to the use of PF_5

for phosphorus. As expected, fluorine emission was detected in the spectra of several of the mass-analyzed beams that resulted from partial dissociation of these molecules in the ion source. However, strong silicon, boron, and oxygen emission was also observed, presumably as a result of interaction of fluorine with the walls of the pyrex ionization chamber, the major constituents of pyrex being SiO_2 and B_2O_3. This allowed studies of silicon and boron to be accomplished simultaneously with those of sulfur and phosphorus. Our beam-foil spectra of sulfur and silicon have been reported previously (Ir 73d). Figure 6 shows a section of the spectrum recorded from unresolved SF^+, SiF^+, BF_2^+ beams in which boron and silicon features are prominent. Fluorine emission was positively identified only below 700 Å, and the observed transitions are shown in Fig. 7.

A consequence of working with multi-element beams is the increased probability of line blending and, in particular, the difficulty in unambiguously identifying unknown lines. However, blending has been only an occasional problem in these studies. Very often, emission from certain ions can be enhanced with respect to that from others by a suitable choice of ion energy (see Section 3.2 and Ch. V). Alternatively, unresolved molecular components containing elements of interest may be produced in different

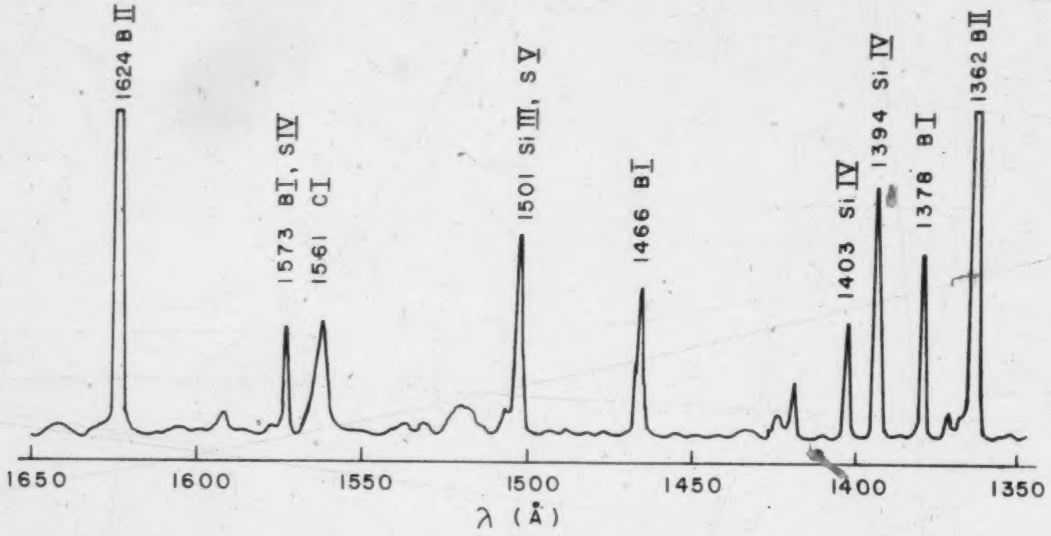

Fig.6. Section of beam-foil emission spectra from unresolved beams of SF^+, SiF^+, and BF_2^+ incident at 1.6 MeV upon a carbon foil.

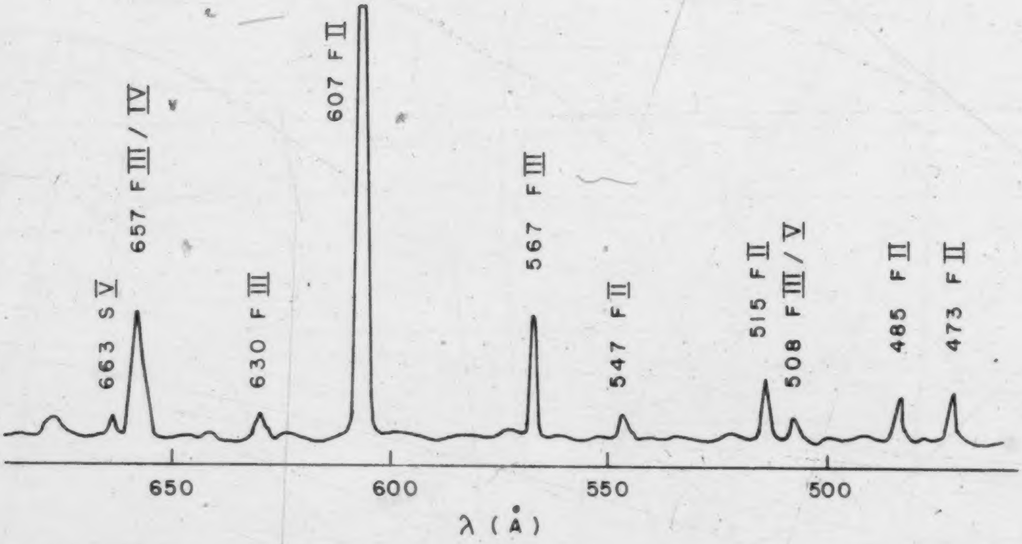

Fig.7. Section of spectra from unresolved beams of SF_3^+ and SiF_3^+ at 1.0 MeV.

proportions for various mass beams, so that an unwanted element can sometimes be suppressed by the choice of an appropriate mass beam. For example, Fig. 8 illustrates the relative amounts of silicon and phosphorus found in each of the observed mass beams from the PF_5 source. The element contributions are based upon the observed relative intensities of the isoelectronic 3s-3p transitions in Si IV and P V in each beam. The $-F_2^+$ and $-F_4^+$ beams are most favorable for studying phosphorus, whereas the $-F_3^+$ beam is best for silicon.

3.2 Foil Ionization

Perhaps the outstanding feature of the ion-foil interaction is its capability of producing numerous ionization stages of the beam element(s), even for a single ion energy. By variation of the incident ion energy, this capability can be extended, or else used to suppress selectively the higher or lower stages of ionization. Two sections of the argon spectrum recorded at various ion energies are shown in Fig. 9. Lines of Ar I and Ar II dominate at low energy, but are rapidly suppressed with increasing energy. Higher ionization stages are clearly represented at all energies except 0.2 MeV, and at 0.4 MeV the presence of both Ar I (1048 Å) and Ar VIII (700 Å) implies that

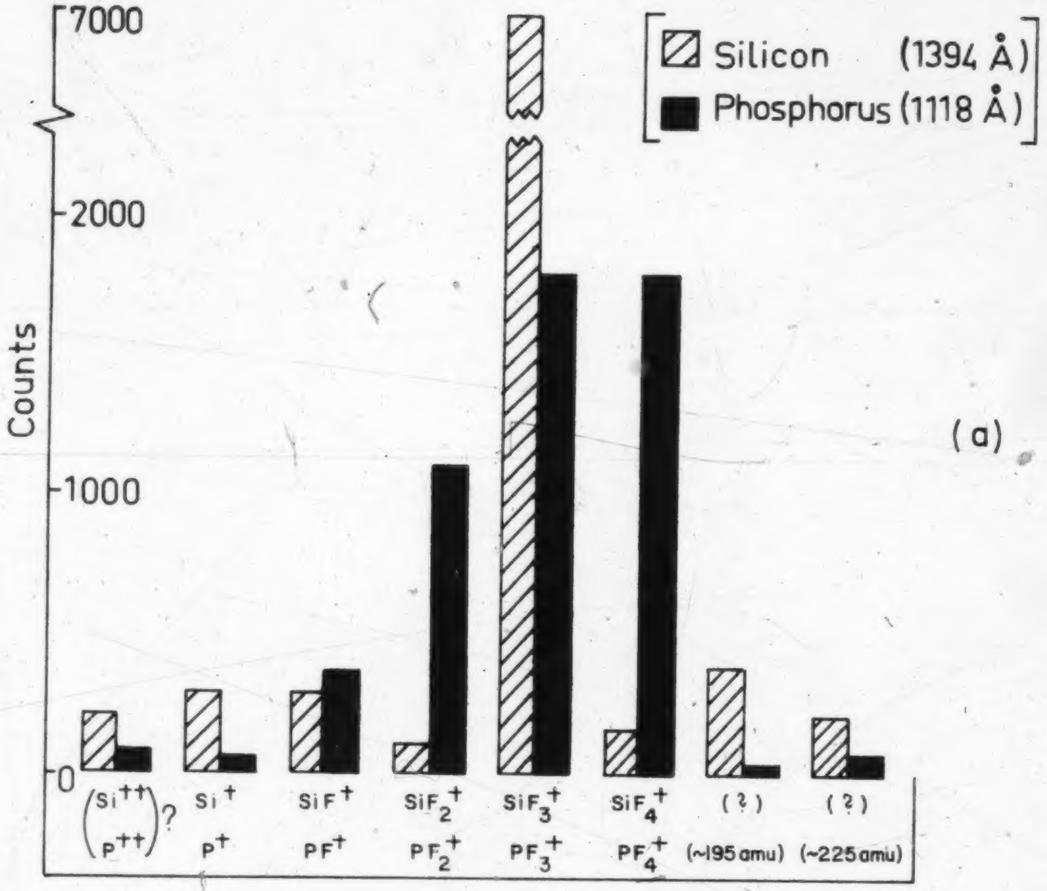

Fig.8. In (a), the relative contributions of silicon and phosphorus in each of the indicated unresolved beams are estimated, based upon the relative intensities of the 1/2-3/2 components of the isoelectronic 3s-3p transitions in Si IV and P V, shown in (b).

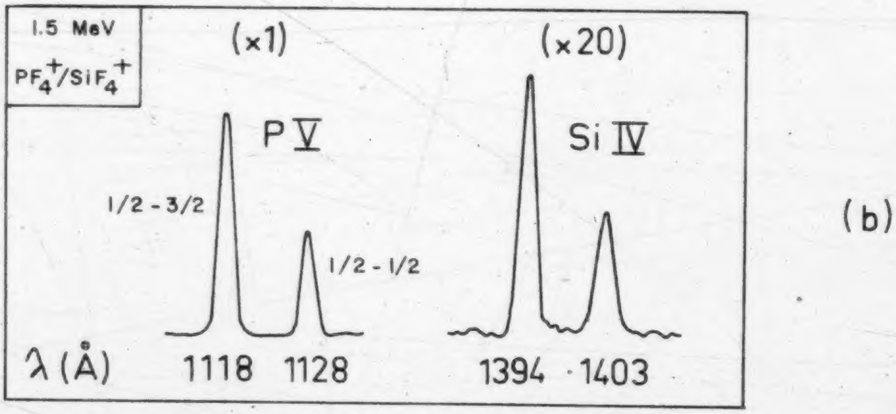

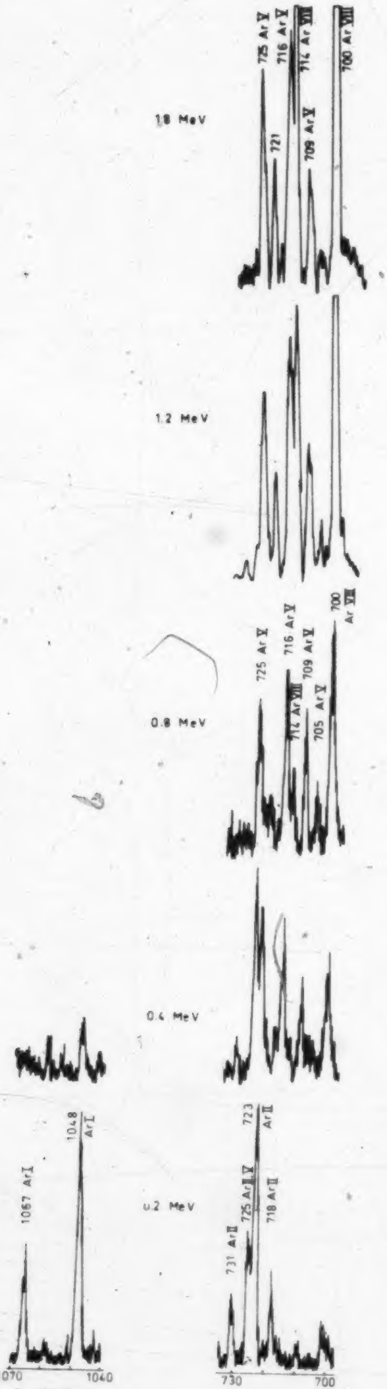

Fig.9. Sections of beam-foil spectrum of argon, recorded at the indicated argon (Ar^+) energies.

eight stages of ionization in argon can be observed simultaneously (see also Ch. V). Different intensity/energy characteristics are apparent between the Ar V and Ar VIII lines as well, with Ar VIII dominating at the highest energy. On this basis, the line at 721 Å should belong to a high ionization state of argon, although the assignment is not known (see Ch. V). Similar features for the beam-foil spectra of neon have been discussed in our report on that element (Ir 73b).

3.3 Spectra

Beam-foil spectra are normally recorded in analog form by photoelectric detection, although some early work utilized photographic methods. A section of the beam immediately downstream of the foil normally yields highest line intensity, as well as giving the best approximation to the actual relative intensities of transitions at the time of excitation. Transitions possessing very short decay times can be easily overlooked if even as little as the first millimeter of beam is excluded from the section accepted by the spectrometer. Several additional factors that affect the reliability of beam-foil spectra are discussed below.

Residual gas excitation

As mentioned in Ch. I, the high vacuum conditions in the target chamber eliminate several possible effects that could otherwise be caused by residual gas atoms or molecules. One such effect is the collisional excitation of both beam and gas molecules that occurs for sufficient residual gas pressure (e.g. beam-gas spectroscopy typically employs a gas pressure of ∿0.1 torr). A result of this effect is illustrated in Fig. 10. A 1.0 MeV Kr^+ beam was directed into the target chamber (in which the foil slide had been removed) and the pressure allowed to rise above 10^{-4} torr. Gas excitation of the two strongest Kr I lines, as well as ion excitation of prominent multiplets in O I and H I from residual gas atoms, was observed. No other features were seen between 1050 Å and 1800 Å. Such excitation is not observed at normal beam-foil chamber pressures (less than 10^{-5} torr). It is obvious that high vacuum conditions must be maintained if all emission is to be attributed to the ion-foil interaction.

Wavelength resolution

Two factors contribute to limitations in wavelength resolution in beam-foil spectra. The emission intensity is intrinsically low, necessitating the use

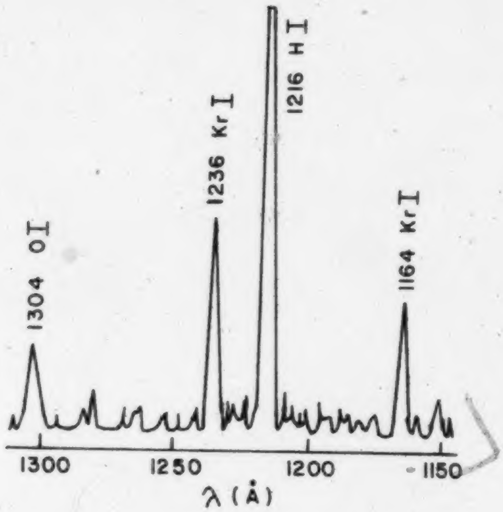

Fig.10. Spectra of beam-gas emission for Kr$^+$ incident upon residual gas at 10^{-4} torr.

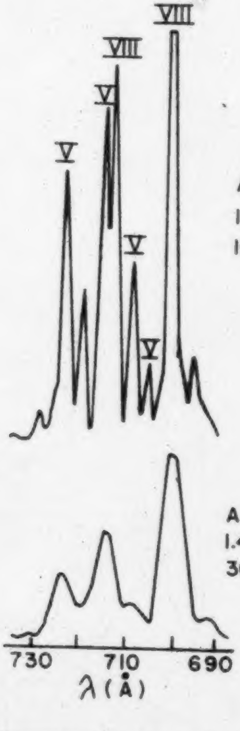

Fig.11. Comparison of different wavelength resolution capabilities for the argon spectrum.

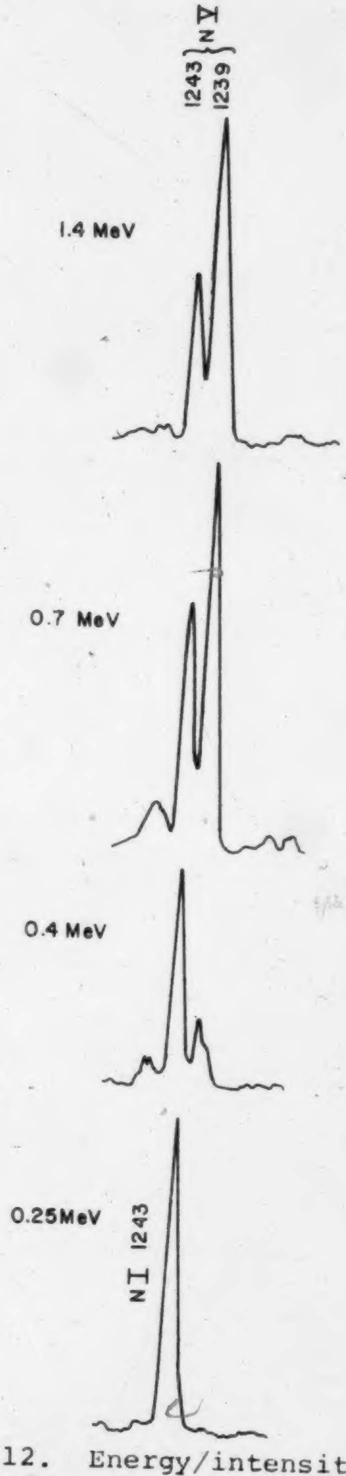

Fig.12. Energy/intensity dependence of N I and N V transitions.

of relatively fast optical systems or wide spectrometer slits. Also, the motion of the source with respect to the observer causes significant Doppler broadening of emission lines in many instances. The latter problem is a consequence of the finite acceptance angle of the spectrometer, which thus receives radiation emitted within a fixed angle about the direction of the optical axis of the system. If the ion speed, v, is much less than the speed of light, c, then the Doppler broadened linewidth is simply

$$\Delta\lambda = 2\lambda \frac{v}{c} \sin(\theta/2)$$

for an acceptance angle θ and radiation of wavelength λ. For the ion speeds and acceptance angles employed during this project, the condition

$$\Delta\lambda/\lambda < 5\times10^{-4}$$

was always fulfilled. This represents less than 0.5 Å at 1000 Å and, compared with our typical instrumental linewidth of about 2 Å, was usually not significant. Since Doppler broadening is proportional to wavelength, the effect becomes large in the visible region, and techniques have been developed specifically to eliminate it (St 71).

The importance of achieving good wavelength resolution is illustrated in Fig. 11 for a complex region of the argon spectrum. Our 1971 experiment on argon (Li 72a) was limited to minimum slit widths of 300 μm by instrumental problems (Ir 74a). Our more extensive 1972 experiment had no such limitation, and a comparison of spectrum traces for the same regions from each experiment reveals that a great deal more information is provided simply by the improvement in wavelength resolution.

Energy dependence of spectrum line intensity

The variation of intensity for transitions from different ionization stages has been illustrated earlier in this chapter for argon. This important characteristic of beam-foil spectra is exploited in nearly all studies of ions in several stages of ionization, both in experimental techniques and to assist in the interpretation of results (see Ch. V). The principal reason for the variation is actually the energy dependence of the charge state distribution resulting from the beam-foil interaction, as studied, for example, by Smith and Whaling (Sm 69).

An instructive example of spectrum analysis employing the energy dependence of line intensity is shown in Fig. 12. The high-wavelength member of the resonance doublet in N V is blended with a strong N I multiplet at 1243 Å. At 0.25 MeV the N I feature is isolated, and at 1.4 MeV the N V doublet appears with the characteristic 2:1 intensity ratio predicted by LS coupling. Clearly, a lifetime measurement performed at 1243 Å at an intermediate energy could yield an ambiguous result, particularly since the mean lives of the two upper states differ by less than 30% (Ke 74). In practice, a measurement at 1239 Å should clarify the N V situation, but the N I transition should be measured at low energy to obtain a reliable result.

Photon-counting spectrum measurements

Beam-foil spectra often display complicated blends of emission features, usually resulting from limited resolution, combined with the presence of radiation from more than one stage of ionization. In many instances, careful analog recording yields adequate results, but more detailed studies are found to be necessary at times. For example, the sulfur spectrum near 660 Å contains an unresolved feature in our analog data (Ir 73d), involving several multiplets of S IV and S V. To resolve these transitions, photon counting at uniformly spaced wavelength positions (0.125 Å) was performed in the second grating order using 75 μm slits, the data being accumulated automatically with the stepping/pulse-counting system described in Ch. II. Fine-structure components representing three different multiplets have been resolved, as shown in the lower section of Fig. 13. The results are in excellent agreement with the same section of a beam-gas spectrum of sulfur reported recently by Beyer et al (Be 73). Using this information, we have been able to perform the first reliable mean-life measurements for these multiplets (Ir 74a). It is interesting to note that beam-foil excitation is seen to be more efficient than beam-gas excitation for the production of highly ionized atoms, even at significantly lower ion energy, as previously noted for argon by Bridwell et al (Br 70).

A worse blending situation is the coincidental overlap of the resonance multiplets in 0 II and 0 III (834 Å), involving seven components of similar intensity (Ke 73) distributed over 3 Å (see Fig. 14). The data in Fig. 14 represents photon counting under the same conditions used for the sulfur example above, yet full resolution has not been achieved. The use of even higher grating orders or significantly narrower slits could improve the situation, but the intensity loss would be severe. Despite these difficulties, we have been able to distinguish the mean lives of the two states involved (1.2 ns for 0 II, 1.6 ns for 0 III) by measuring decays at high energy at 835.5 Å and at

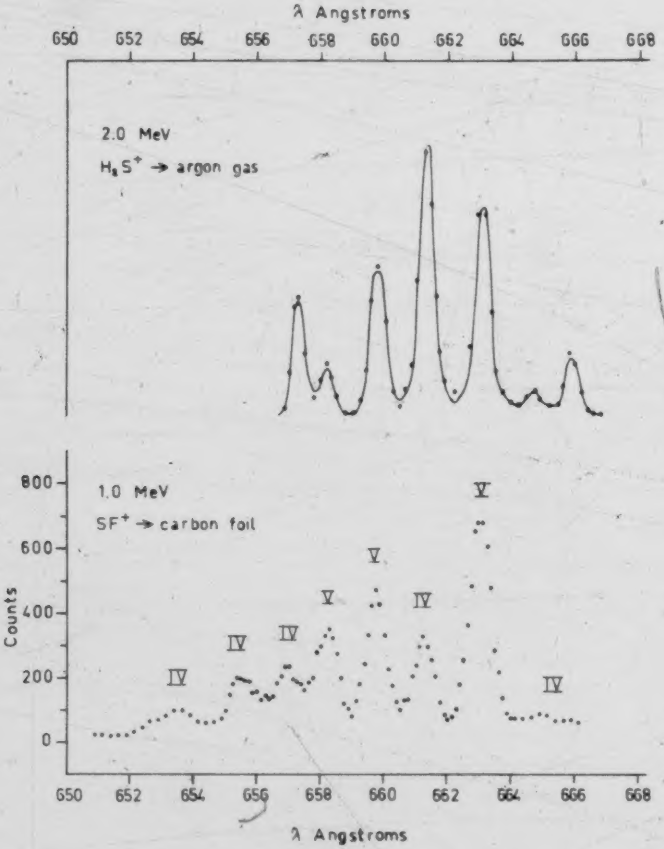

Fig.13. Photon-counted spectrum of sulfur:
(above) from the beam-gas results of Beyer et al (Be73),
(below) from the beam-foil results of this project.

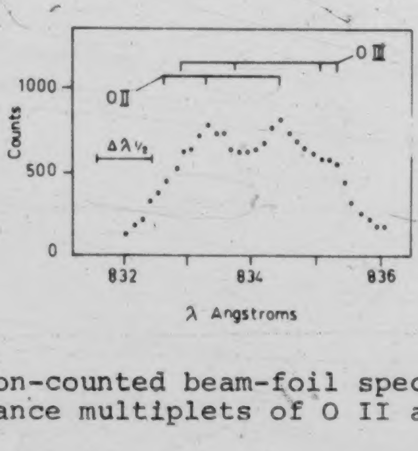

Fig.14. Photon-counted beam-foil spectrum of the blended resonance multiplets of O II and O III.

low energy at 834.5 Å.

3.4 Ion-velocity measurements

The ion velocity downstream from the foil must be known precisely if a precise time scale for lifetime measurements is to be obtained. A technique for measuring the ion velocity directly, using the Doppler shift in wavelength of the emitted radiation, was developed in this laboratory by Pinnington and Lin and has been applied to emission in the visible region (Pi 69, Pi 70). During this project, the method has been utilized in the vacuum ultraviolet region (between 1200 Å and 1800 Å), using magnesium fluoride overcoated mirrors. The Doppler shift for a given velocity is proportional to wavelength, so the shifts in this region are only about one-third the magnitude of those in the visible. Analog recordings of the oxygen spectrum detected at 90° with respect to the beam axis (unshifted) and at 30° from the axis (blue-shifted) are shown in Fig. 15. All identifiable oxygen features are shifted by more than 10 Å, whereas the emission from foil-ejected carbon and hydrogen atoms is essentially unshifted. These results show the speeds of foil-ejected particles to be much less than those of the beam particles. This can be used, for example, to verify that the prominent unassigned line at 1727 Å is emitted by a beam ion.

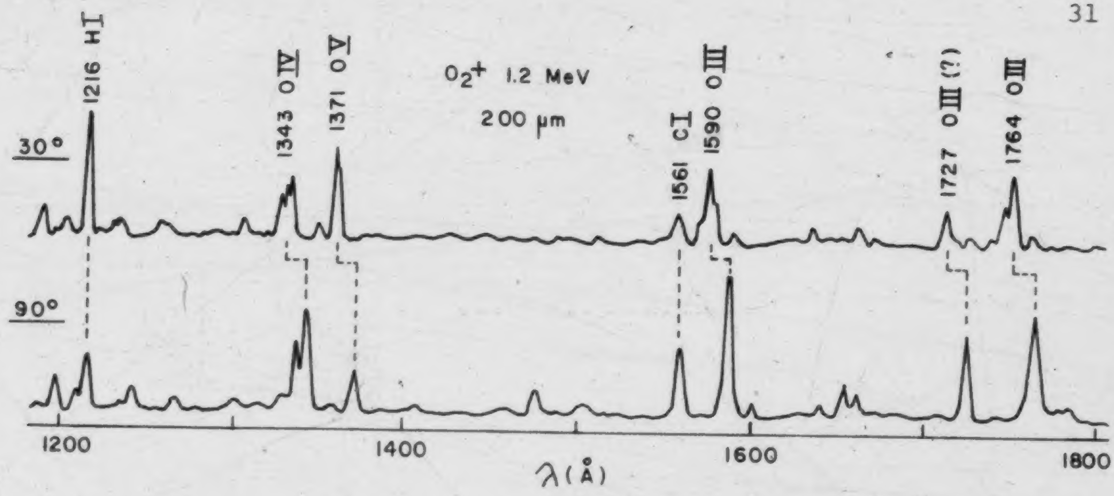

Fig.15. Comparison of beam-foil spectra of oxygen for emission observed at 90° and at 30° to the beam axis.

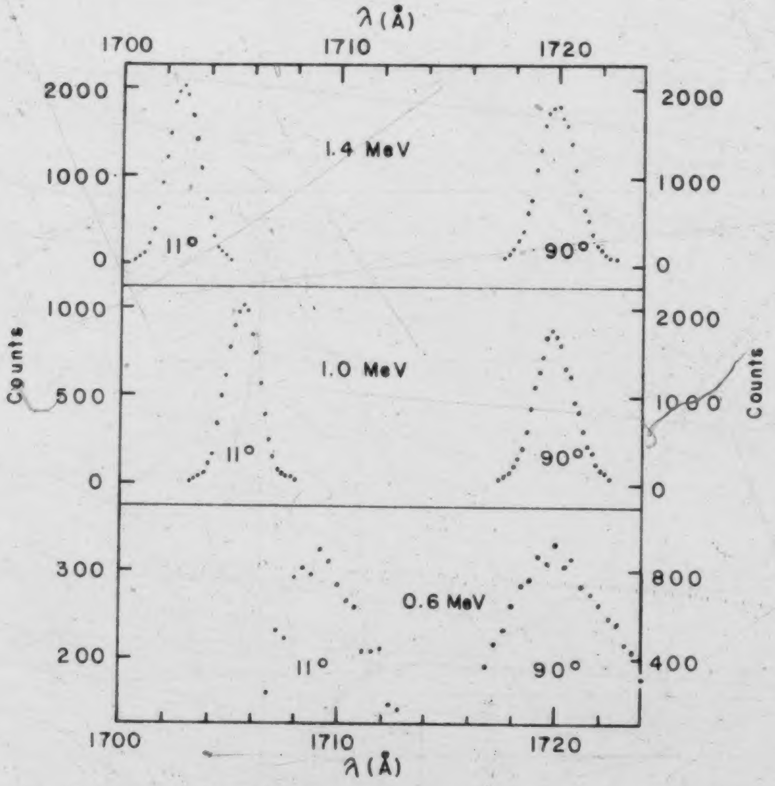

Fig.16. Photon-counted peaks for the N IV 2s2p $^1P^o$-2p^2 ^1D transition (1718 Å) observed at 90° and at 11° to the beam axis at different ion energies.

Precise velocity measurements, however, require photon counting with suitable lines. The strong N IV 2s2p $^1P^o-2p^2\ ^1D$ transition at 1718 Å is an ideal candidate in this region since it is an isolated single line with high wavelength, and consequently greater shift. Photon-counted peaks for this transition, detected at 90° and 11° to the beam axis at three different energies, are shown in Fig. 16. The 11° mirror has been aligned by laser to better than 0.1°. The peaks are counted, using the stepping-motor system described in Ch. II, from the low-wavelength side of the 11° peak, through both peaks, without interruption, to avoid possible systematic errors in determining the wavelength difference. The optics is manually shifted from 11° viewing to 90° viewing while the stepping motor approaches the 90° peak.

By repeated measurements, the ion speed can be determined to within one or two percent at higher energies, and good agreement is obtained with velocities predicted from the electronic energy loss values of Northcliffe and Schilling (No 70) for ions in carbon. At lower energies, where the nuclear energy loss becomes important and predicted speeds are less certain, the Doppler-shift method is also less precise. Wavelength shifts are smaller and suitable peaks are harder to find. However, virtually all mean-life measurements during this project involve ions and energies for which the nuclear energy loss is negligibly small.

3.5 Decay measurements

A number of important characteristics of beam-foil spectra are naturally reflected in the techniques for the decay measurement of line intensity. A compromise between emission intensity and wavelength resolution (that is, the choice of slit width) should be considered for every measurement, and intensity/energy properties should be exploited whenever possible. The conditions of the beam and the foil become more important now, since precise relative intensities are desired. Finally, the recognition of geometrical limitations and time-resolution capabilities of the system is mandatory for the production of reliable decay data.

Photon counting

Decay data has been accumulated during this project by photon counting techniques, which average over beam fluctuations and provide data in a form directly suited to numerical analysis. The stepping system described in Ch. II was employed for all decays measured after 1971. To obtain good counting statistics over sufficient portions of the decays, counting times were normally chosen to yield at least 2000 counts at the decay peak. This procedure provides better than 10% statistics over at least three decay times of the primary decay component ($e^3 \approx 20$). Since the decays were nearly always followed to below the 100-count level, data were thus obtained over more than three primary lifetimes. Where significant cascading was present, much longer decay distances were monitored.

Counting periods at each point were normalized to a preset integrated beam current. This approach is frequently used in beam-foil work in an attempt to eliminate the effects of beam-current fluctuations upon the emission rate. The distance between foil and cup was kept constant so that scattering of beam ions by the foil did not introduce a systematic error in the normalization. Beam-current normalization was found to be unsatisfactory only when large current instabilities persisted during a decay measurement.

Choice of wavelength position

An obvious problem in low-resolution beam-foil spectra is the isolation of a particular transition or multiplet of interest for decay measurement, especially for complex regions such as those described in Section 3.3. Reliable spectral data is a fundamental requirement for the planning of lifetime investigations, since the relative intensities of known transitions and the possible appearances of new lines or impurity lines normally are unpredictable in beam-foil spectra. Extensive wavelength surveys at several ion energies and under various beam conditions have been performed for all elements studied during this project, using the highest resolution for which reasonable intensity could be obtained. Where blending or near-blending of lines was indicated, the wavelength position for a decay was carefully chosen and narrow slit widths were often used, this usually demanding a significant increase in counting time. In addition, decay measurements were frequently performed at more than one energy for a given transition to reveal or eliminate suspected blends.

Foils

A single decay was always performed using only a single foil. Decay data that was interrupted by foil breakage has been rejected (except possibly where breakage occurred very near the end of the decay). For heavier ions and lower energies the foils tend to break much more quickly than for lighter ions and higher energies. The maintaining of a uniform beam density over the entire foil area was observed to increase foil survival time.

For intact foils, there was found to be no significant dependence of decay times upon foil "age" under ion bombardment, although changes in the visual appearance of a foil were often observed. Ageing effects would probably be most noticeable with respect to ion energy losses, as a result of apparent structural changes in the foil. For all but a few of our decays, however, the energy loss involved is only a few percent, and hence changes in the energy loss would not affect our lifetime results. The decay of a given transition was almost always measured more than once, often under different foil conditions.

Time resolution

Characteristic mean lives of terms that are de-populated by vacuum ultraviolet transitions are found to be $\sim$0.1 to 1 ns, much shorter than those for terms de-populated only by higher-wavelength transitions. For typical ion velocities, these values represent decay lengths (i.e. distances over which the intensity falls by a factor of e) of $\sim$0.1 to 10 mm. In measurements of these short decays, the geometrical limitations of the apparatus must be considered. Thus, a transition which decays by a factor of e in a distance of 0.1 mm would decrease in intensity by a factor of more than 20,000 over 1 mm! Failure to initiate a decay measurement immediately after the foil, or the spacing of data points by distances much greater than the actual decay length, can result in the true primary decay being overlooked. Very often only the long-lived cascade components, which are normally present, would then be observed. The elimination of such time resolution problems was one specific aim of this project. Some results will be presented in Ch. V.

The geometrical limitation involved in beam-foil measurements is illustrated in the lower part of Fig. 17. The finite acceptance angle of the spectrometer, α, determines a finite length of beam, ℓ, from which light is received. The integrated intensity received from this length of beam is proportional to the actual beam intensity at the mid-point of the segment observed. Clearly, there exists a "first meaningful" data point at a distance $\ell/2$ from the foil. In an otherwise-fixed geometrical system, ℓ is determined by the width of the grating. We have introduced masks in front of the grating to decrease the acceptance angle, and thus allow the first meaningful point to occur closer to the foil. Although this decreases the total intensity received, this technique does enhance the intensity of a primary decay component with respect to its cascade component. Equally important, we utilize very small steps between data points (0.1 mm) during the initial part of a decay measurement

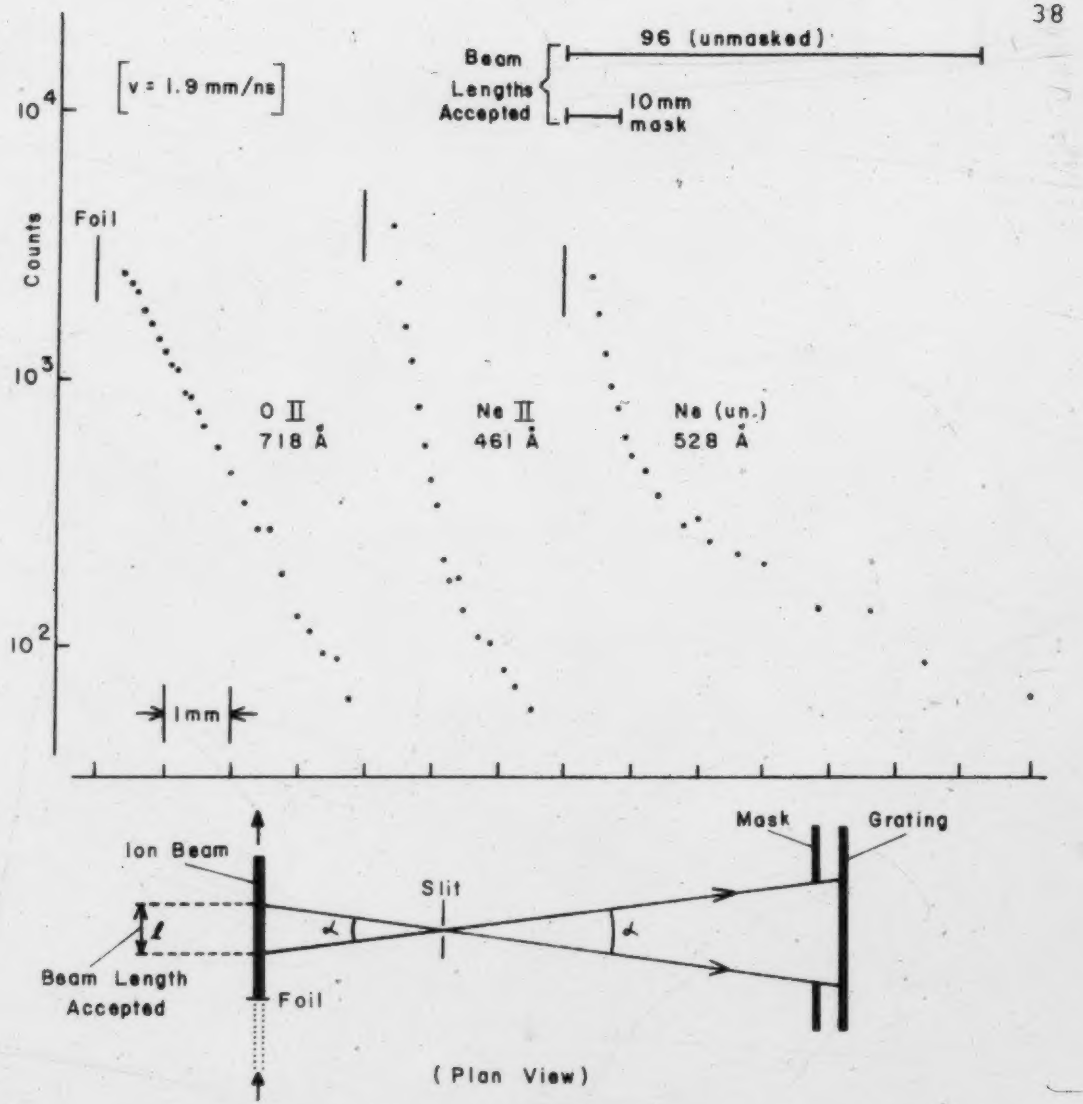

Fig.17. Schematic illustration of the geometrical limitation for beam-foil intensity decay measurements (below), and decay data for three transitions (above), chosen to illustrate different degrees of cascading and the importance of good spatial resolution along the beam.

The integrated intensity at x, I(x), is related to the actual intensity, $y(x)=A\exp(-bx)$, by

$$I(x) = \frac{2}{b}\sinh(b\frac{s}{2})\ y(x),$$

where s is the beam length accepted.

to accumulate more information in this critical region.

The upper part of Fig. 17 displays actual decay data (on a common semi-logarithmic plot) for three typical transitions, as well as the beam lengths subtended by an unmasked and masked grating (on the same horizontal scale) in our system. The decays were all measured using the 10 mm mask, as implied by the distance between the foil and first data point indicated for each. They were chosen to illustrate three qualitative degrees of cascading, ranging from almost non-existent to relatively strong. The O II transition displays no apparent cascading and should be readily measurable for any reasonable resolution at any section of beam below the foil, depending on the initial intensity. On the other hand, the 528 Å decay is more typical, and inspection of the diagram reveals that the use of an unmasked grating would reduce the relative contribution of the primary component in an intensity measurement at any position. The extraction of a reliable primary mean life from the data would then become more difficult. The necessity for closely-spaced data points is also apparent. Analysis of this decay indicates that the primary component contributes significantly to the intensity only for the first few points. Each such point is particularly important, and the data suggest that even smaller steps would not be inappropriate for this type of decay. It is certainly not true that the smallest step size should be at least as large as the length of beam from which light is collected at any given setting.

Growing-in cascades

Good time resolution is also important for a transition in which the initial rate of intensity decay is slower near the foil than it is farther downstream. This characteristic is often called "growing-in", and normally can be attributed to repopulation of the radiating level by a cascading transition from a level having shorter lifetime (De 68, Pi 69). A fast cascade of sufficient strength can contribute significantly to the intensity near the foil, and should be accounted for in a precise decay analysis (namely, as a negative exponential component).

The 3s-3p doublets of sodium-like ions all are expected to exhibit this type of cascading from their 3d terms. Decay data for the 3s-3p transition in S VI (934 Å) and its 3p-3d cascade (712 Å) are shown in Fig. 18. The computer fits to these decays are indicated, and they are each consistent with the fits obtained for three other measurements of each doublet. (Data representing the low-count tail of each decay has been omitted in Fig. 18 for compactness.) The growing-

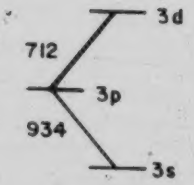

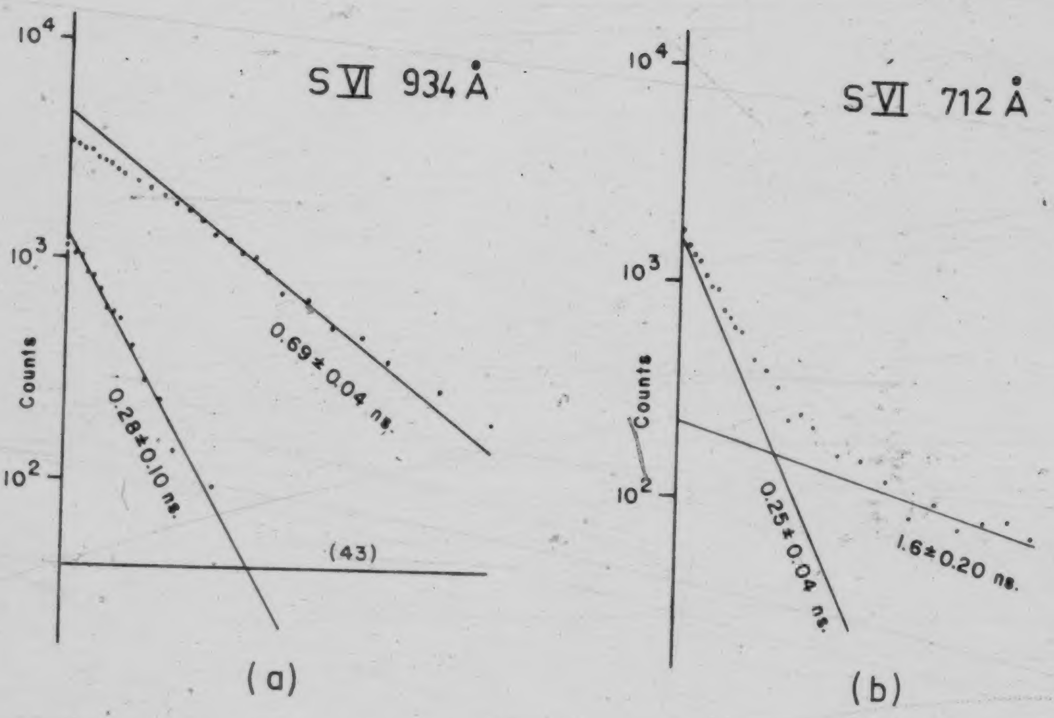

Fig.18. Decay data and computer fits for the S VI resonance transition (934 Å) and its dominant cascade (712 Å), showing the appearance of the 3d mean life as the growing-in cascade component of the 3p decay curve.

in characteristic is evident for 934 Å. The values obtained by subtracting the decay data of 934 Å from its 0.69 ns fitted component have also been plotted in (a), and the negative decay component of the 934 Å fit has been superposed. The linearity of these values on the semi-log plot indicates that the growing-in may be attributed to a single fast decay component. The consistency between the growing-in mean life (0.28±0.10 ns) and the 3d mean life (0.25±0.04 ns) strongly suggests that the 3p-3d transition is the only significant fast cascade into the 3p term.

These characteristics thus demonstrate that decay data very near the foil is required for the recognition of such fast cascades. The failure to account for this type of cascading could lead to mean lives that are too long.

CHAPTER IV

ANALYTIC TECHNIQUES

The analysis of beam-foil decay data may be subdivided into three phases: (1) the preparation of data for the curve-fitting program; (2) the preliminary numerical analysis of the data, involving one or two curve-fitting "runs" on each data set; (3) the final analysis and interpretation, involving further computer runs, comparisons of related decay fits for consistency, recognition of the physical situation for each transition, and comparison of the final results with theoretical or other experimental values and with systematic trends. Details of these phases will be described below.

4.1 Preparation of Data

The experimental decay data is accumulated directly on punched paper tape (see Ch. II). This is converted by the computer to a punched-card format for convenient access to individual data sets (all computer analysis has been performed on the IBM 360/67 at the University of Alberta Computing Center). Ion velocity and detector dark count are incorporated into each decay data set, and a truncation of one or more of the initial data points of each decay is performed to ensure that no data before the first meaningful data point (see Ch. III) is used for the curve fitting. (The original data always remains on the data cards, however.) Modifications such as truncation and dark-count correction are accomplished indirectly by the insertion of appropriate control parameters into each data set, these being monitored by the curve-fitting program and applied to the data before fitting begins.

4.2 Preliminary Numerical Analysis

All fitting of decay data is performed using the computer program HOMER (Ir 74b). This program yields a nonlinear, least-squares fit to multi-exponential decay data, providing intensities and decay times that represent a fit to 2, 3, 4, 5, or 6 parameters. Initial estimates for the iterative routine are calculated automatically from the data, and error estimates are provided for the final parameters of the fit. The program is designed to attempt a 4-parameter (2-exponential) fit and, if this succeeds, a 6-parameter fit. The fits to 2, 3, or 5 parameters are available as default options that can be triggered for certain statistical or physical reasons during a 4-fit or a 6-fit. Initial estimates may be inserted manually, as well, causing the initial-estimates subroutines to be bypassed.

The preliminary numerical analysis involves a first run for each decay, followed by inspection of the results for indications of inappropriate truncation and for the failure of an iteration sequence to converge to a solution. Further truncation is normally required when the first fitted data point (i.e. that closest to the foil) lies significantly below the fitting value, with subsequent points lying above their fitting values, as indicated below. This situation frequently

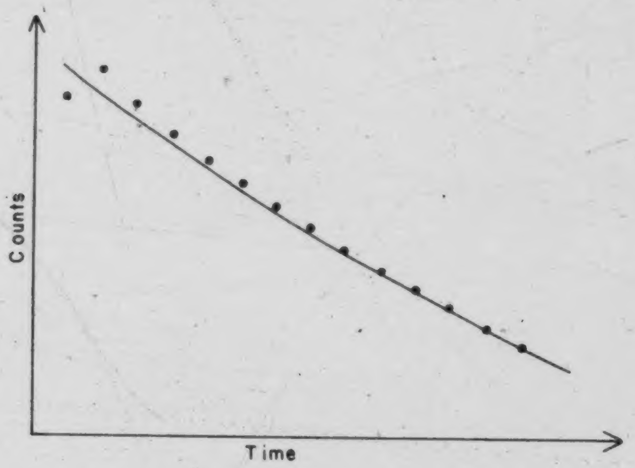

characterizes a decay that is measured using a foil with relatively large unsupported area ($\sim 1\ \mathrm{cm}^2$ during this project), as a result of foil bulging caused by the beam-ion pressure. In principle, this may also indicate a growing-in component, although more evidence is required to confirm such a phenomenon - see Section 4.3.

Failure to converge sometimes may be overcome simply by increasing the allowed number of iterations (normally 30) and re-running the data, although non-convergence is more often an indication that the number of parameters used for the fit is inappropriate. The latter situation requires the insertion of initial estimates. However, if the goodness-of-fit indicator (χ^2/d.f.)* monotonically increases as iteration proceeds it is possible that the number of parameters is correct, but that the initial estimates are poor.

---

* Chi-square (χ^2), for a set of N fitted values $\{y_i\}$, is defined as

$$\chi^2 = \sum_{i=1}^{N} \frac{(y_i - f_i)^2}{f_i + b_i} ,$$

where $\{f_i\}$ are the fitting values. If the $\{y_i\}$ are assumed to be governed by the Normal distribution (which is essentially the same as the Poisson distribution for reasonably large values of y_i) then, for the proper fit to the data, χ^2 is approximately equal to the number of degrees of freedom (d.f.) of the data set, i.e. N-p, where p is the number of fitting parameters. Thus, χ^2/d.f. should be close to the value 1.0 for a fit with the appropriate number of parameters to data that obeys Poisson statistics. This factor, χ^2/d.f. is referred to as the "reduced-χ^2".

In general, the object of the preliminary analysis is to obtain at least one satisfactory fit, with appropriate truncation, for each set of decay data.

4.3 Final Analysis and Interpretation

Following the preliminary analysis, further runs may be necessary to achieve the best fit to the data, but various consistency checks as well as the recognition of the experimental and physical situation are now correlated with the numerical analysis.

Consistency checks

(a) Systematic discrepancies

Poor fits to the beam-foil decay data are always indicated by high reduced-χ^2 (see footnote, page 46) values and usually are characterized by systematic discrepancies between fitting values and fitted values. A typical situation is illustrated (qualitatively) below, which might occur with a 4-parameter (2-exponential)

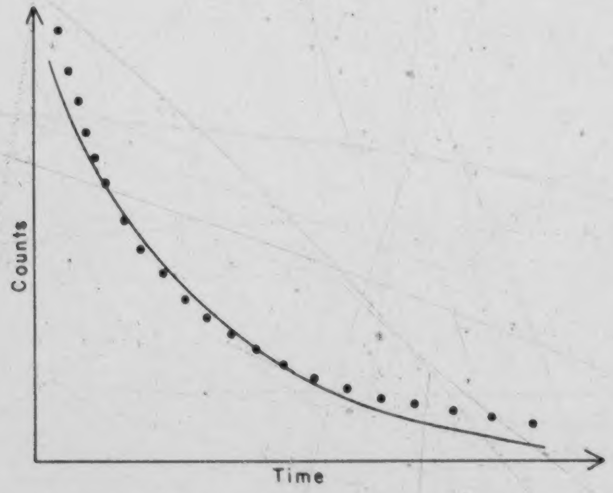

fit to 6-parameter decay data. The fitting curve is systematically below the data at the head and tail of the decay, and above the data at the center of the decay. This type of fit clearly indicates that more parameters are needed.

(b) Data rejection

It is to be expected that occasionally an individual datum value will show a significantly larger deviation from the fitting function than the remainder of the data in the set. This may result from an extreme fluctuation in the Poisson distribution or from some non-statistical source of scatter. A mechanism whereby such anomalous values can be rejected from the fitted data set has been incorporated into HOMER (Ir 74b). This procedure is invoked sparingly during the analysis, primarily where an apparent "best fit" yields a high reduced-χ^2 value. Normally, the rejection of one or more anomalous values in such a data set will noticeably decrease the reduced-χ^2 value without affecting the parameter values significantly, thus enhancing the reliability of the fit.

(c) Repeated measurements

The best way to verify an experimental result or to estimate its uncertainty, is to measure it a number of times. A mean life can be re-measured in a number of ways: using the same transition, or using another multiplet member or branch transition, under the same conditions; or using any of these under different conditions (in particular, with different ion energy). Consistency among primary and cascade components is important during comparisons of these results, although discrepancies can arise for a number of reasons. For example, one or more multiplet members or branch transitions may be affected by blends. If the blending transition represents a different ionization stage, the contribution may be energy dependent. Time resolution is velocity dependent (and hence energy dependent) so that low-energy measurements of fast decays may yield primary mean lives which are too long, and are longer than measurements performed at higher energy. Repeated measurements using different transitions and/ or ion energies are most useful for distinguishing these systematic effects. However, several measurements under identical conditions are usually needed for the subsequent determination of a reliable best-fit to a particular decay.

The experimental situation

The experimental conditions that existed during a decay measurement may sometimes account for the inability to obtain a satisfactory multi-exponential fit or for the disagreement among the results of repeated measurements. Unreliable data may be produced for a number of reasons: unstable beam conditions, changing foil properties (e.g. undetected foil deterioration prior to an observed breakage), or low-count data. Of course, such conditions are noted during a measurement, but the most satisfactory procedure is to re-measure the decay, if possible under improved conditions.

Disagreement among repeated measurements can frequently be attributed to unreliable data, although real differences may exist if the wavelength resolution, time resolution, or ion energy has been altered for the re-measurement. In particular, a change in wavelength resolution or ion energy could allow certain decay components to appear, to disappear, or at least to display different relative intensities. However, this would normally indicate the presence of blending and thus be helpful in the analysis, as mentioned earlier. Time resolution is dependent upon ion velocity, as mentioned previously, as well as upon the acceptance angle of the spectrometer and the step size between data points (see Ch. III). All of these considerations are relevant when comparing the results of repeated measurements.

The physical situation

Apart from resolution effects and the energy dependence of intensity, which are physical effects that can be controlled by experimental techniques, the foremost problem in the analysis of beam-foil mean lives is cascade repopulation. Cascade contributions usually necessitate multi-exponential curve-fitting analyses which, in principle, can be misleading (Wi 70). Fortunately, decays of vacuum ultraviolet transitions rarely exhibit more than one significant cascade, and this is often weak relative to the primary component. The accurate determination of cascade mean lives from secondary decay components is difficult, however, owing to the low intensity of these components relative to the primary as well as the possibility that one or more weaker cascades are also contributing to the decay. Unless a realistic comparison can be made with a directly measured (dominant) cascade mean life, the approach taken during this work has been to seek the best fits for which agreement with repeated measurements is demonstrated. (The best fit is generally taken to be that which, under given truncation and rejection conditions, displays the lowest reduced-χ^2 value without possessing a large ($\gtrsim$ 50%) statistical uncertainty for any fitting parameter.) More detailed techniques for handling cascade corrections have been developed by Curtis (Cu 70b). One comparison involving one such technique will be discussed in Ch. V.

A particular type of cascade that occurs relatively infrequently is the growing-in cascade. It is characterized by a negative exponential component in the decay, representing a short cascade mean life (see Fig. 18 and the accompanying discussion in Ch. III). Since growing-in effects normally are significant only very near the foil, they may be confused with the effects of a bulging foil. Confirmation of the growing-in component from the results of several decay measurements, involving different foil conditions, is therefore desirable. Often, a fast cascade can either be predicted or measured directly to verify that the growing-in component is real.

Comparison of the mean-life results with those of other experiments or theory, either directly or with regard to systematic trends, is also important when assessing the physical situation. Other beam-foil measurements should, of course, yield the same primary mean life and should also display similar cascading. Large discrepancies may indicate line blending (perhaps due to beam impurities) or, for short decays, time resolution limitations. Different analytic techniques may also contribute to disagreements. Several such comparisons are to be discussed in Ch. V.

Reliable theoretical mean lives are normally available for only a few transitions of an ion. They are particularly useful for indicating large errors in experimental results, for example, where a mean life is well below the resolution capabilities of a system and only the cascade mean life will be observed. Alternatively, predictions based upon configuration-interaction calculations can indicate where anomalously long mean lives are to be expected. Often these cannot be measured with the beam-foil method since the transition intensity does not decay sufficiently over the length of the chamber.

Systematic trends among experimental and theoretical values can be equally powerful, however, both in the direct prediction of individual results and in the indication of characteristics of atomic structure. Regularities along isoelectronic sequences are often employed in this manner, and a large number of these trends are to be discussed in Ch. VI.

4.4 Final Results

The final value for a mean life is obtained by calculating the weighted mean of the results of repeated measurements. The weight is defined to be the inverse square of the error estimate provided by HOMER. The statistical uncertainty of this final value is taken to be either the weighted standard deviation of the individual results or the weighted mean of the HOMER error estimates, whichever is larger. These two quantities are frequently of comparable magnitude, which suggests that the HOMER error estimate generally provides a reasonable approximation to the statistical uncertainty of the mean life. The uncertainty in the measured beam velocity (see Ch. III), including the uncertainty in foil thickness, is combined with the statistical uncertainty to provide an error estimate for the mean-life value. This error estimate should be regarded as representing one standard deviation.

CHAPTER V

SPECTRUM AND MEAN-LIFE RESULTS

Beam-foil emission spectra have been recorded during this project for the elements nitrogen, oxygen, neon, silicon, phosphorus, sulfur, argon, and krypton over the wavelength region 400-2000 Å. In each case, spectra were recorded at several ion energies. A few emission features from fluorine and boron were also studied. A summary appears below of the ions investigated and the approximate number of terms for which mean lives were measured in each element.

Ions	Terms Measured
B I, II	4
N I-V	40
O I-VI	60
F I-IV	4
Ne I-VII	30
Si II-IV	15
P I-V	20
S III-VI	15
Ar I-VIII	60
Kr I-VIII	50

The results of these investigations either have been published or are being prepared for publication, and a number of reports on this work have been presented at scientific meetings and international conferences (see Appendix I). The discussions in this and the following chapter summarize some of the more interesting results, concentrating on original analysis and interpretations.

5.1 Spectra

Ion energies ranging from 0.2 to 1.8 MeV were used to record spectra and measure decays. Emission was observed in the vacuum ultraviolet for both neutral and ionized atoms, but only for those ions formed by removal of up to (n-1) electrons from the n-electron outermost shell. This comprises, for example, four atomic species in silicon, and eight in argon. More-highly-ionized states usually require greater ion energies (see Bashkin et al (Ba 73b)), and many of the prominent transitions in their spectra occur in the XUV region, which we are unable to detect.

The low-wavelength response of our system down to 250 Å is shown in Fig. 19 for the oxygen spectrum. The spectrum is weak below about 500 Å, primarily as a result of rapidly decreasing efficiency of the reflection grating for decreasing wavelength. However, all features are readily identified as oxygen transitions. Three different relative intensity scales are used in Fig. 19 to indicate how the observed intensities

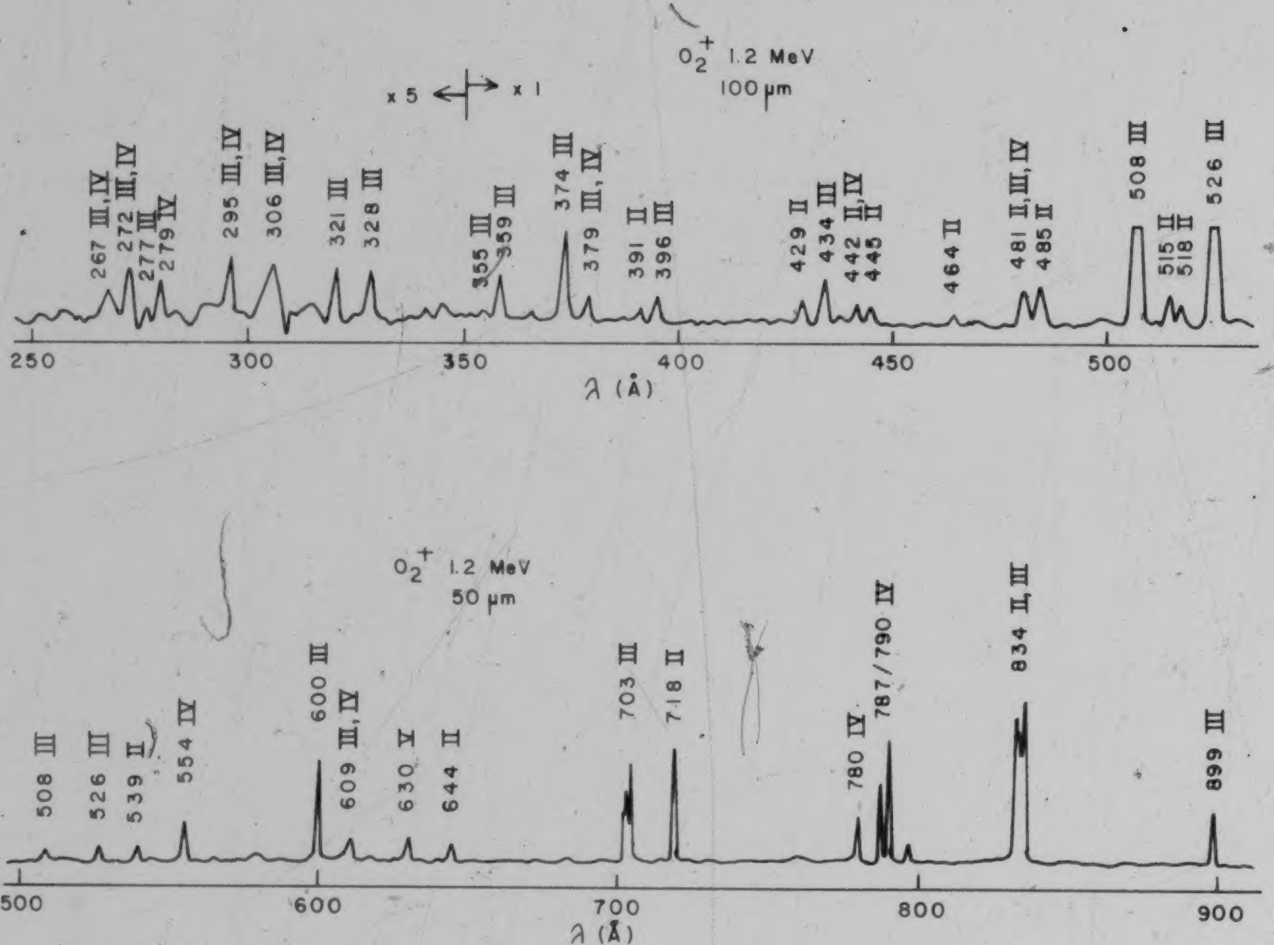

Fig.19. Composite spectra of oxygen recorded with different sensitivities and slit-widths.

vary within this spectrum. The lower trace also indicates the maximum wavelength resolution capability of our system.

Of the eight elements for which we performed extensive studies, the spectra of oxygen and nitrogen are the best known, and we have been able to classify nearly all the emission features observed in our beam-foil spectra of these elements using standard wavelength compilations (Ke 73). Most of the observed strong transitions in the higher Z elements studied have also been routinely classified in this way, although a large number of new lines appear at high energy in the neon, argon, and krypton spectra. Mean-life results have been reported for twelve unassigned neon transitions as part of our beam-foil survey of this element (Ir 73b). In that report we also presented lifetimes for several recently assigned (unpublished) Ne V and VI transitions. Similarly, investigations of sulfur and argon have yielded lifetimes for recently assigned transitions in Ar V (725 Å) and S V (696 Å). These results are discussed in Ch. VI in the context of trends for isoelectronic sequences (Figs. 47 and 64 , respectively). Spectra and preliminary lifetime results for several second period and third period elements have been reported at the Third International Conference on Beam-Foil Spectroscopy (Ir 73c, Ir 73d).

A systematic study of the beam-foil spectra of argon has been undertaken during this project, with emphasis on the region below 1000 Å where the most prominent transitions are found. An early report (Li 72) on a fairly low-resolution study of this element presented a large number of new lifetime results, particularly for multiply-ionized species. Many unassigned argon transitions were observed between 1100 Å and 1700 Å during that investigation. At low ion energy, this wavelength region is complicated by a high density of weak Ar II and III lines as well as (in beam-foil spectra) numerous impurity lines from foil-ejected carbon atoms and ions. Features which persist at higher energies should fall into neither of these categories, except possibly for a few very strong, well-known carbon multiplets. In Table 5.1 are presented lifetime results for those transitions studied that do not become weak at higher energy. (The 649 Å and 721 Å lines are the only prominent transitions below 1000 Å not yet assigned. They will be discussed below and are only included here for completeness.) Argon spectra between 1050 Å and 1700 Å, recorded during a higher-resolution study, are shown in Figs. 20 and 21. The features above 1100 Å in Table 5.1 probably represent transitions

Table 5.1

Unassigned Transitions in Argon

	Decay Components (ns)	
λ[a] (Å)	Strongest	Other
649	0.21±0.03	1.5±0.5
721	0.9 ±0.2	–[b]
1163	0.35±0.06	5 ± 1
1303	1.0 ±0.2	3.5±0.9
1409	1.0 ±0.2	–
1416	1.0 ±0.2	–
1425	0.37±0.06	1.7±0.3
1435	1.3 ±0.6	–
1454	0.50±0.05	4 ± 1
1516	0.45±0.05	–
1585	0.8 ±0.1	3.5±1.0
1614	2.5 ±0.5	–
1625	1.1 ±0.3	–
1632	0.8 ±0.2	–
1638	0.7 ±0.1	–
1648	0.8 ±0.1	9 ± 2

(a) Estimated wavelength uncertainty: ±1 Å.

(b) A constant background component is usually present in these single-exponential cases; it may reflect the presence of very long-lived cascades.

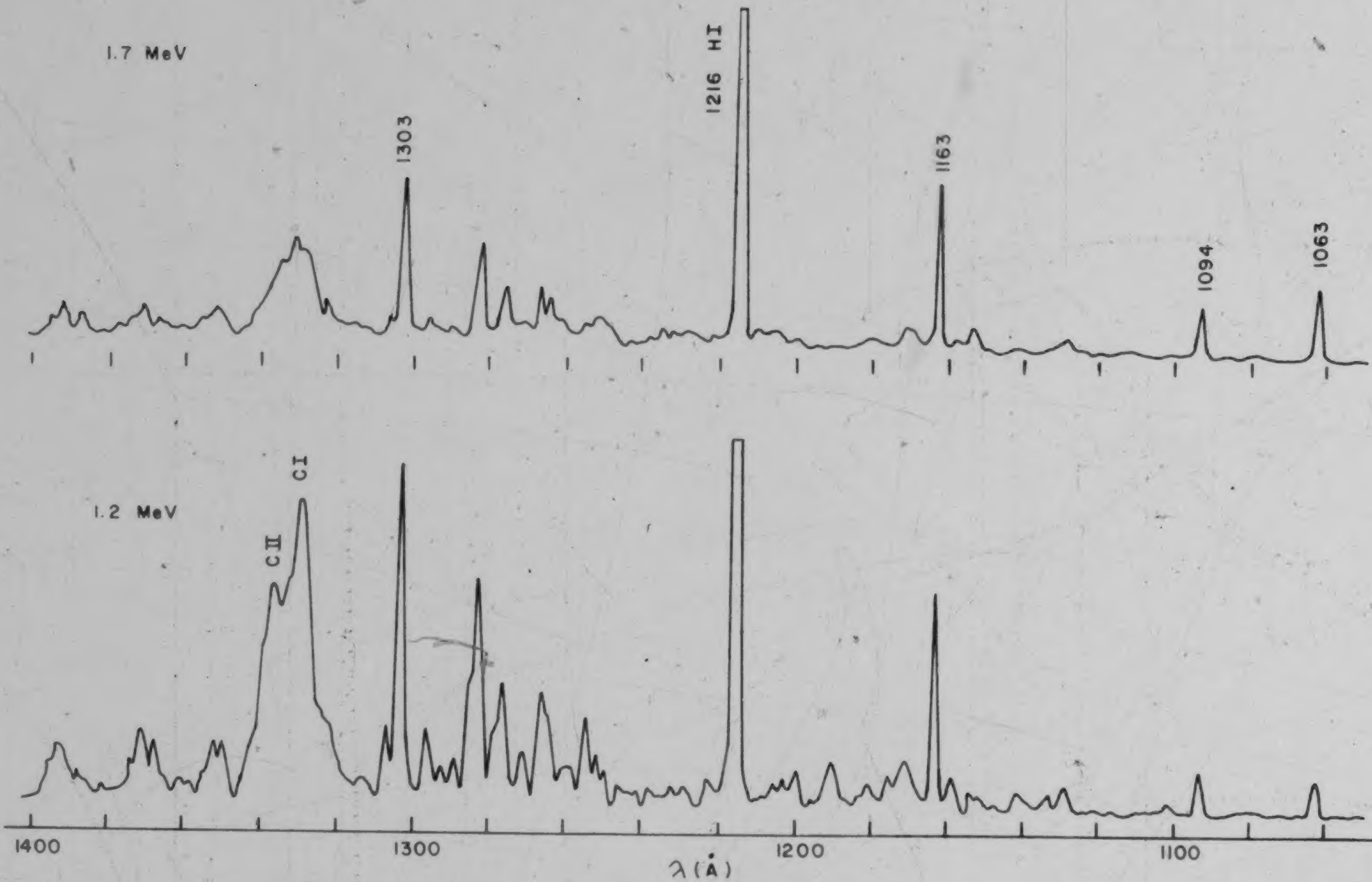

Fig 20 Beam-foil spectra of argon.

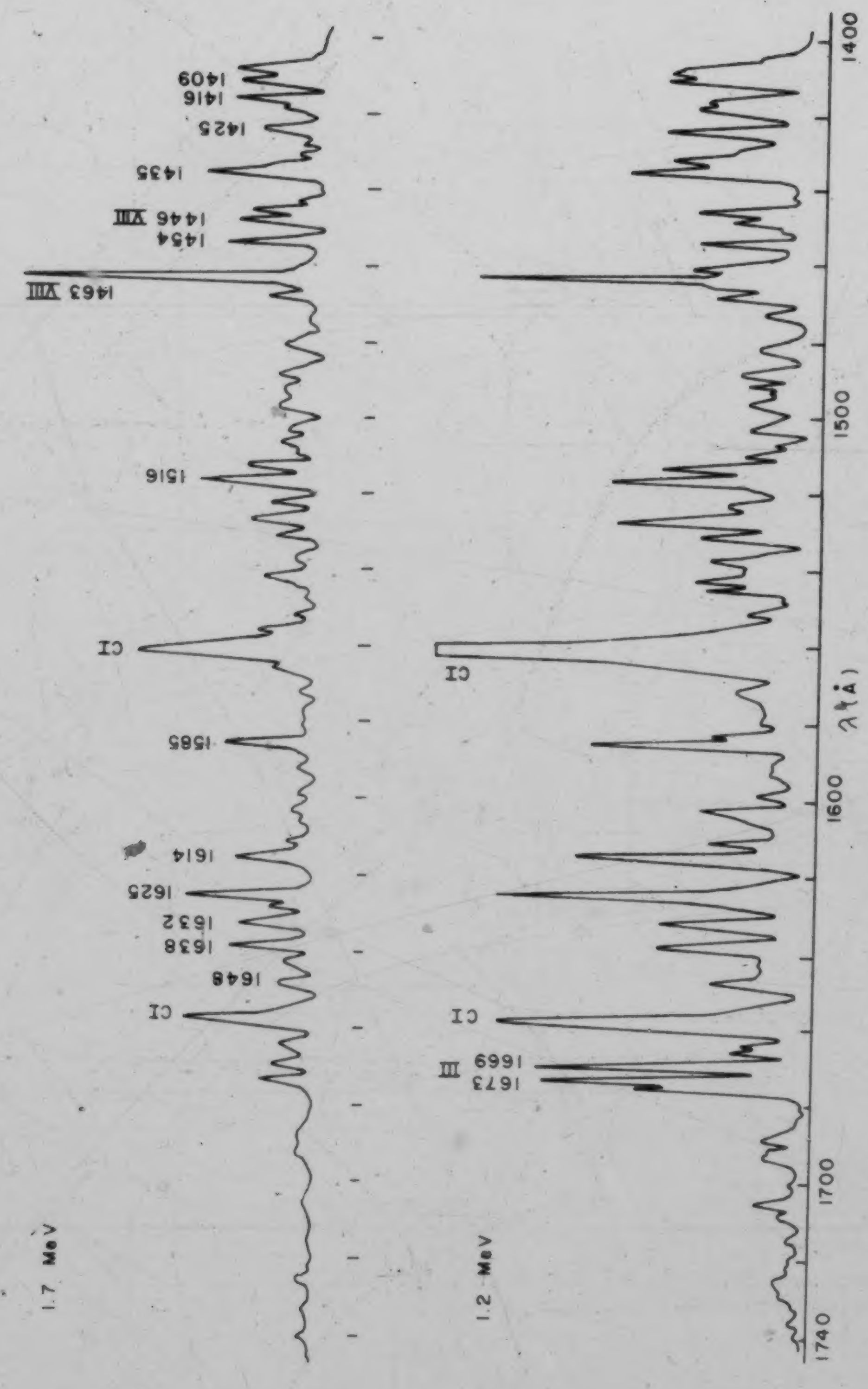

Fig.21. Beam-foil spectra of argon.

involving high-lying terms in Ar IV and higher ionization stages.

The more recent investigation of this element employed better resolution for both wavelength and decay measurements. In particular, spectra were recorded between 400 Å and 1000 Å using ion energies of 0.2, 0.4, 0.8, 1.2, 1.8 MeV. These are shown in Figs. 22 to 26. Decays were measured for all prominent transitions in these spectra. Many of the lifetime results are incorporated into the discussions of oscillator strength trends along isoelectronic sequences in Ch. VI.

A detailed study of observed wavelengths, intensities, and lifetimes in these spectra, along with comparisons of energy levels and oscillator strengths for isoelectronic ions, has resulted in a number of new proposed classifications in argon. Two classifications of observed phosphorus transitions have also resulted from this investigation. The results are summarized in Table 5.2. All of these transitions display intensity/ion-energy properties that are characteristic of transitions from several-times-ionized atoms.

The two phosphorus multiplets and their isoelectronic counterparts in Ar VII are discussed in

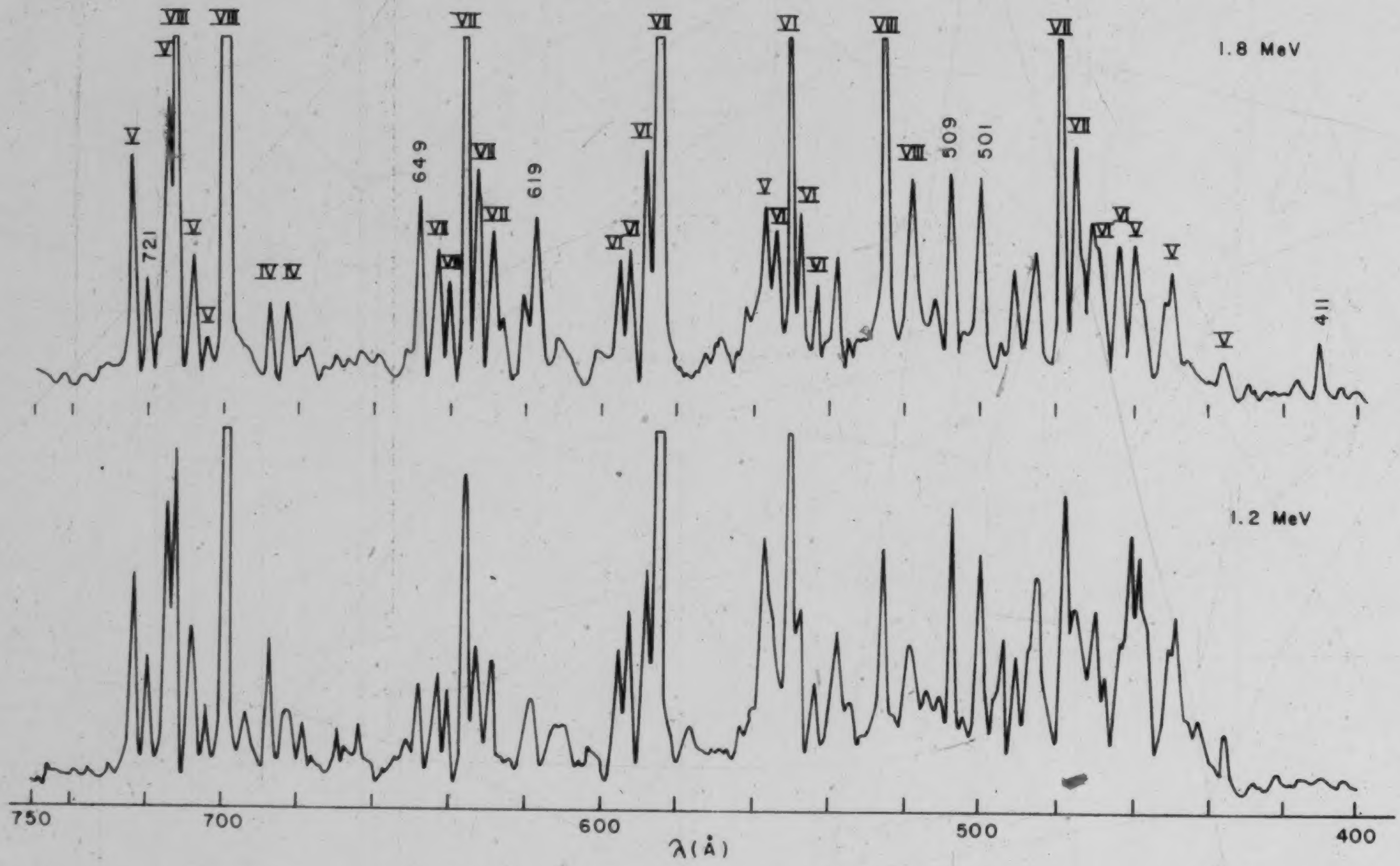

Fig.22. Beam-foil spectra of argon.

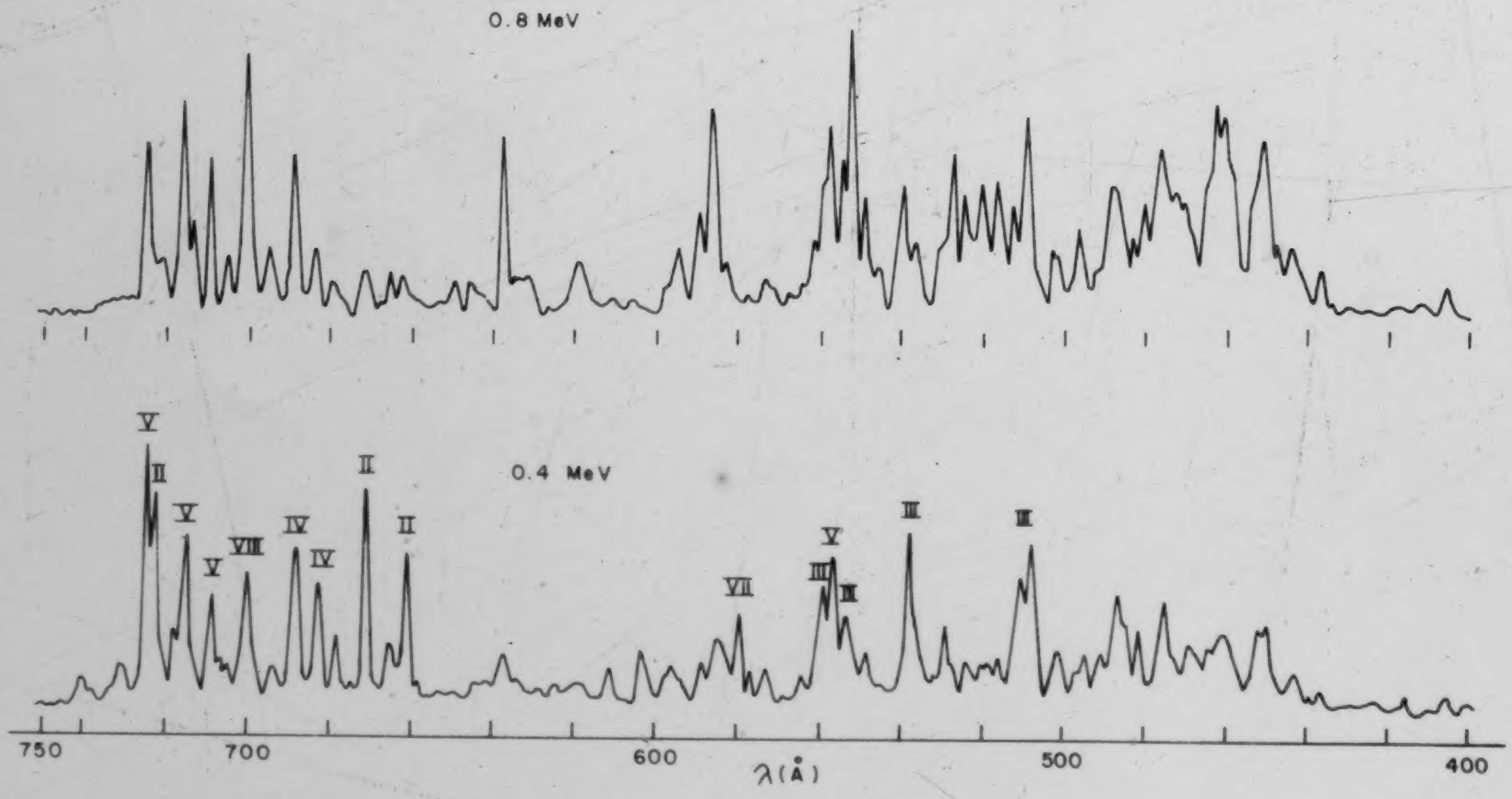

Fig.23. Beam-foil spectra of argon.

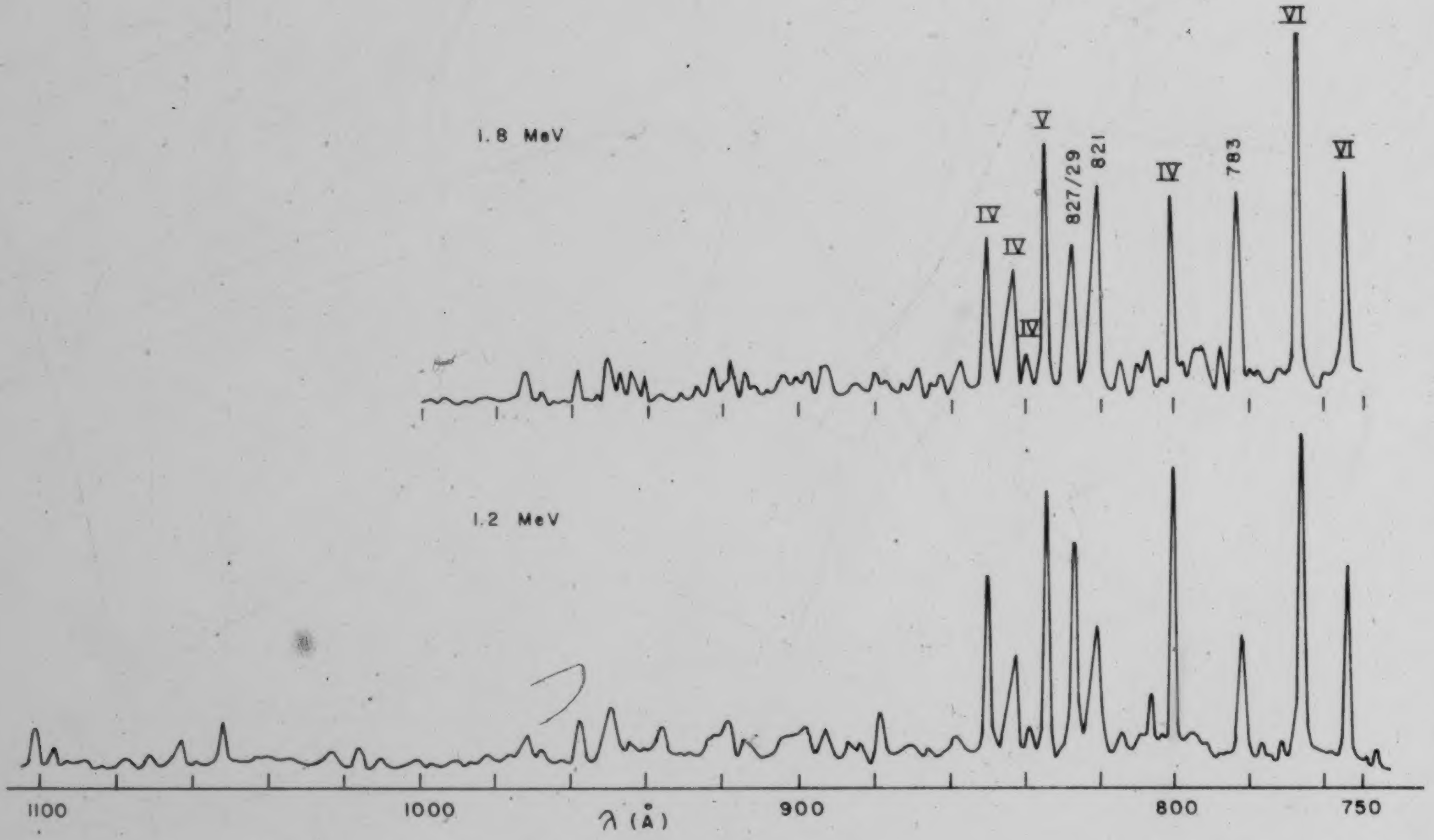

Fig.24. Beam-foil spectra of argon.

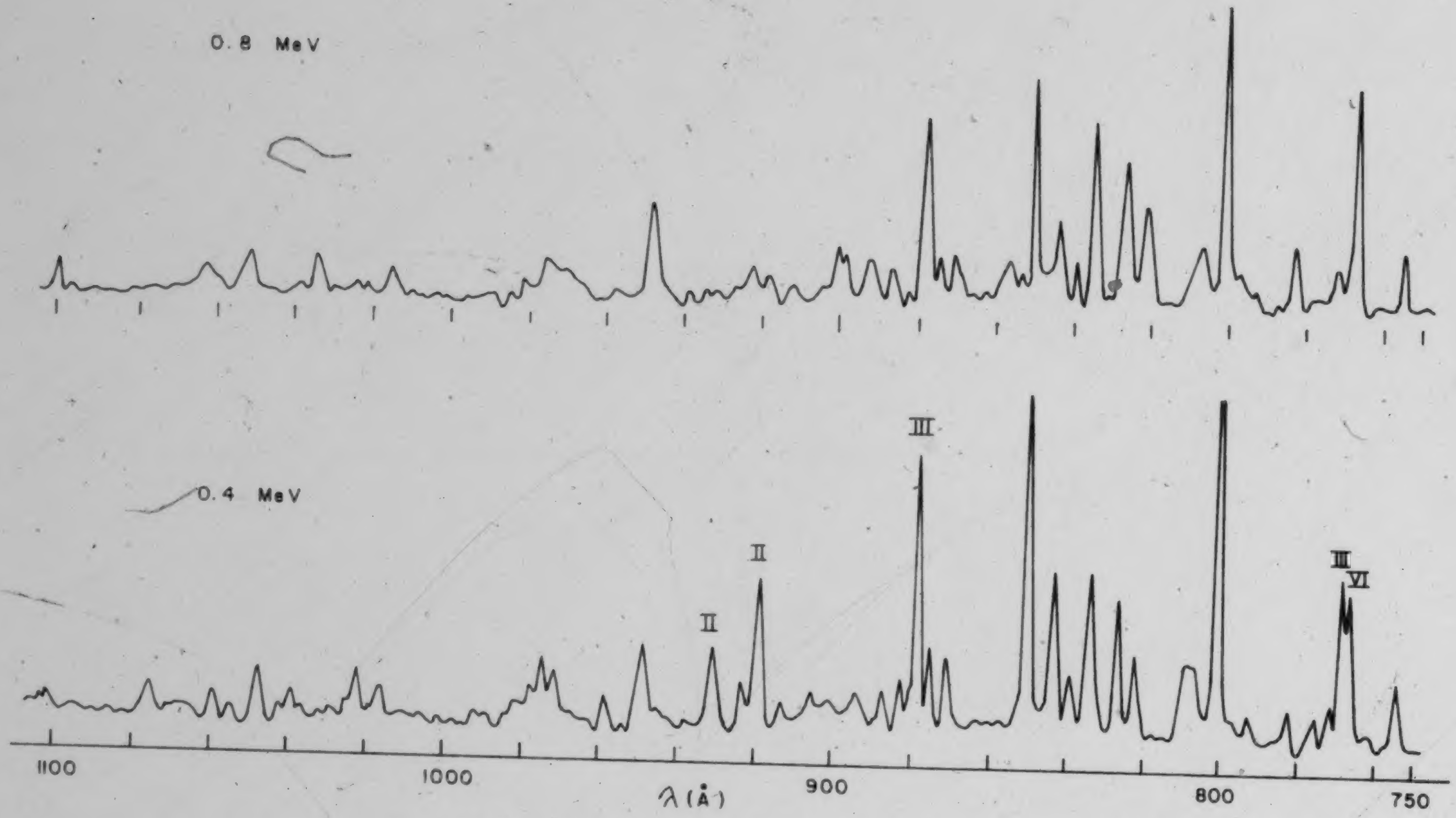

Fig.25. Beam-foil spectra of argon.

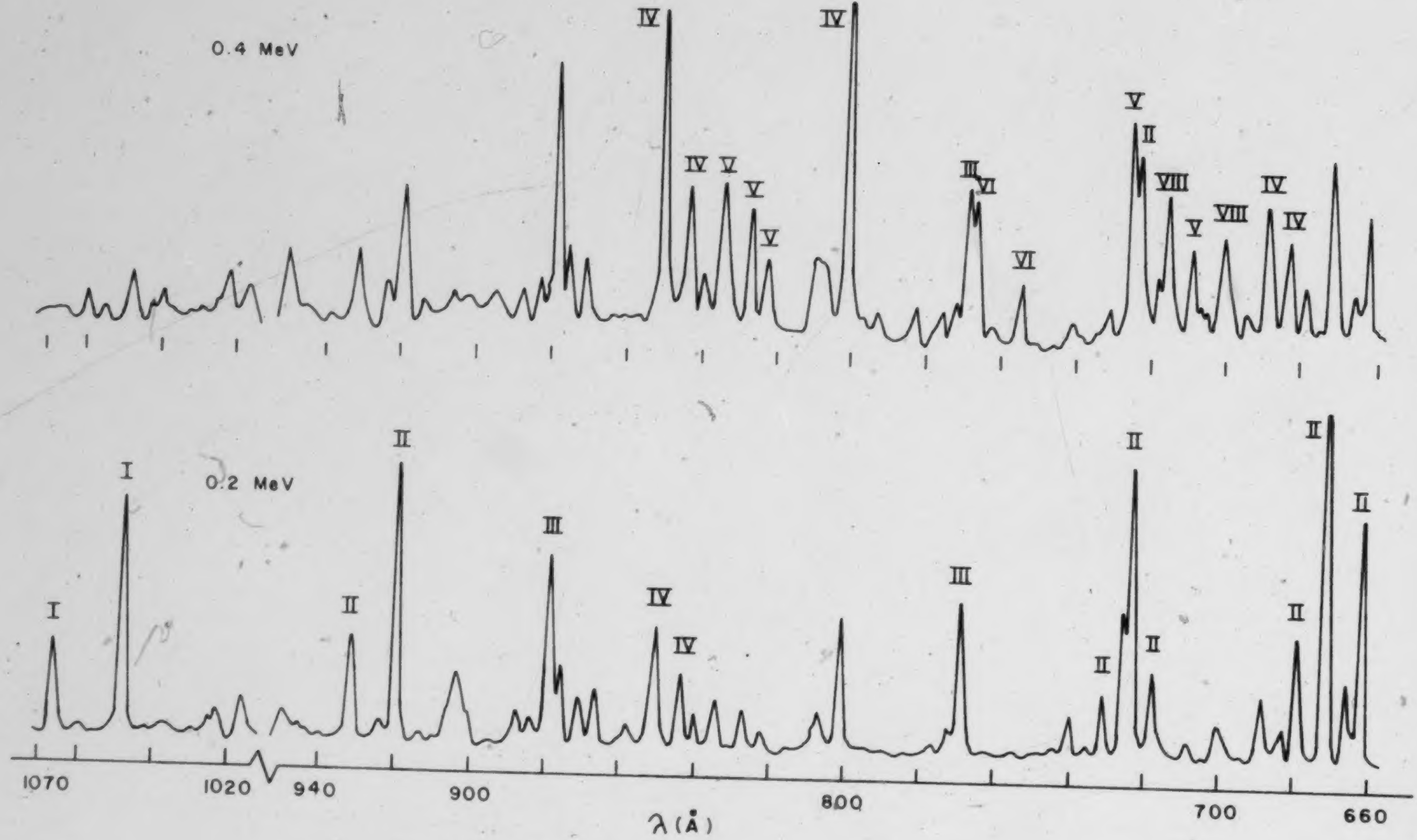

Fig.26. Beam-foil spectra of argon.

Table 5.2

Proposed Classifications in Argon and Phosphorus

Ion	λ[a] (Å)	Transition	Mean Life (ns) Primary	Mean Life (ns) Cascades
Ar VI	619	$3s3p^2\ ^2D-3p^3\ ^2P^o$	0.26±0.03	1.2±0.3
Ar VI	783	$3s3p^2\ ^2D-3p^3\ ^2D^o$	1.4 ±0.3	(0.6±0.1 bl?)[b]
Ar VII	411	$3s3d\ ^3D-3s4p\ ^3P^o$	-	-
Ar VII	501	$3s3p\ ^1P^o-3s3d\ ^1D$	0.12±0.02	1.0±0.2
Ar VII	509	$3s3d\ ^1D-3s4p\ ^1P^o$	0.15±0.02	0.5±0.1,3±1
Ar VII	821 829	$3s3d\ ^3D-3p3d\ ^3F^o$	0.7 ±0.2	-
Ar VII	1063	$3s3p\ ^1P^o-3p^2\ ^1D$	-	-
P IV	877(?)	$3s3p\ ^1P^o-3s3d\ ^1D$	0.21±0.03	1.2±0.2
P IV	1367 1373 1378	$3s3d\ ^3D-3p3d\ ^3F^o$	3.1 ±0.6	-

(a) Estimated wavelength uncertainty: ±1 Å.

(b) This shorter component is considerably weaker than the 1.4 ns component and probably represents a weak blended transition.

Ch. VI with regard to f-value trends along the Mg I isoelectronic sequence (see Figs. 64 and 67). R. Hallin (private communication to Ekberg (Ek 71)) has independently suggested tentative wavelengths of 501.07 Å and 1063.55 Å for the 3s3p $^1P^o$-3s3d ^1D and 3s3p $^1P^o$-3p^2 ^1D transitions in argon, respectively, in agreement with the values in Table 5.2. The 501.07 Å value determines the previously unknown 3s3d ^1D level and, since the 3s4p $^1P^o$ level is known (Mo 49), the 3s3d ^1D-3s4p $^1P^o$ transition wavelength may be determined precisely as 510.03 Å. This is in fair agreement with our observed transition at 509 Å. The P IV 877 Å feature actually has two possible classifications, the other being 3s3d ^3D-3s4f $^3F^o$, also in P IV (Ke 73). The classification in Table 5.2 is proposed primarily on the basis of the lifetime results, in comparison with adjacent members of the Mg I isoelectronic sequence. The f-value derived from the primary lifetime appears to favor the classification in Table 5.2 (compare Figs. 64 and 68 in Ch. VI), and the degree of cascading observed is consistent with our observations of cascading for the same transition in Ar VII (501 Å, Table 5.2) and S V (696 Å, (Ir 74)). The 3s3d ^1D level position that would result from this classification agrees well with the energy level trend for the sequence (see Fig. 60).

Sections of beam-foil spectra showing both P IV multiplets from Table 5.2 appear in Fig. 27. The 3s3d ^3D-3p3d $^3F^o$ multiplet in P IV has been found at 1367/73/78 Å. The observed wavelengths and measured mean life are consistent with recently reported results for this multiplet in S V and Cl VI (Ba 73b). The relative intensities of the resolved components are approximately those expected for LS coupling (i.e. ~4:3:2). This multiplet has also been identified in argon, with the two strongest components appearing at 821/29 Å. There is serious blending of both components with the 822/27 Å components of the resonance multiplet in Ar V. Inspection of Fig. 23 reveals, however, that the Ar VII lines dominate at 1.8 MeV. Fortunately, the Ar V multiplet displays a relatively long mean life (4 ns) so that the 3p3d $^3F^o$ mean life (0.7 ns) is obtainable even with the blending. These decay components were observed in the analysis of our earlier argon results (Li 72), although the source of the blending was unidentified at that time. The f-value derived from the 3p3d $^3F^o$ mean life is also consistent with the sequence trend (Ch. VI, Fig. 67).

The remaining classifications (at 619, 783, 411 Å) are proposed on the basis of wavelength agreement with the transitions predicted by estimation of upper

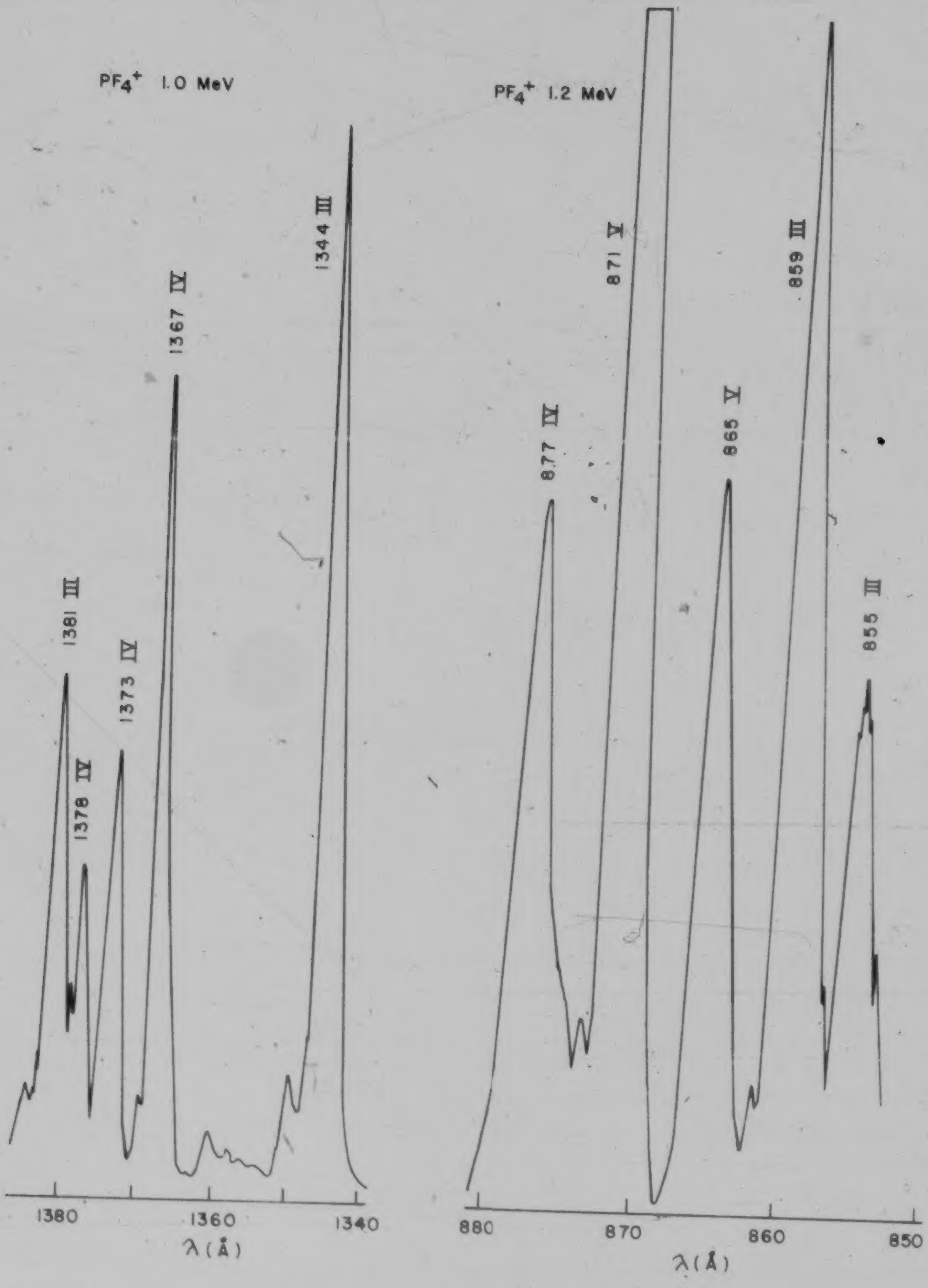

Fig.27. Sections of beam-foil spectra of phosphorus.

term positions, using extrapolation along the isoelectronic sequences. Only two of the prominent unassigned lines in this region, 649 Å and 721 Å, could not be classified by this method.

A systematic study of the vacuum ultraviolet spectra of krypton has also been undertaken. Spectra have been recorded at various ion energies for wavelengths from 400 Å to 1800 Å. The Kr IV to Kr VIII systems are poorly determined in the vacuum ultraviolet, with only eleven multiplets involving allowed transitions below 2000 Å having been classified in these five ions (Ke 73). As in argon, these prominent multiplets all lie below 1000 Å. Fig. 28 shows the beam-foil spectrum of krypton in this region, recorded at high ion energy to enhance the emission from higher ionization stages. All but the weakest of the eleven known multiplets have been identified in this spectrum and many prominent unassigned lines are also observed. Transitions from Kr I-III have been identified in spectra recorded at lower energies.

A striking similarity is apparent between the wavelength values of homologous transitions in argon and krypton. For $\Delta n = 0$ transitions the wavelengths are nearly the same (usually slightly lower in krypton),

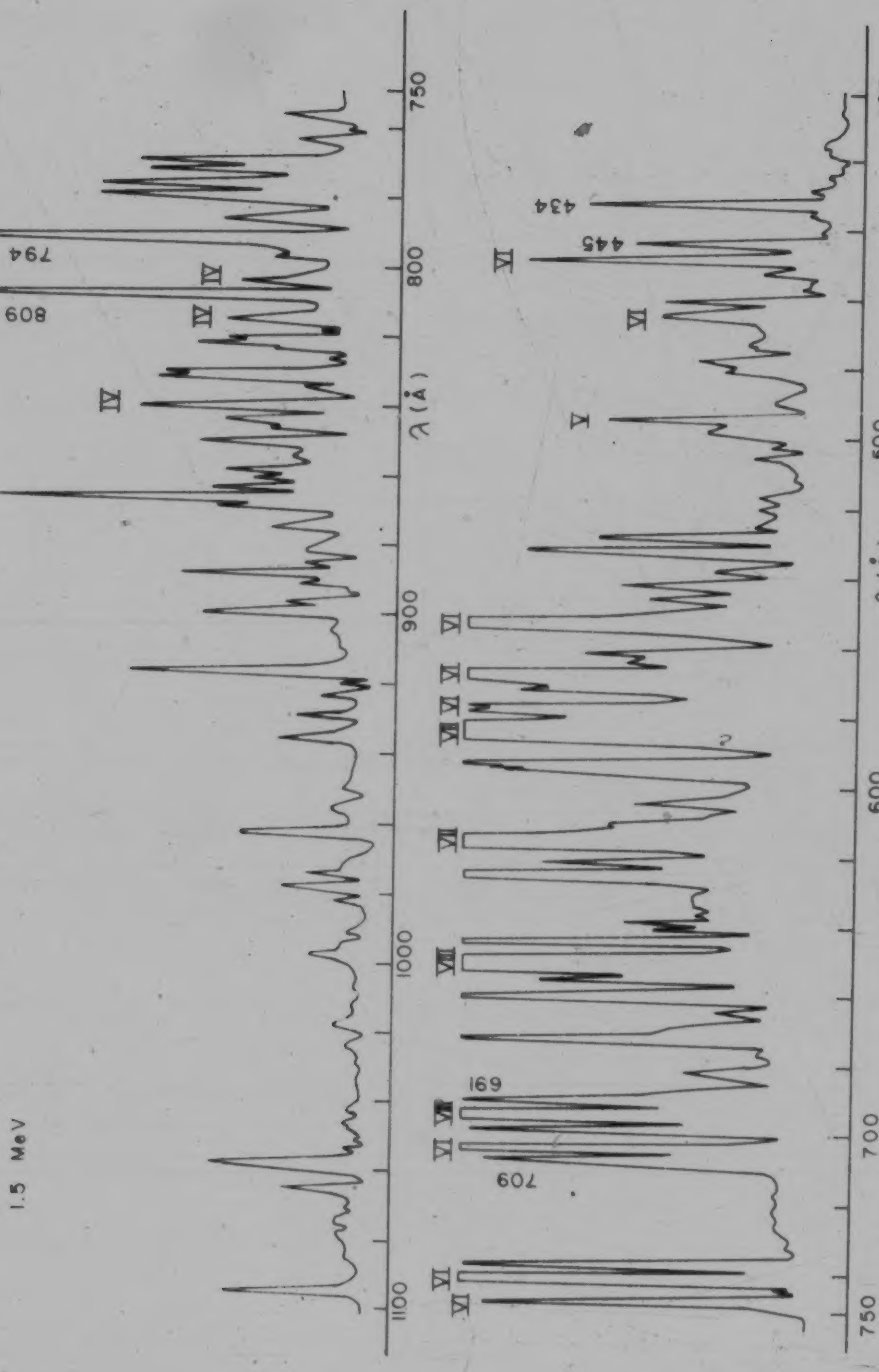

Fig.28. Beam-foil spectra of krypton.

a correspondence that is not observed between homologous transitions in neon and argon. For $\Delta n \neq 0$ transitions, however, a pronounced increase in wavelength is observed for the krypton transitions. (Much the same characteristics are displayed between krypton and xenon transitions.) Electronic shells having $n > 2$ appear to be radially far enough removed from the nucleus to allow approximate preservation of relative term-energy spacings within an outer shell along a homologous group of elements. The relative separation of different electronic shells decreases with increase of nuclear charge Z along a group, however, resulting in higher wavelengths for transitions connecting these shells.

This correspondence is very useful for comparing krypton spectra with argon spectra, the latter being better understood in all stages of ionization. In addition, since f-values of homologous transitions are normally about equal if coupling characteristics are the same (Wi 69), the similarity of wavelengths implies that mean lives of upper terms for $\Delta n = 0$ transitions also should be nearly equal. Using these wavelength and mean-life guidelines, along with relative multiplet intensities and intensity/ion-energy characteristics, several classifications in Kr IV, V, and VII are proposed.

Table 5.3 summarizes wavelength and mean-life information for prominent homologous transitions in the first to eighth spectra of argon and krypton. All mean lives have been measured during this project. The proposed classifications in krypton are indicated by asterisks.

For all the transitions measured in Kr IV-VIII the mean life is found to be shorter than that for the argon transition. In about half the cases the difference is fairly small (10-20%), although several transitions display larger discrepancies. It is interesting to note that the large discrepancies exist only for transitions that are known to be strongly affected by configuration interaction in argon (these are denoted by the superscript "b" in Table 5.3). In each case the oscillator strength in argon has been significantly reduced by the interaction, which is reflected as an increase in the mean life. The krypton results suggest that the corresponding configuration interaction effects in the fourth period are weaker than those in the third period. Several third-period sequences involving such interactions are discussed in Ch. VI.

The correspondence between mean lives for argon and krypton appears to break down for p-s transitions in the neutral and singly-ionized atoms (the three final entries in Table 5.3). This is

Table 5.3

Mean Lives for Homologous Transitions in Argon and Krypton

ARGON				KRYPTON	
Ion	λ (Å)	τ (ns)[a]	Transition	λ (Å)	τ (ns)[a]
VIII	700/14	0.50	$s\ ^2S-p\ ^2P^o$	652/96	0.35
	519/26	0.15	$p\ ^2P^o-d\ ^2D$	491	-
VII	586	0.18	$s^2\ ^1S-sp\ ^1P^o$	585	0.16
	630-44	0.20	$sp\ ^3P^o-p^2\ ^3P$	619	0.18
	475/79	0.13	$sp\ ^3P^o-sd\ ^3D$	434/45*	0.11
VI	755/67	2.8	$p\ ^2P^o-sp^2\ ^2D$ [b]	706/43/49	1.1
	545-56	0.11	$p\ ^2P^o-sp^2\ ^2P$	544-80	0.10
	457/62	0.11	$p\ ^2P^o-d\ ^2D$	450/65	0.10
V	822/27/36	4.0	$p^2\ ^3P-sp^3\ ^3D^o$ [b]	809*	2.7
	705/9/16	1.3	$p^2\ ^3P-sp^3\ ^3P^o$ [b]	691*	0.8
	725	1.7	$p^2\ ^1D-sp^3\ ^1D^o$ [b]	709*	1.0
	458-64	0.11	$p^2\ ^3P-pd\ ^3P^o$	484-507	0.10
IV	840/44/51	4.5	$p^3\ ^4S^o-sp^4\ ^4P$ [b]	806/17/42	3.5
	800-02	2.7	$p^3\ ^2D^o-sp^4\ ^2D$ [b]	794*	2.2
III	871-87	3.5	$p^4\ ^3P-sp^5\ ^3P^o$ [b]	837-98	3.5
	769	1.8	$p^4\ ^1D-sp^5\ ^1P^o$ [b]	786	-
II	920/32	4.5	$p^5\ ^2P^o-sp^6\ ^2S$ [b]	917/65	0.3
	718-31	0.35	$p^5\ ^2P^o-p^4s\ ^2P$	826-84	0.7
I	1048	1.6	$p^6\ ^1S-p^5s\ \frac{1}{2}[\frac{1}{2}]$	1165	3.
	1067	6.0	$p^6\ ^1S-p^5s\ \frac{3}{2}[\frac{3}{2}]$	1236	3.

(a) Uncertainties in mean lives: Argon 10-15%; Krypton ~20%.

(b) See text discussion.

(*) Proposed classifications.

partly due to the existence of significant deviations from LS coupling for these transitions. Intermediate coupling calculations by Aymar et al (Ay 70) show that the coupling characteristics differ sufficiently among these transitions in Ne I, Ar I, Kr I, and Xe I to disrupt uniform f-value trends. Of course, the homologous wavelengths differ considerably in these $\Delta n \neq 0$ transitions as well, and cause further f-value (and hence mean-life) discrepancies. Our mean-life values agree well with intermediate coupling calculations for the five p-s transitions for which theory is available (i.e. for all but the Kr II transition).

5.2 Mean Lives

Mean-life results obtained during this project represent the first experimental determinations for about 100 terms in 50 ions of 10 elements. Nearly 200 other term mean lives have been measured for which comparison can be made with previous experimental work. Significant discrepancies from the earlier work have been found for neon and sulfur and, to a lesser extent, for silicon and phosphorus. The silicon results have been fully reported elsewhere (Ir 73a) and will not be discussed here.

Neon

Our beam-foil results for neon (Ir 73b) may be compared with results reported previously by Kernahan et al (Ke 72), who had performed the most extensive beam-foil study of neon in the vacuum ultraviolet. Agreement is found for only five of the fourteen comparisons, with discrepancies of more than a factor of two existing in both directions. Comparison of both sets of results can be made with recent, fairly reliable calculations of Nicolaides (Ni 73a). For 12 possible comparisons, our results yield a mean deviation of about 12%. For 8 possible comparisons, the mean deviation of the Kernahan et al results is about 40%. Furthermore, examination of oscillator strength trends along isoelectronic sequences (see Ch. VI) confirms the reliability of our neon results.

Since five of the nine discrepancies involve a significantly _lower_ mean life in the earlier report, insufficient time resolution cannot account for all differences. This may be the cause of the four discrepancies in which we report the lower value, however, since the mean lives are very short in each case and large step sizes (0.5 mm compared to our 0.1 mm) were used in the earlier experiment (Kernahan, private communication). Somewhat higher ion speeds than ours were employed in that work, which should partially compensate for the lower spatial resolution.

One probable source of error is the use of graphical fitting in their analysis of the decay components of the multi-exponential curves. When cascading is weak, or when only two components with very different mean lives are present, reliable results can be obtained with this simple method. Neither situation is common in these neon decays. Of the four transitions for which we detected little significant cascading, Kernahan et al report nearly the same result in three cases, their fourth result being a factor of two low. The remaining transitions all show stronger cascading, and results obtained graphically are expected to be less reliable.

Sulfur

The first detailed study of beam-foil spectra and lifetimes of sulfur was performed by Berry et al (Be 70b), who investigated the wavelength region 600-4000 Å. As pointed out in that report, the mean lives found for the five transitions in S IV, V, VI observed below 1000 Å are systematically much longer than would be predicted by isoelectronic comparisons. It was suggested that inability to detect fast decay components was responsible for the discrepancies. Their decays were measured by viewing a 5 mm beam length and using 2.5 mm steps between data points. The consequent time resolution limitations were significant, since each step corresponds to 3-10 predicted mean lives (at their highest ion speed) for typical transitions below 1000 Å. We performed a beam-foil study of sulfur in the vacuum ultraviolet specifically to obtain the correct mean lives for these transitions and to investigate other prominent sulfur transitions in this region. Our accepted beam length was less than 1 mm and our minimum step size was 0.1 mm. We obtained shorter mean lives (by factors of 2-10) for all five transitions, and the results show excellent agreement with trends along isoelectronic sequences (see Ch. VI). In addition, we confirmed the result of Berry et al for the long-lived resonance multiplet in S IV and measured mean lives for ten other multiplets in S III-VI below 1000 Å, none of which have been determined experimentally elsewhere. A report on our complete results in sulfur is about to be presented for publication (Ir 74a).

Phosphorus

Curtis et al (Cu 71b) have studied beam-foil spectra and lifetimes in P I-V between 600 Å and

2200 Å. We have recently re-measured most of their transitions, along with several transitions that have not been previously studied (Li 74). Reasonable agreement with their results has been obtained for only about half of the 15 comparisons. This seems to be unsatisfactory in view of the various techniques that were employed by Curtis et al to reduce the uncertainties in their decay-curve analysis. A number of examples in Chapter VI reveal that, where disagreement occurs, our results for phosphorus are systematically in better agreement with the experimental trends along isoelectronic sequences than are those of Curtis et al.

One method used in their work is the arbitrarily-normalized-decay-curve (ANDC) cascade analysis technique (Cu 71a). By this procedure, arbitrarily normalized primary and cascade decay curves are integrated over various (common) intervals to generate a family of linear relationships between the primary lifetime and the replenishment ratio (Cu 70a). A sharp intersection among the various lines is required to indicate that all significant cascading has been accounted for, and the lifetime can then be read directly off the graph. Curtis et al used this technique to analyze decays for the 3p $^3P^o$-3d ^3D

(825 Å) transition and its strong cascade from 4p $^3P^o$ (1488 Å). We have also measured these decays, but we find disagreement with both their results, as shown below:

Transition		Mean Life (ns)	
		This work	Curtis et al
825 Å(3p $^3P^o$-3d ^3D)	Primary:	0.25±0.03	0.36±0.05
	Cascades:	2.1 ±0.3	1.5, 3.3
1488Å (3d ^3D-4p $^3P^o$)	Primary:	2.1 ±0.2	1.1 ±0.3
	Cascade:	-	3.3

Our results represent the mean of three different decay measurements for each transition. It should be noted here that the 3d ^3D mean life obtained directly from the ANDC plot of Curtis et al (Cu 71b) is actually about 0.40±0.01 ns, although the above value (0.36 ns) is reported in their table of results.

The ANDC technique has been applied to our data for these decays and the results appear in Fig. 29. Plots (a) and (b) represent different decay measurements for 825 Å combined with the same measurement of 1488 Å. Although the intersection in (b) is somewhat diffuse, both plots are consistent in indicating the 3d ^3D mean life to be about 0.32±0.02 ns.

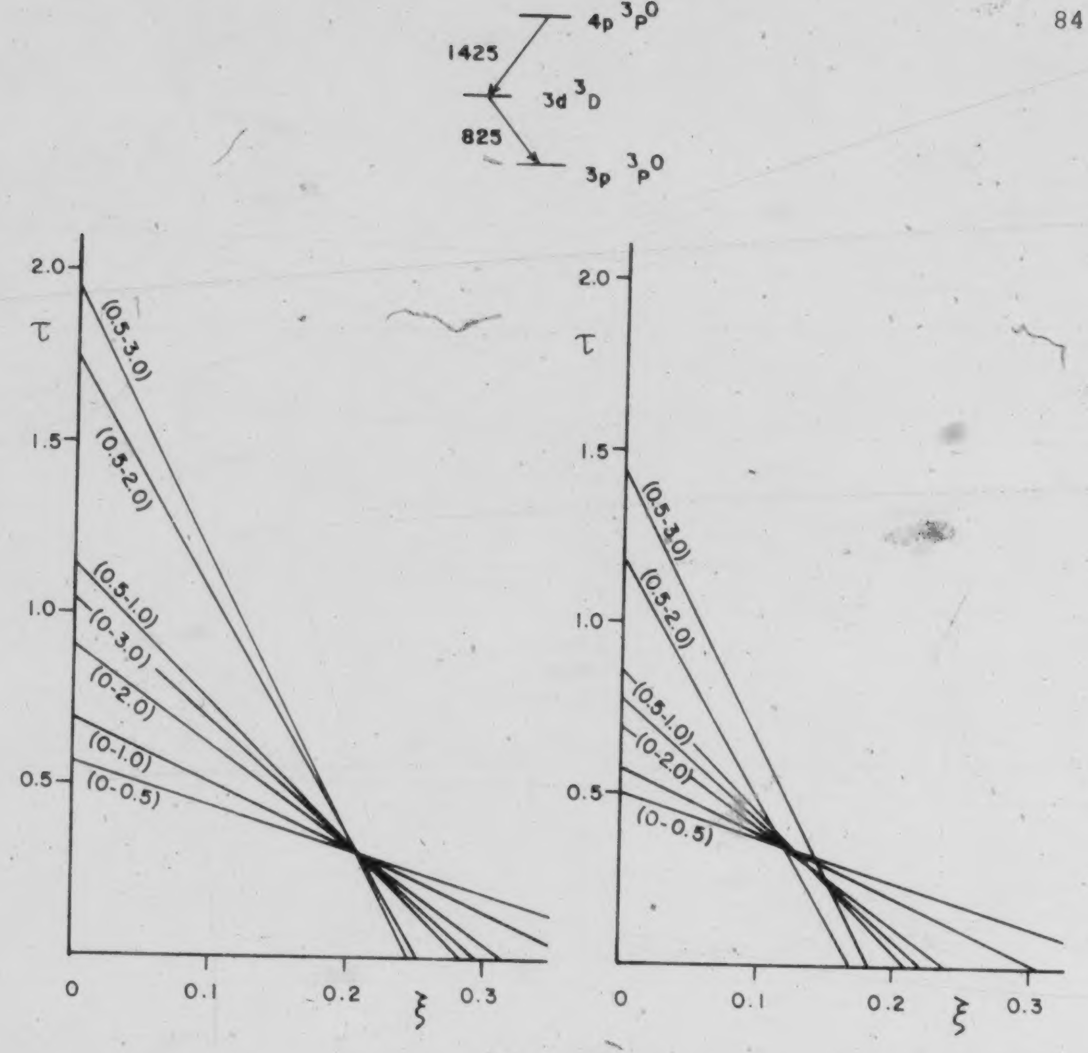

Fig.29. Results of ANDC analysis (Cu 71a) applied to decay data from this project for the 825 Å and 1425 Å transitions in P IV. The two plots represent different decay data for 825 Å combined with the same data for 1425 Å.

This value is almost mid-way between our result and that quoted by Curtis et al. The plots are not really conclusive as to the source of the discrepancy between the experimental results. However, the contrast between the intersections in (a) and (b) reveals that the ANDC technique can be very sensitive to different data for the same transition. Furthermore, the f-value plot for the 3p $^3P^o$-3d ^3D transition along the Mg I sequence (Ch. VI, Fig. 39) indicates that both the Curtis et al result and the ANDC result for our data are inconsistent with the well-determined experimental trend, whereas our curve-fitting result agrees well with the trend.

On the basis of the above example and of similar f-value comparisons for phosphorus in third-period isoelectronic sequences (Ch. VI, Figs. 35-38), the various methods applied by Curtis et al to reduce uncertainties in the lifetime analysis of decay curves apparently have not produced results as reliable as those obtained with our direct curve-fitting techniques, in some cases.

CHAPTER VI

REGULARITIES AND SYSTEMATIC TRENDS AMONG OSCILLATOR STRENGTHS ALONG ISOELECTRONIC SEQUENCES

It has long been known that atomic energy levels exhibit certain regularities, both for individual atoms (e.g. the spectral series) and for groups of atoms that possess similar electronic structures (e.g. homologous atoms, and ions forming an isoelectronic sequence). Regularities for the intensities of spectral lines have more recently been recognized among these same systems (Wi 68a, Wi 68b). The most extensively studied trends involve the variation of oscillator strength (f-value) with nuclear charge along isoelectronic sequences (Wi 68a, Sm 71a). The beam-foil technique has proved to be ideally suited for experimental studies of these trends. Spectra can be produced for virtually all ionization stages of any element that can be extracted from an ion accelerator, and precise measurement can be made of atomic mean lives, these yielding either the oscillator strengths directly or at least their upper bounds. The expressions relating line strength, oscillator strength, transition probability, and lifetime are summarized by Wiese et al (Wi 66, Wi 69).

In the second and third periods of the periodic table most transitions among low-lying terms appear in the vacuum ultraviolet region of the spectrum, particularly for ionized systems. The systematic studies of lifetimes for many second- and third-period elements that were performed during this project have provided new f-value information for a large number of transitions below 2000 Å along 16 different isoelectronic sequences. Also, our measurements in krypton have extended this survey to the fourth period where little previous work has been done. Trends for selected transitions along various sequences are presented below to illustrate the extent and consistency of our beam-foil results and to suggest or support the discussion of some physically interesting characteristics of oscillator strengths and their relation to atomic structure.

The f-value dependence upon nuclear charge (actually Z^{-1}) is normally used to study trends along isoelectronic sequences. This choice arises from the appearance of Z^{-1} as the natural independent variable in a series expansion formulation of f based upon conventional perturbation theory (see Wiese and Weiss (Wi 68a):

$$f = f_o + f_1 Z^{-1} + f_2 Z^{-2} + \ldots \quad .$$

Thus one expects a plot of f versus Z^{-1} to be approximately linear for low values of Z^{-1} (higher sequence members), and for higher order terms to become increasingly important toward the neutral end of the sequence. In practice, the quadratic approximation is found to be sufficient, so that the "basic" f-value dependence on Z^{-1} resembles a simple parabola. As we shall see, significant departures from this basic dependence are frequently found. These may be attributed either to cancellation in the transition integral or, more commonly, to configuration interaction effects for particular sequence members. We note that the hydrogenic limit of f (i.e. as $Z^{-1} \rightarrow 0$) is simply f_o. In the hydrogenic limit all configurations become hydrogen-like so that all configurations involving the same outer n-shell become degenerate. Thus the energy of a transition between two such configurations becomes zero. Since f-value is directly proportional to transition energy, the hydrogenic limit of f for any $\Delta n = 0$ transition is zero, and this provides a convenient interpolation point from lower sequence members for this class of transitions. When $\Delta n \neq 0$, $f_o \neq 0$ in general and it must be explicitly calculated.

Various theoretical results will be referred to for comparison with experiment and for explanation of the physical significance of particular trends. These results represent either single-configuration Hartree-

Fock (HF) calculations or one of several types of configuration-interaction (CI) treatments. The HF results cannot account for interaction between configurations, and are useful primarily as reference values to which other calculations and experiment can be referred in assessing the effects of such interactions. The CI calculations vary in sophistication, including as few as two and as many as 100 different contributing configurations. In particular, the Z-expansion technique (Co 64, Cr 65) incorporates only those configurations that lie within the same electronic shell (the same "complex") and is most reliable for highly-ionized atoms. The superposition-of-configurations (SOC) approach of Weiss (We 67a) normally includes several dozen configurations and yields fairly reliable results in most cases. The non-closed-shell-many-electron-theory (NCMET) of Sinanoğlu and coworkers (We 69b, Ni 73b) considers more detailed electron correlation in the multi-configuration calculations and provides the most reliable theoretical results for several transitions. Limited-CI calculations have been performed by Nussbaumer (Nu 69) and by Froese Fischer (Fi 68).

The oscillator-strength results from this project in Figs. 30-69 are listed with their respective mean-life values in Appendix II.

6.1 Uniform Trends Along Second-Period Sequences

Examples of very uniform f-value trends can probably be found for every isoelectronic sequence. Normally, however, they are not common for transitions between low-lying terms in atomic systems with 4 or more electrons, due to the existence of significant interaction effects among various electron configurations, especially those involving the upper terms of transitions. A few uniform trends in the Li I, Be I, and B I sequences have been discussed by Wiese and Weiss (Wi 68a) and examples from these and other sequences may be found in the compilation of Smith and Wiese (Sm 71a). Six such trends from the B I, N I, F I, and Be I sequences are discussed below.

B I sequence: $2s2p^2\ {}^4P-2p^3\ {}^4S^o$, $2s^22p\ {}^2P^o-2s2p^2\ {}^2P$

The oscillator strength trends for both these transitions are expected to be uniform over the entire B I sequence since there is no significant configuration interaction for either of the upper terms involved. (None of the nearby configurations contains a ${}^4S^o$ or ${}^2P$ perturbing term.) There are, however, nearby terms that can interact with the lower terms of each transition (see insets in Figs. 30 and 31). The effect of these interactions is a fairly uniform reduction of f

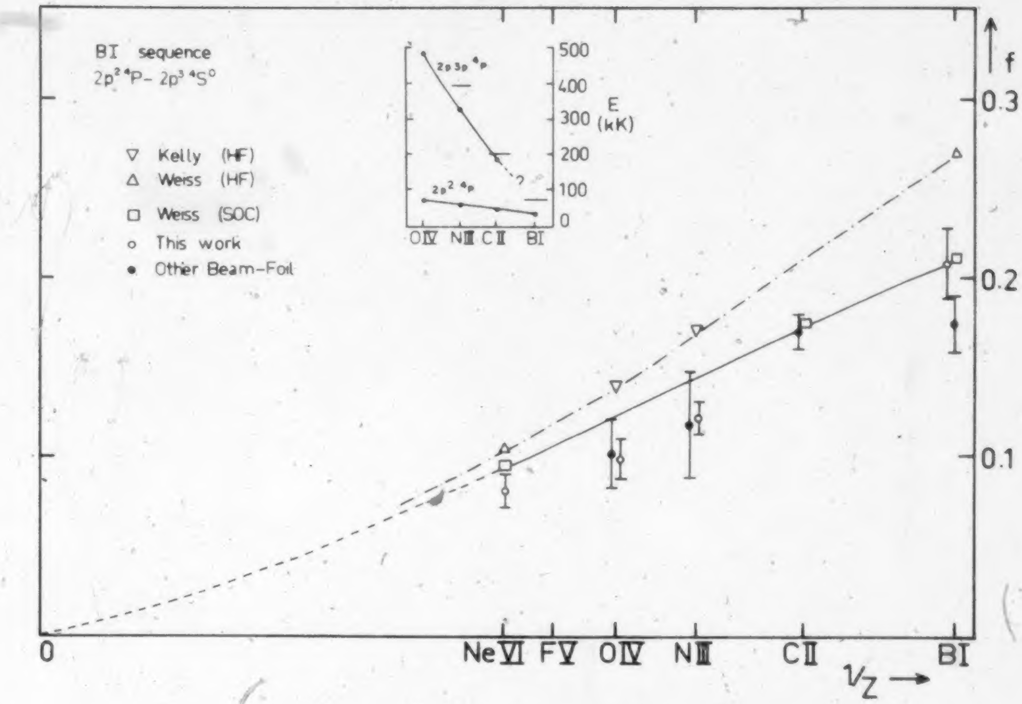

Fig.30. Oscillator strength (f) vs. 1/Z for the $2s2p^2\ ^4P-2p^3\ ^4S^o$ transition in the B I isoelectronic sequence. (The insets in this and subsequent figures show energies above the ground state (in kK=10^3 cm^{-1}) for relevant terms. The horizontal bars represent first ionization limits.) Sources of results: theory: Kelly (Ke64), Weiss (We69a); beam-foil: B I (Ma70b), C II (He69), N III (Du72), O IV (Ma71a).

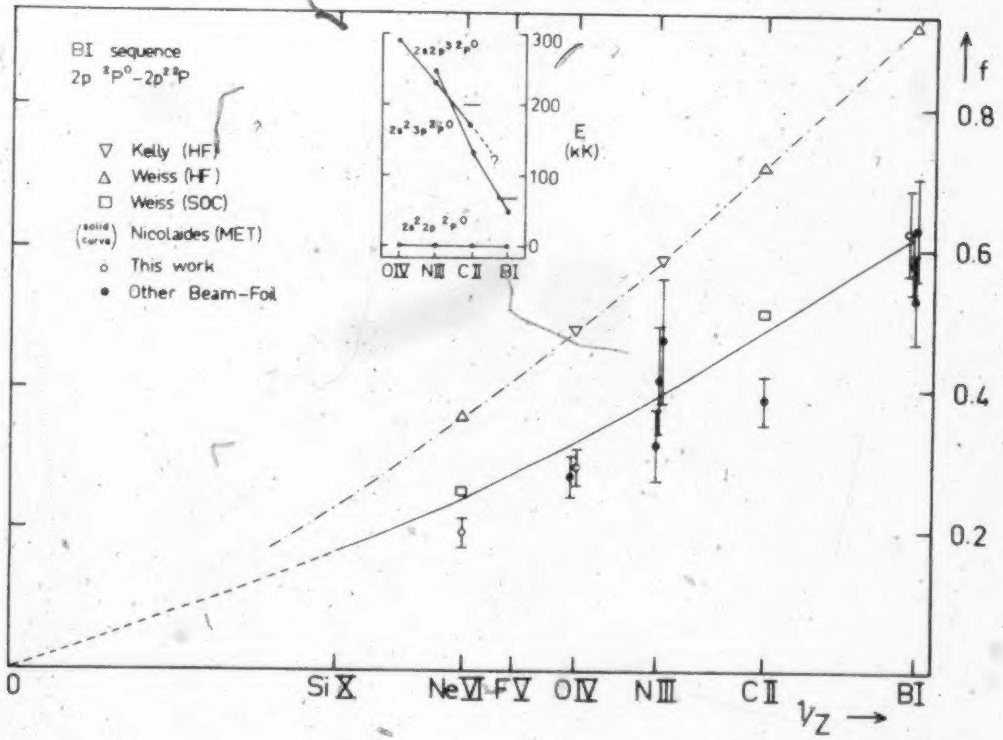

Fig.31. f vs. 1/Z, $2s^22p\ ^2P^o-2s2p^2\ ^2P$ transition, B I sequence. Sources: theory: Kelly(Ke64), Weiss (We69a), Nicolaides (Ni73a); beam-foil: B I (Ma70b,Br71), C II (He69), N III (Du72,He67,Bu72a), O IV (Ma71a).

along the entire sequence, as indicated by a comparison of single-configuration Hartree-Fock results with the configuration interaction treatments of Weiss (We 69a) and Nicolaides (Ni 73a). Experimental measurements (all of which are beam-foil lifetimes) indicate that a further slight decrease in the f-value trend from these CI values is needed for most sequence members.

$2p^2\ ^4P-2p^3\ ^4S^o$

This transition, connecting the two lowest quartet terms in boron-like systems, has only recently been studied experimentally above C II, and 4 of the 8 results from B I to Ne VI represent work done during this project. A systematic discrepancy of 10-20% from the SOC theory is indicated for N, O, and Ne, whereas our measurement for BI agrees with this theory. Earlier measurements for BI and C II deviate only slightly from the trend of our results. The improvement of the SOC calculations over the single-configuration approach is evident, although the lifetime measurements suggest that configuration interaction is even stronger than Weiss has proposed. Weiss (We 69a) has pointed out that Z-expansion calculations by Cohen and Dalgarno (Co 64) agree with the higher, single-configuration trend. This is to be expected here, since the Z-expansion method includes configuration interaction only within the same complex, and there are no other ^4P terms in the $n = 2$ shell for boron-like systems. The interaction probably involves the 2pnp ^4P series ($n = 3,4,5,\ldots$).

$2p\ ^2P^o - 2p^2\ ^2P$

The trend for this ground state transition is similar to the one just discussed. Weiss' SOC calculations for C II and Ne VI confirm the results of Z-expansion calculations in predicting f to be uniformly 30% below single-configuration values. This agreement indicates that the dominant mixing configuration here is $2s2p^3$, despite the appearance of a lower-energy $^2P^o$ term ($2s^23p$) in B I and C II, since the Z-expansion method only accounts for contributions within the same complex. More recent calculations by Westhaus and Sinanoğlu (We 69b) and Nicolaides (Ni 73a), employing additional electron correlation effects, uniformly reduce the trend by a further 5%. The solid curve in Figure 31 represents the more extensive results of Nicolaides.

As before, however, beam-foil lifetime measurements tend to indicate a further slight reduction in f is needed, at least for the ionized members. Our results for O IV and Ne VI are particularly consistent in displaying this discrepancy, while our B I value agrees with theory, as for the previous transition.

The scatter of results at N III deserves comment. The highest value is a result reported by Dumont (Du 72), who used graphical curve-fitting of analog decay curves. This can be a source of serious systematic error and, although Dumont's results are generally in good agreement with ours, the reliability of any one result is somewhat uncertain. The middle result represents a very early beam-foil measurement by Heroux (He 67). It is seen to be inconsistent with the trend of his own subsequent measurement of the C II value (He 69). The lowest value was reported by Buchet et al (Bu 72a), whose recent extensive investigation of nitrogen lifetimes has yielded generally reliable results. A simple weighted mean value of the three results yields $\bar{f} = 0.36$ (using the inverse square of the quoted uncertainty as the statistical weight). This value agrees well with the trend suggested by the other members of this sequence.

N I sequence: $2s^22p^3\ ^2P^o - 2s2p^4\ ^2S$

In the N I sequence, transitions from the ^2S term of the $2s2p^4$ configuration reflect the effects of configuration interaction much more uniformly than do those involving the remaining ^2P, ^2D and ^4P terms. The "anomalous" f-value trends for these other transitions may be attributed to the near degeneracy of these terms with terms from interacting configurations, as will be discussed later. However, no other low-lying ^2S levels exist in nitrogen-like systems, except possibly in N I, where the $2s2p^4$ term is not known and may be an autoionizing state above the $2p^2(^3P)n\ell$ limit. The trend for the $2s^22p^3\ ^2P^o$-$2s2p^4\ ^2S$ transition (Fig.32) is similar to that discussed earlier for the quartet transition in the B I sequence (Fig.30). Limited-configuration-interaction calculations (involving a single complex) yield uniformly high f-values, indicating that significant mixing occurs with configurations outside the $(n = 2)$ complex. The NCMET calculations of Nicolaides (Ni 73a) are fairly well verified by our lifetime measurements in O II and Ne IV.

F I sequence: $2p^5\ ^2P^o$-$2p^43s\ ^2P$

Complications due to configuration mixing would usually be expected for this transition since, as will be seen later, interaction normally occurs between the $2s^22p^n3s$ and $2s2p^{n+2}$ configurations. However, in fluorine-like systems, $2s2p^{n+2}$ is $2s2p^6$, which generates only a ^2S term. So interaction with $3s\ ^2P$ can arise only from higher configurations, such as $3d\ ^2P$, and the influence of these on $3s\ ^2P$ is normally small. Gruzdev (Gr 71) has employed the (single-configuration) Coulomb approximation with intermediate coupling to calculate

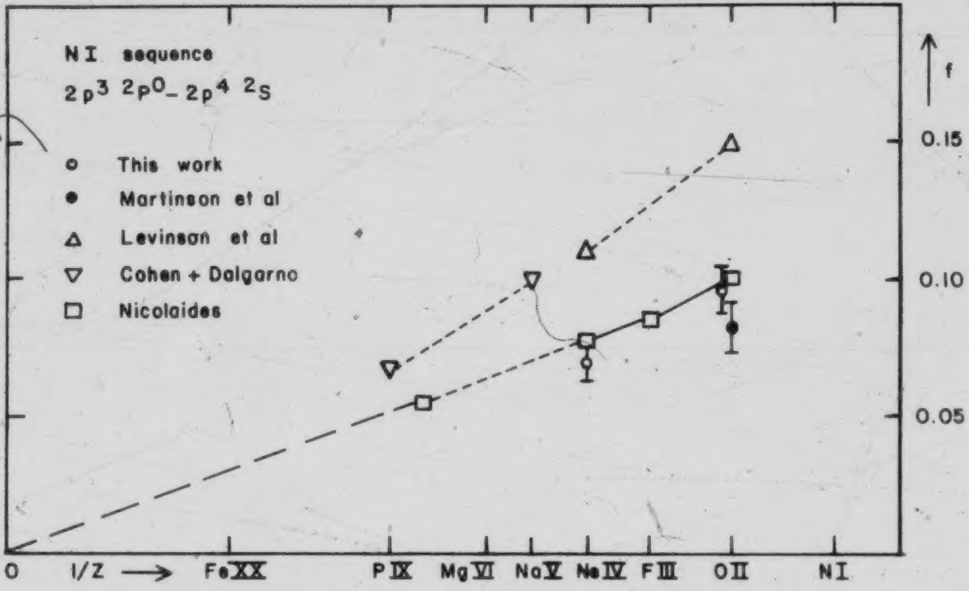

Fig.32. f vs. 1/Z, $2s^22p^3\ ^2P^o$-$2s2p^4\ ^2S$ transition, N I sequence. Sources: theory: Levinson et al (Le 56), Cohen & Dalgarno (Co 64), Nicolaides (Ni 73a); beam-foil (Ma 71a).

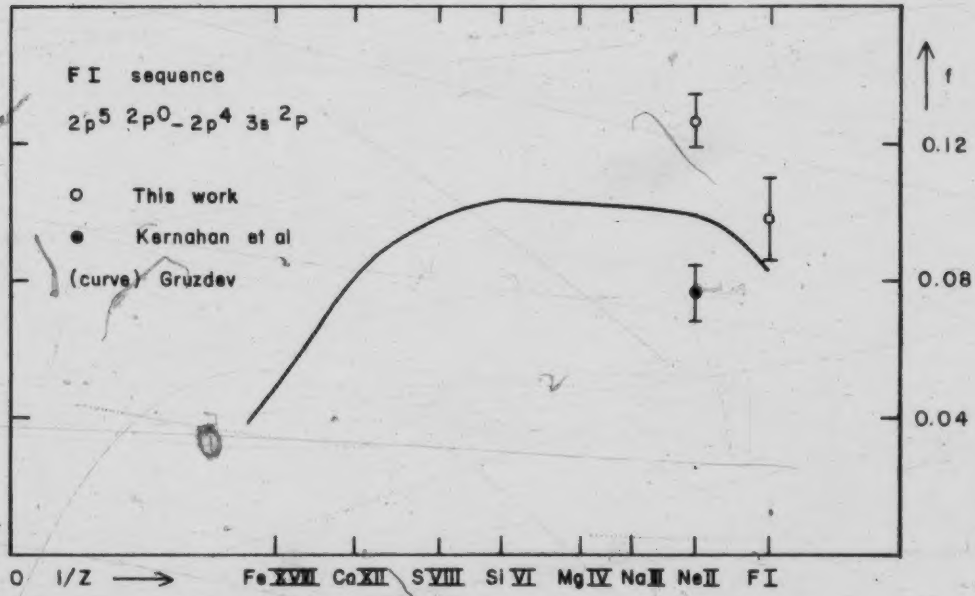

Fig.33. f vs. 1/Z, $2p^5\ ^2P^o$-$2p^43s\ ^2P$ transition, F I sequence. Sources: theory (Gr 71); beam-foil (Ke 72).

oscillator strengths for this transition from F I to Cu XXI and has shown that the trend is fairly smooth throughout the sequence (Fig.33). Our mean-life measurements for F I and Ne II represent the only reliable experimental results for this transition (see Ch.V for a discussion of the neon results of Kernahan et al). We have verified the initial trend of Gruzdev's f-values, but have shown them to be 10-20% low.

The initial depression of the trend at F I is probably due to an anomaly in the energy of the 3s ^2P term in this atom, rather than to a reduced transition integral (multiplet strength). This would be reflected in the oscillator strength through its dependence upon transition wavelength (λ) in addition to multiplet strength (S), i.e.

$$f \sim S/\lambda \sim S\Delta E \quad .$$

An anomalously low upper term would produce a low f. Such slight depressions in f for neutral sequence members are commonly observed in the Na I sequence, for example (see Smith and Wiese (Sm 71a)-pages 104 and 175-185, as well as the first two third-period examples discussed below). We note that Gruzdev's results explicitly show the deviation from LS coupling to be negligibly small for early sequence members (< 1%), and hence not responsible for the dip. In addition, his single-configuration treatment implies that configuration interaction is not responsible either.

It is particularly interesting to follow his f-value trend to high sequence members where a pronounced fall-off is predicted. Above Si VI Gruzdev found that departure from LS coupling in the $2p^4 3s$ configuration steadily increased, with mixing being strongest between the $^2P_{3/2}$ and $^4P_{3/2}$ levels. The LS coupling label for the $^2P_{3/2}$ level becomes meaningless by V XV where the contributions from $^2P_{3/2}$ and $^4P_{3/2}$ are equal. In addition to the reduction in f shown here, Gruzdev reported a large increase in f for the normally spin-forbidden transition $2p^5\ ^2P - 2p^4 3s\ ^4P$, arising from the relaxation of LS coupling selection rules with the increase of intermediate coupling. These calculations emphasize how important the deviations from LS coupling can be in affecting the oscillator strengths of certain transitions in highly-ionized atoms. Unfortunately, there are no experimental f-value results available for this transition above Ne II. (Note that the hydrogenic limit of f for this $\Delta n \neq 0$ transition is not necessarily zero.)

Be I sequence: $2s^2\ ^1S-2s2p\ ^1P^o$

This transition is noteworthy as having probably the most extensively studied theoretical oscillator strength trend among atomic systems containing more than 3 electrons. The theoretical and experimental situation up to early 1972 was fully summarized at the last international beam-foil conference (Sm 73, Vi 73). During the past two years a further 5 beam-foil lifetimes have been measured (4 during this project) and at least one additional theoretical investigation has been reported. In this recent calculation, Sims and Whitten (Si 73) claim a high degree of precision, and their results appear to provide a stringent test of the reliability of lifetime measurements.

The f-value plot is shown in Fig.34, where the results of Sims and Whitten for Be I, C III, and O V have been connected with a solid line and the trend extended to the hydrogenic limit (this being $f = 0$ for a $\Delta n = 0$ transition). They obtained their results by calculating upper and lower state wave functions, including interelectron coordinates explicitly, and using these to calculate dipole-length f-values, along with upper and lower bounds. Their results indicate that the neglect of core ($1s^2$) and intershell electron correlations in previous configuration interaction calculations can yield f-values that are incorrect by

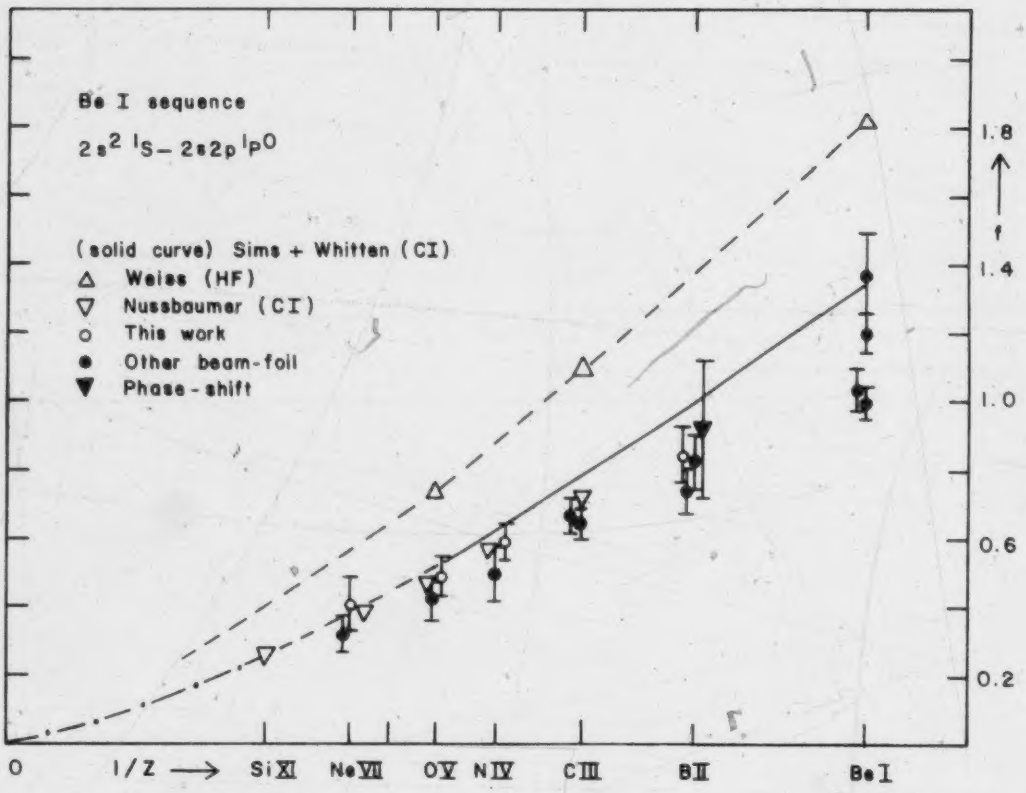

Fig.34. f vs. 1/Z, $2s^2\ {}^1S$-$2s2p\ {}^1P^o$ transition, Be I sequence. Sources: theory: (Si 73, Wi 66, Nu 72); phase-shift (La 66); beam-foil: Be I (Br 71, Be 69, An 69b, Ho 72), B II (Br 71, Ma 70b), C III (He 69, Po 71), N IV (Bu 72a), O V (Ma 71a), Ne VII (Be 72b).

as much as 5-10% in Be I and by lesser amounts in higher ions. Sims and Whitten quote "rigorous" upper and lower bounds of ±7-10% and "probable" uncertainties of ≤±2% for the f-values in this sequence, with the exception of Be I where ±1% is quoted. However, all configuration interaction treatments yield the same results (within ≤2%) for all except the Be I member, for which 5 theoretical results are distributed within ±7% of the Sims and Whitten value (see Victor and Laughlin (Vi 73)).

Since only one of the four experimental results for Be I agrees well with any of the theoretical values, the situation in Be I remains unsatisfactory. For ionized sequence members, the experimental trend of earlier beam-foil measurements indicates a slight negative discrepancy from theory for B II to Ne VII. Our results for B, N, O, and Ne show systematically better agreement with theory than do these previous results. It appears now that the discrepancy from theory is real only for B II, and perhaps C III, among ionized members. (In view of the ±20% uncertainty quoted for the phase-shift result in B II, the apparent indication of closer agreement with theory by that measurement is not really significant.)

This type of disagreement has, in the past, been routinely attributed to either insufficient correction for cascading in the beam-foil work, or the failure to completely account for configuration interaction in the theoretical calculations. Sims and Whitten claim that their theoretical uncertainties are too small for the error to lie with the theory. At the same time, it is hard to accept that the five different beam-foil laboratories represented by the boron and carbon results could all have failed to correct their decays for cascading in such a consistent manner. In fact, the cascade component here is relatively weak in all ions and should have little effect on the decays. Our results show it to become progressively weaker from neon to boron, where it represents about 5% of the initial decay intensity. This means that its possible effect on the primary decay component should be least in B II. Furthermore, our beam-foil results have displayed consistency and reliability for numerous transitions along many isoelectronic sequences, including agreement with theory for two other boron transitions. All the experimental evidence thus suggests that the discrepancy from theory indicated by our boron result is real.

6.2 Uniform Trends Along Third-Period Sequences

In the third period (sodium to argon) extensive theoretical f-value calculations have been performed mainly for the Na I and Mg I sequences, since these are essentially one- and two-electron systems, respectively, outside a neon-like core. The next five transitions to be discussed were presented by Smith and Wiese (Sm 71a) in their 1970 compilation as predominantly theoretical sequences, only a few experimental results in the neutral and singly-ionized members being then available. Since 1970 more than 60 experimental f-values have been reported for these transitions so that each has now been studied up to its argon member. Nearly all of these results are derived from beam-foil lifetime experiments, about one-third being produced during this project (specifically, results for Si, P, S, and Ar for all five transitions). Since each transition represents the only decay branch from the upper term involved, the mean life yields the multiplet f-value directly.

Early beam-foil experiments mainly involved the first 3 or 4 sequence members and, with a few exceptions, roughly verified theoretical predictions. However, our first results for argon (Li 72a) and those of Bashkin and Martinson for chlorine (Ba 71) indicated slight systematic deviations below theory at higher Z.

Further evidence was needed to determine the magnitudes of these deviations along each sequence. The scatter among earlier results and the existence of some very large quoted uncertainties were unsatisfactory for this purpose; hence our systematic investigation of the four multiply-ionized sequence members Si, P, S, and Ar.

Considerably less experimental and theoretical work has been done for the other 3rd-period sequences (Al I, Si I, etc.). We shall see later that configuration interaction effects are even more significant than in the second period for transitions involving low-lying levels in these sequences, simply because there are many more possible configurations within the n = 3 shell. For this reason, uniform f-value trends are less common. One example in this category will be discussed from the Al I sequence.

Na I sequence: 3s ^2S-3p $^2P^o$

The f-value trend for the resonance multiplet in sodium-like systems has been reasonably well predicted by various theoretical calculations (see Fig. 35), although our measurements now clearly demonstrate the existence of a systematic 10-20% negative discrepancy from theory, at least above Al III. We agree very well with the trend indicated by the Cl VII value by Bashkin and Martinson (Ba 71) and with unpublished results of

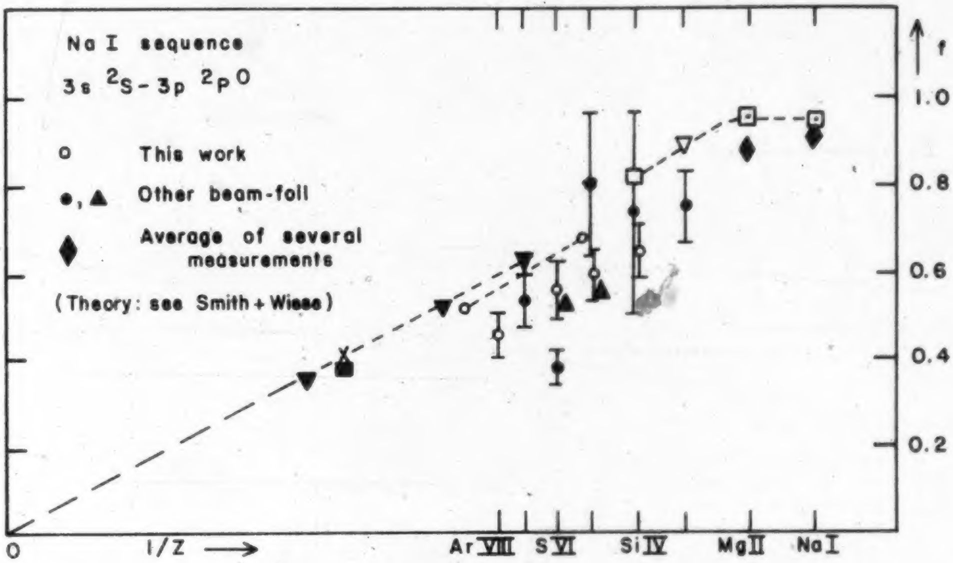

Fig.35. f vs. 1/Z, 3s ^{2}S-3p ^{2}P^o transition, Na I sequence. Sources: theory (Sm 71a); experiment: Na I (Be 70a, An 70b, An 72), Mg II (Be 70a, Sm 71b, An 70a, Lu 73), Al III (Be 70a), Si IV (Be 71a), P V (Cu 71b, So 73), S VI (Be 70b, So 73), Cl VII (Ba 71).

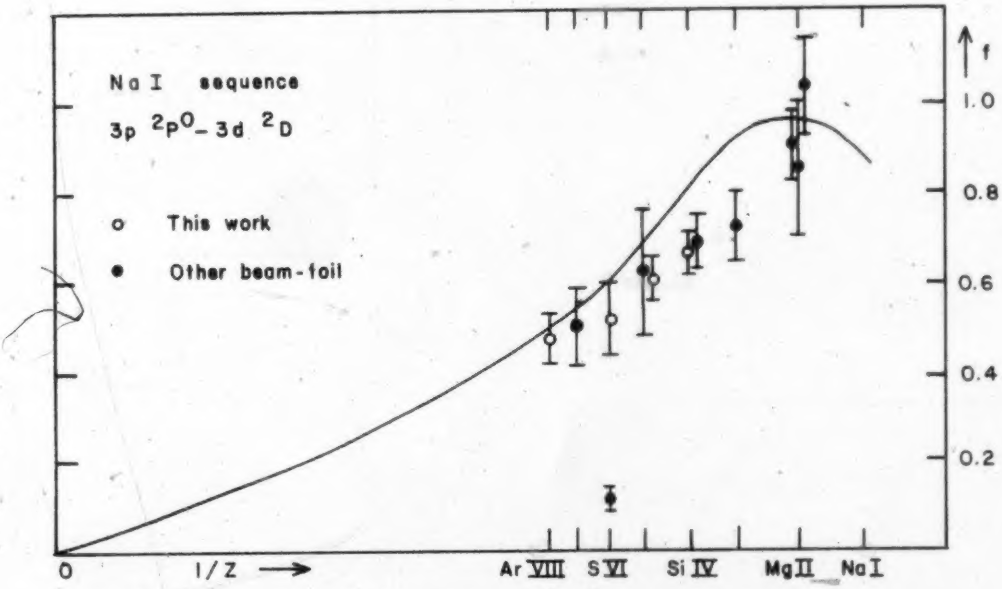

Fig.36. f vs. 1/Z, 3p^{2}P^o-3d ^{2}D transition, Na I sequence. Sources: curve (Sm 71a); beam-foil: Mg II (Be 70a, An 70a, Lu 73), Al III (Be 70a), Si IV (Be 71a), P V (Cu 71b), S VI (Be 70b), Cl VII (Ba 71).

Anderson and Sørensen for P V and S VI (So 73). The discrepancy from theory is significant since it is nearly equal to the maximum uncertainty attributed by Wiese et al (Wi 69) to these calculated values. The individual theoretical values plotted by Smith and Wiese are reproduced here, since their "best-fit" curve does not indicate the spread among these values. (Their curves will be retained for the following four transitions, where the scatter among various theoretical values does not exceed a few percent and the theoretical trends are smooth.)

Since $\Delta n = 0$ for this transition, the hydrogenic limit of the f-value (as $Z \to \infty$) is zero, which means that the lifetime results imply a shallower slope in the trend at the very high Z. The indication that such a trend may be expected in the Na I sequence was reported by Kunze and Datla (Ku 71) for the 3d-4p transition. Their experimental and theoretical analysis indicated that the linear extrapolation of Wiese et al (Wi 69) and Smith and Wiese (Sm 71a) between the existing theoretical value at Si IV and the hydrogenic limit is not correct, but that a smooth depression of f is observed for all sequence members above Si IV. Similar results have recently been presented by Laughlin et al (La 73b) and discussed by Dalgarno (Da 73) for the 3d-4p and 4p-4d transitions, demonstrating that the trend is not restricted to $\Delta n \neq 0$ transitions. Here the Z-expansion method was employed to calculate directly the slopes of the f vs. 1/Z curves at high Z. These results for 3d-4p are nearly identical to those of Kunze and Datla above the sixth member of the sequence (S VI), where the Z-expansion method is normally becoming reliable for third period sequences (We 67b). Dalgarno (private communication) feels that this trend may well apply to other transitions in the third period.

Our results for the 3s-3p transition (as mentioned above) and for the three transitions to be discussed in the Mg I sequence also confirm such a qualitative effect for transitions involving lower-lying terms. In these cases, however, theoretical results exist for all the members up to calcium, and also for iron.

3p $^2P^o$-3d ^2D

A trend somewhat similar to the previous case is exhibited for this transition (Fig.36), although the beam-foil results appear to converge more rapidly with the high-Z trend indicated by Z-expansion theory than they did for the resonance multiplet. The consistency of all the experimental results here is striking, if the one very low value at S VI is ignored, for reasons discussed previously (see Ch. V). A recent measurement for the Mg II transition by Lundin et al (Lu 73) shows good agreement with the results of Andersen et al (An 70a) and Berry et al (Be 70a), the latter author having extracted the mean life from the decay of an unresolved blend. The experimental f-value trend is firmly established for the entire sequence, except possibly at Na I where the transition occurs in the infra-red region (8191 Å) and has not been studied experimentally.

Mg I sequence: $3s^2\ {}^1S-3s3p\ {}^1P^o$

The resonance transition in the Mg I sequence has been studied extensively both theoretically and experimentally, resulting in apparent consistency for Mg, Al, and Si, but with the familiar discrepancy from theory appearing at higher Z for the four uniformly low experimental results (Fig.37). In this 2-electron system, configuration interaction effects are often very important, and extensive calculations incorporating such effects have been performed by Weiss (We 67b) and by Zare (Za 67). The consistency between these calculations, and their smooth merging with the more limited-CI values from the Z-expansion technique, has prompted Wiese et al (Wi 69) to attach uncertainty limits of ±10% to the theoretical f-values over the entire sequence. Weiss suggested an uncertainty of ±25% for his own calculations, which involve the Mg,

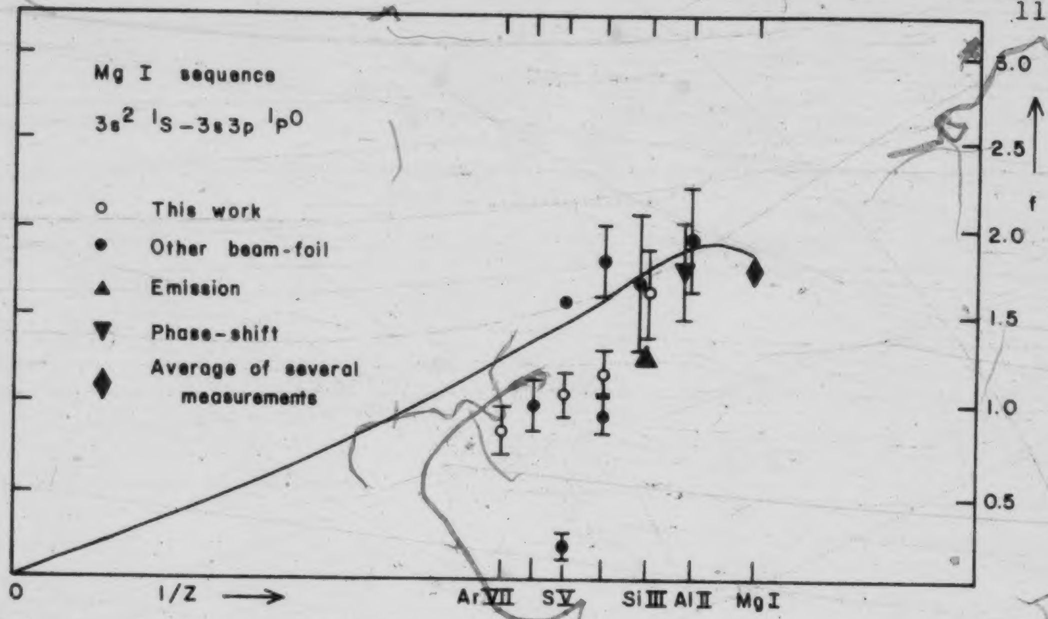

Fig.37. f vs. 1/Z, $3s^2\ ^1S$-$3s3p\ ^1P^o$ transition, Mg Isequence. Sources: curve (Sm 71a); experiment: Mg I (Be 70a, Sm 71b, An 70a, Lu 73), Al II (Be 70a, Sm 71b), Si III (Be 71a, Ho69), P IV (Cu 71b, So73), S V (Be70b, So73), Cl VI (Ba 71).

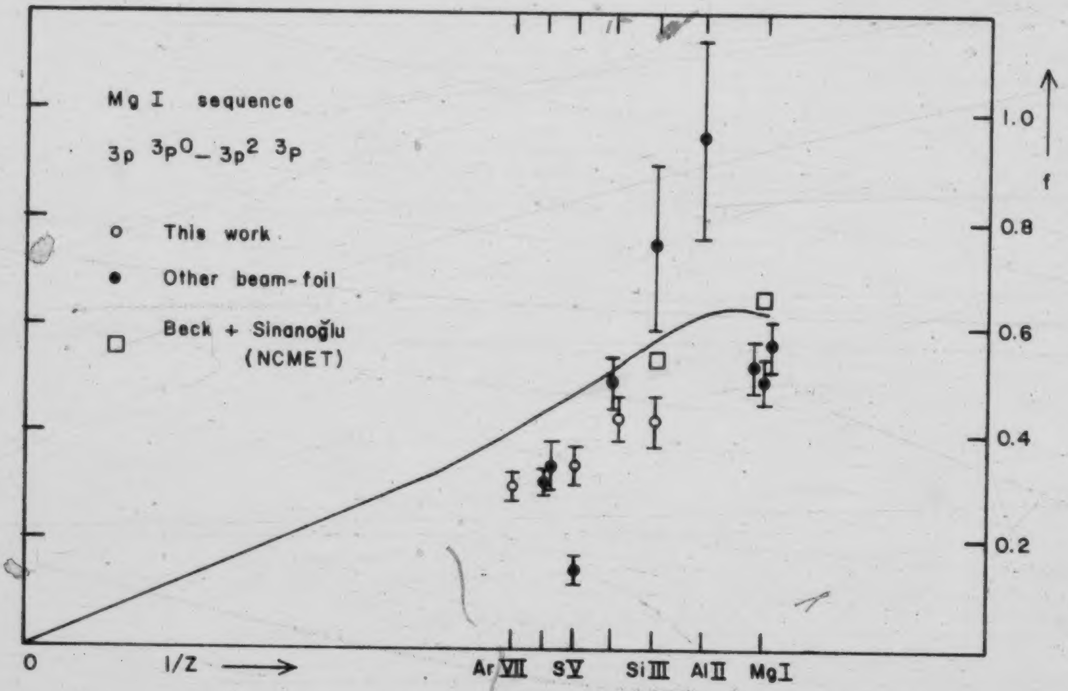

Fig.38. f vs. 1/Z, $3s3p\ ^3P^o$-$3p^2\ ^3P$ transition, Mg I sequence. Sources: curve (Sm71a), theory (Be72a); beam-foil: Mg I (Be70a, An70a, Lu73), Al II (Be70a), Si III (Be71a), P IV (Cu71b), S V (Be70b), Cl VI (Ba71, Ma71b).

Al, and Si members. In either case, the discrepancy of 20-30% indicated by the smooth trend of our results for higher sequence members is significant. The departure from theory appears to begin above Si III. The stabilized arc emission f-value of Hofmann for Si III is probably a little low, in accordance with similar discrepancies shown by his silicon results for transitions to be discussed later. Considerable scatter is evident among earlier beam-foil results for S V and P IV. The low sulfur values for certain transitions measured by Berry et al have been discussed earlier (see Ch. V). The high sulfur value was reported by Sørensen (So 73) without an estimation of uncertainty. The slightly low value for phosphorus is from unpublished results of Mølhove and Sørensen (So 73). The high value in P IV is disturbing since Curtis et al (Cu 71b) performed a detailed study of phosphorus decays using an analysis technique designed to reduce the effects of cascade contributions. We may note that, for the five 3rd-period transitions being discussed here, in three cases the Curtis et al phosphorus f-value is significantly higher than our value, while in one case it is much lower (see Figs.35-39).

$3s3p\ ^3P^o - 3p^2\ ^3P$

This transition has been somewhat less thoroughly studied than the resonance transition. At the time when we reported our early argon result (Li 72a), the sequence trend was characterized by severe disagreement between Weiss' SOC calculations and beam-foil measurements in Al II and Si III (the high f-values in Fig.38). Since then we have verified that the early Si III value is too high (Ir 73a). Our results, along with several Mg I measurements, now show the trend to be systematically some 15-20% below theory (SOC and Z-expansion calculations). In contrast to the three previous examples, the discrepancy here extends uniformly to the neutral (high Z^{-1}) end of the sequence. Recent calculations by Beck and Sinanoǧlu (Be 72a), which are in general more reliable than SOC methods, show little difference from the earlier theory for Mg I and Si III, since L-shell (n = 2) electron correlation effects unique here to the Sinanoǧlu theory are very small for this transition.

$3s3p\ ^3P^o$-$3s3d\ ^3D$

The experimental trend for this transition along the Mg I sequence was unclear until our recent results above Al II and reliable results for Mg I became available. Once again the trend appears to fall uniformly below the consistent predictions of SOC and Z-expansion calculations, although the discrepancy here is much less than that for the previous transition.

Owing to the very short mean life of the 3s3d ^{3}D term for Ar VII (0.13 ns), our early measurement of this decay in second order (Li 72a) failed to detect the primary component. We remeasured this decay in first order during a recent extensive study of argon and obtained the f-value shown in Fig. 39, with a cascade component equal to our earlier result. The consistency of the new result with our values for Si, P, and S is evident. Bashkin et al (Ba 73b) have very recently reported the 3s3d ^{3}D mean life for Cl VI, yielding an f-value in excellent agreement with our trend and replacing the lower limit of f (0.36) for this transition reported previously by Bashkin and Martinson (Ba 71). The results for P IV by Curtis et al (Cu 71b), for S V by Berry et al (Be 70b), and for Mg I by Berry et al (Be 70a) do not conform to the trend established by the more recent work for this transition.

On the basis of experimental lifetime results for these three transitions in the Mg I sequence it would appear that even extensive configuration interaction calculations yield f-values that are too large, particularly for the higher 3rd-period members of the sequence, where the results of this project indicate good consistency among several neighboring elements. It is significant to note that the most uniform discrepancy from Mg I to Ar VII occurs for the 3s3p ^{3}P^o-

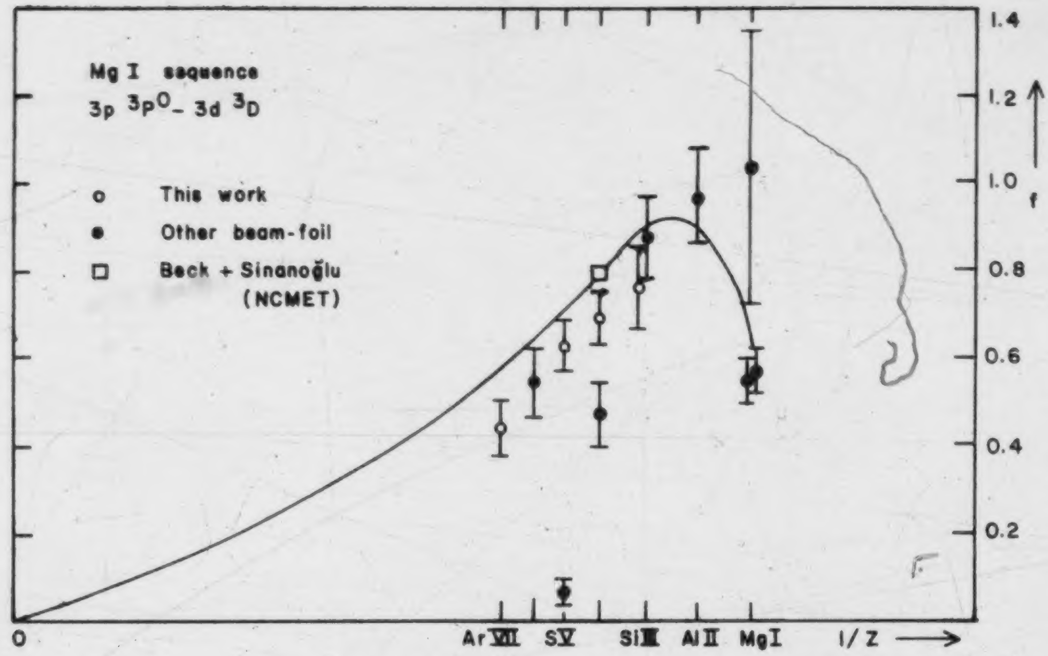

Fig.39. f vs. 1/Z, 3s3p $^3P^o$-3s3d ^3D transition, Mg I sequence. Sources: curve (Sm71a), theory (Be72a); beam-foil: Mg I (Be70a, An70a, Lu73), Al II (Be70a), Si III (Be71a), P IV (Cu71b), S V (Be70b), Cl VI (Ba71).

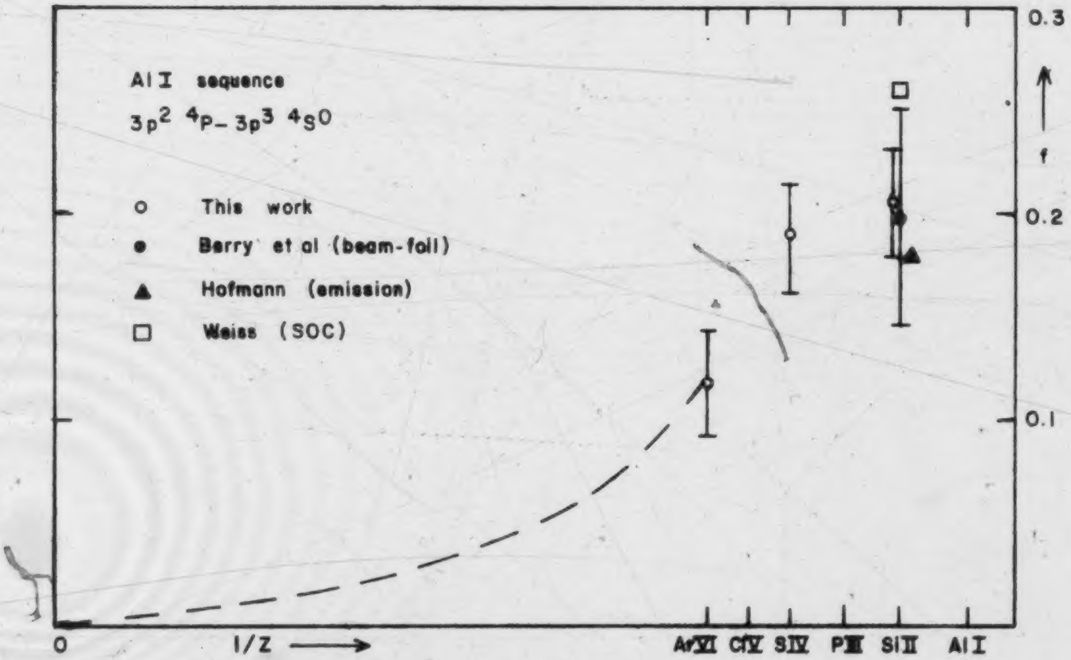

Fig.40. f vs. 1/Z, 3s3p^2 ^4P-3p^3 $^4S^o$ transition, Al I sequence. Sources: theory Weiss (see Wi69); emission (Ho69), beam-foil (Be71a).

$3p^2\ ^3P$ transition, where configuration interaction appears to be least pronounced. Weiss' results (We 67b) show that the inclusion of higher configurations (involving principal quantum number $n > 3$) yields little improvement over the results based upon $n = 3$ interactions alone for this transition. This suggests that the source of the discrepancy is not simply the failure to include a sufficient number of higher interacting configurations in the calculations.

Al I sequence: $3s3p^2\ ^4P-3p^3\ ^4S^o$

This transition is not expected to exhibit strong effects of configuration interaction since no other $^4S^o$ terms are produced by nearby configurations. Our results for Si II, S IV, and Ar VI suggest that the trend does conform to the characteristic fall-off toward $Z^{-1} = 0$ normally found in such cases (see Fig. 40, where the dashed line represents a qualitative extrapolation to the hydrogenic limit). The SOC value calculated by Weiss (Wi 69) for Si II appears to be slightly high. There is a suggestion that the trend is beginning to level out between sulfur and silicon, which would be consistent with a slight drop in f-value near the neutral member, as in the Na I and Mg I sequences discussed previously.

6.3 Anomalous Trends

Recently, reliable lifetime measurements in the vacuum ultraviolet have demonstrated that "anomalous" departures from uniform f-value trends are real and are relatively common among prominent transitions for nearly all isoelectronic sequences. These f-value anomalies are almost always found near the neutral end of the sequence and are usually attributable to configuration interaction resulting from the close spacing of energy levels that characterizes the lowest sequence members. Frequently, the energies of configurations involving different principal quantum numbers extensively overlap for the neutral atom, so that interpolated term "crossings" must occur along the sequence as each configuration converges on its hydrogenic energy at $Z^{-1} = 0$. Ions near these crossings can exhibit dramatic abnormalities in the f-values for transitions involving the crossing terms.

The sequences to be discussed below involve atomic systems with normal outer electron configurations of the type ns^2np^a (a = 0-5) in the second (n = 2) and third (n = 3) periods, specifically the B I - F I and Mg I - S I sequences. In these systems, the dominant interactions are found to occur between $s^2p^{a-1}\ell$ and sp^{a+1} configurations (or $sp^{a-1}\ell$ and p^{a+1}), with ℓ

representing either an s or d electron (a p electron would give opposite parity and hence no interaction with sp^{a+1}). The d electron is a "nonpenetrating" electron, which labels any spectral series of the type (core) + nd (n = 3,4,5,...) as a nonpenetrating series. In particular, the series we shall be referring to are s^2p^{a-1} nd (n = 3,4,5,...) in the second and third periods. Similarly, $s^2p^{a-1}ns$ is called a penetrating series, where $n \geq 3$ in the second period and $n \geq 4$ in the third period. The significance of considering a series of configurations will become more apparent later. Often only the lowest configuration of the series interacts with sp^{a+1}, although in some cases several series members and even other configurations can also contribute. Examples are presented below of a few interactions involving first penetrating series, then nonpenetrating series, followed by instances where both interactions seem to be involved. Finally, examples from five different third-period sequences will illustrate in more detail the particular importance of configuration mixing with nonpenetrating series for elements with Z > 11.

6.3.1 Penetrating Series Interaction

The effects on oscillator strength of interaction involving a penetrating series and a perturbing term are clearly illustrated in Figs. 41 and 42 for the B I sequence. As shown in the inset of Fig. 41, the ^2S terms of the $2s2p^2$ and $2s^23s$ configurations cross between B I and C II, with the $2p^2$ term in B I settling between the 6s and 7s members of the $2s^2ns$ series. The next lowest configuration for which there is a ^2S term is 2s2p3p. This level is well-separated in energy from the two lower ^2S levels and has little effect on them, except possibly in B I. Early superposition of configurations (SOC) calculations by Weiss (We 67a) indicated that strong mixing of the $2s2p^2$ and $2s^23s$ configurations yields two dominant components to the transition integral for the $2s^22p$-$2s^23s$ transition which nearly cancel each other. The resulting f-value in C II was found to be about five times smaller than the prediction of single-configuration calculations, and showed qualitative agreement with the beam-foil result of Heroux (He 67) for N III - the only experimental value then available for this transition in the B I sequence. Since that time Weiss has performed SOC calculations for B I and Ne VI as well, and beam-foil lifetimes have been reported for the first four sequence members, including our results for N III and O IV. Confirmation of the

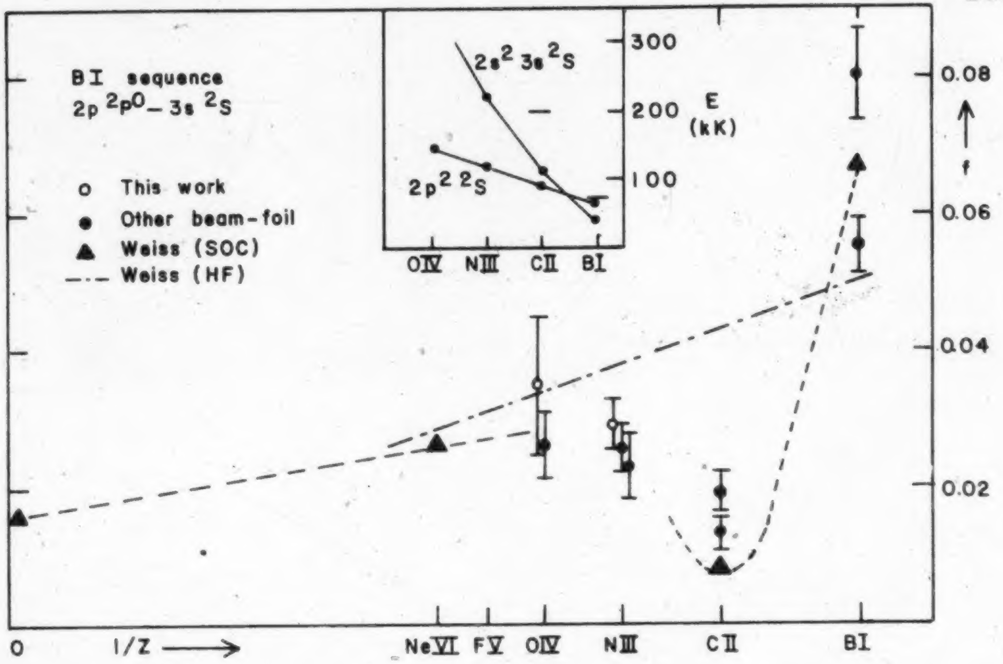

Fig.41. f vs. 1/Z, 2p $^2P^o$-3s ^2S transition, B I sequence. Sources: theory: Weiss (We69a); beam-foil: B I (Be69, An69b), C II (Ma70c, Po73), N III (He67, Bu72a), O IV (Bu72b).

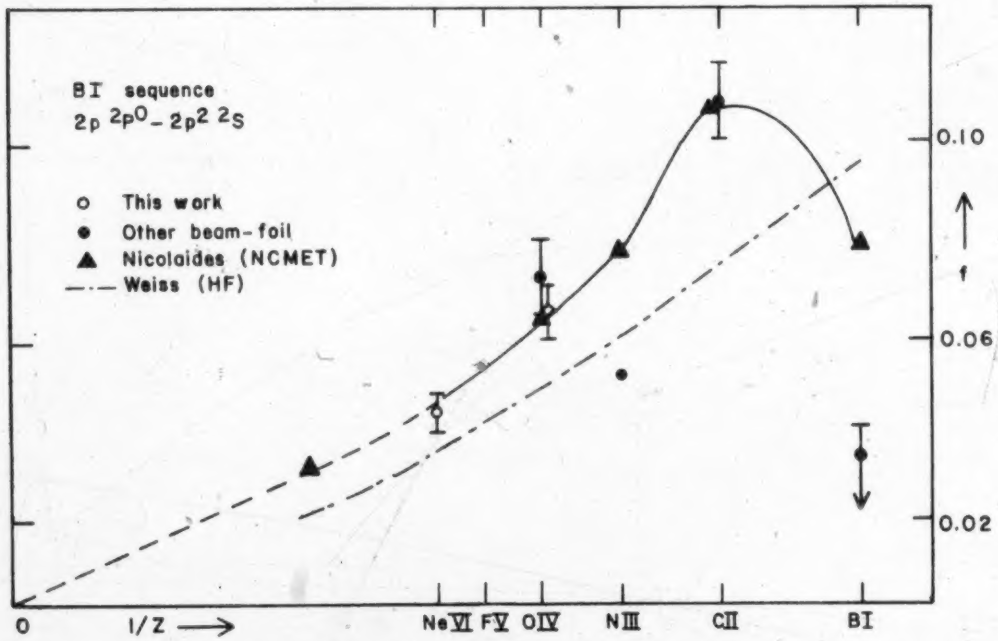

Fig.42. f vs. 1/Z, $2s^22p$ $^2P^o$-$2s2p^2$ ^2S transition, B I sequence. Sources: theory (We69a, Ni73a); beam-foil: B I (Ma70b), C II (He69), N III (Bu72a), O IV (Ma71a).

theoretical trend is evident, although significant disagreement exists among all experimental and theoretical results for B I and C II. We note that our result for the 0 IV transition (279 Å) represents by far the lowest wavelength for which a beam-foil decay measurement has been reported using a normal-incidence spectrograph. The low intensity of this line in our spectra (see Fig. 19) is reflected in the uncertainty of the f-value result.

The trend for the transition from the $2s2p^2\ ^2S$ mixing term (Fig. 42) was also first indicated by Weiss for C II and Ne VI (We 69a) and has been recently confirmed by more extensive calculations of Westhaus and Sinanoğlu (We 69b) and Nicolaides (Ni 73a), the latter author extending the treatment up to Si X and presenting the first theoretical result for B I. Beam-foil results experimentally verify the trend for ionized sequence members, our results appearing for 0 IV and Ne VI, but there is large disagreement at B I. Nicolaides (Ni 73a) points out that for neutral atoms, calculated oscillator strengths of $2s^2 2p^n - 2s2p^{n+1}$ transitions are particularly sensitive to the details of correlation and/or cancellation effects, and therefore are of rather unpredictable accuracy. The beam-foil result of Buchet et al (Bu 72a) for N III (f = .053) is presented only for completeness.

This transition is normally blended with the resonance line of N IV in beam-foil spectra, and our investigation of nitrogen indicates that the N IV transition dominates at the ion energy employed by Buchet et al for this lifetime measurement. Their quoted mean lives for these two transitions are not significantly different. (The N IV transition has been discussed earlier - see Fig. 34).

An analogous configuration-mixing situation occurs for the $2p^2\ ^1S$ and $2s3s\ ^1S$ levels in the Be I sequence (not shown here). The f-value trends for the transitions connecting these with the $2s2p\ ^1P^o$ level are predicted to be very similar to those just discussed (Sm 71a, Sm 73). Experimental agreement is somewhat less good for these transitions, however. In particular, the beam-foil result of Martinson et al (Ma 70b) contradicts the SOC prediction by Weiss of a very low f-value (∿0.001) at B I for the $2s2p\ ^1P^o - 2s3s\ ^1S$ transition (see Smith et al (Sm 73)), the difference being about a factor of 50. If the theory is correct, this transition should be very weak, and the possibility of significant blending in experimental spectra due to other weak transitions increases. This could account for the discrepancy from theory shown by the Martinson et al result. They indicate that their decay curve was corrected for a "cascade", but unfortunately do not quote this lifetime component.

(Note: It has been pointed out by Weiss (We 72) that the assignment of the $2s2p\ ^1P^o-2p^2\ ^1S$ transition in Be I is incorrect, and that the $2p^2\ ^1S$ level is still not known.)

In the third period, the same trends are predicted by the SOC calculations of both Weiss (We 67b) and Zare (Za 67) in the Mg I sequence (see Fig. 43). The ^1S levels of the $3p^2$ and 3s4s configurations cross between Al II and Si III, and corresponding positive and negative anomalies result at Si III for the f-values of their respective transitions to the $3s3p\ ^1P^o$ term. The lone experimental result for the 4s ^1S lifetime in Al II indicates considerable discrepancy from theory, but further measurements are required to verify this result and to ascertain the true magnitudes of these anomalies.

Although the complete description of configuration interaction near these types of level crossing is complicated, a qualitative picture is apparent for the positions and directions of the resultant f-value anomalies for P-S multiplets. (The oscillator strength here will refer to absorption from some given initial state.) As the p^2 term approaches the lowest member of the ns series, oscillator strength is transferred from the series to the approaching term, with the greatest transfer occurring for the ion in which the mixing terms

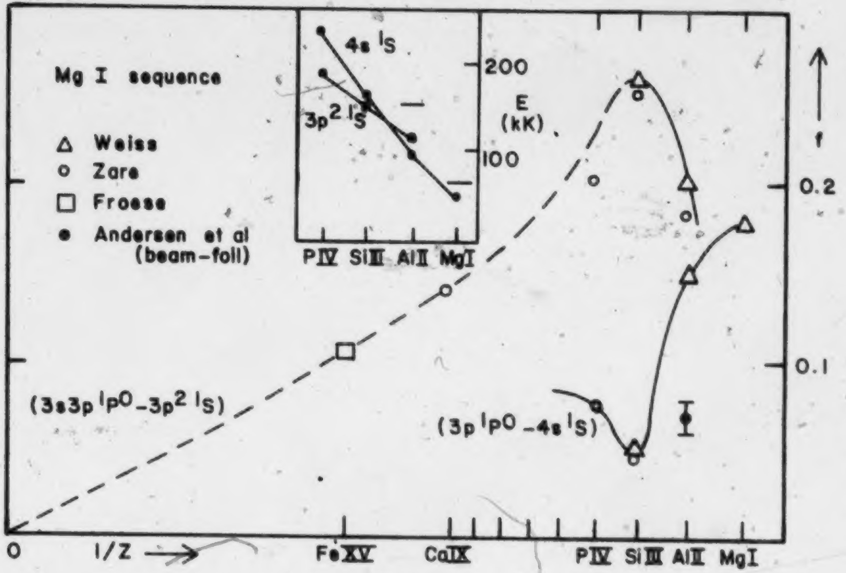

Fig.43. f vs. 1/Z, 3s3p $^1P^o$-3p^2 ^1S and 3s3p $^1P^o$-3s4s ^1S transitions, Mg I sequence. Sources: theory (We67b, Za67, Fr64); beam-foil (An69a).

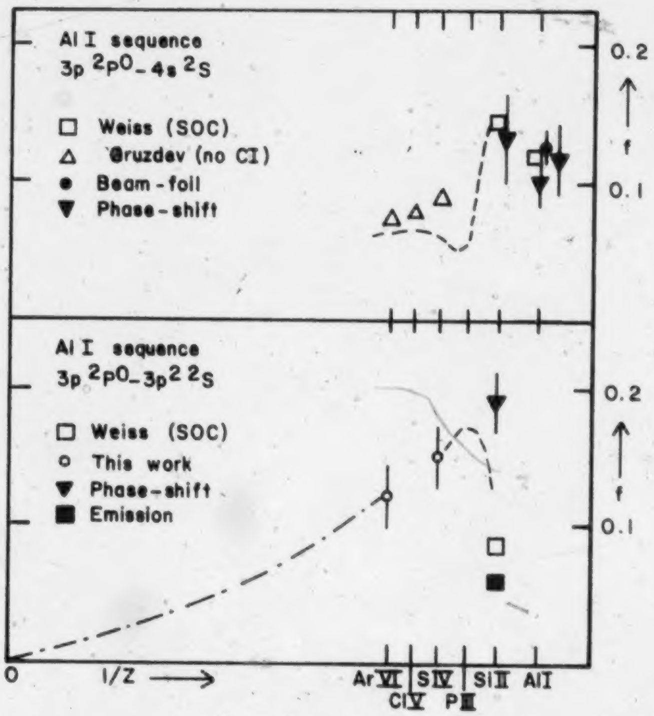

Fig.44. f vs. 1/Z, 3s^{2}3p $^2P^o$-3s^{2}4s ^2S and 3s^{2}3p $^2P^o$-3s3p^2 ^2S transitions, Al I sequence. Sources: theory (Wi69, Gr66); experiment: Al I (An69a, Ma73, De62), Si II (Sa66, Ho69, Cu74).

are closest together before the p^2 term penetrates the series (i.e. before the crossing). After penetration, there is a rapid recovery of oscillator strength by the series member at the expense of the (now higher) p^2 term. The exact f-value of the transition involving p^2 at this point is probably dependent upon how high up the series the p^2 term lies.

On the basis of this picture, we may comment on the f-value trends for transitions involving the analogous interacting terms in the Al I sequence (see Fig.44a), for which there are few theoretical calculations. The ^2S levels of the $3s3p^2$ and $3s^24s$ configurations cross between Si II and P III, so that the f-value anomalies should appear at the P III member. Unfortunately, no results are available for either transition in this critical ion. Severe blending with other phosphorus transitions precluded our obtaining reliable lifetime results. However, a combination of beam-foil and phase-shift measurements confirm the SOC calculations of Weiss for the $3p\ ^2P^o$-$4s\ ^2S$ f-values in Al I and Si II, and we may speculate on the trend for higher ions. The f-value dip should occur at P III and the plotted trend should lie below the single-configuration predictions for at least the next few ions, to conform to the analogous examples previously discussed. (The dashed curve in Fig.44a suggests such a possible trend, although the magnitude of the anomaly is purely speculative.) For the 3p $^2P^o$-3p^2 ^2S transition (Fig.44b), our results for S IV and Ar VI are the only f-values available above Si II and they suggest the qualitative trend expected for multiply-ionized sequence members. In Si II, a recent phase-shift lifetime measurement by Curtis and Smith (Cu 74) disagrees with the emission arc f-value obtained by Hofmann (Ho 69), the latter supporting the SOC calculation of Weiss (Wi 69). The picture that has been developed above tends to favor the two lower results, since the crossing of terms between Si II and P III should result in loss of oscillator strength for the transition involving the 3p^2 ^2S level in Si II. A possible trend below S IV is suggested in Fig.44b. Remeasurement of the silicon f-value using the beam-foil technique may help clarify this discrepancy. Measurements in P III for both transitions of this sequence are clearly needed, although the line blending mentioned earlier will be a problem with low-resolution studies of these relatively weak features.

6.3.2 Nonpenetrating Series Interaction

The redistribution of oscillator strength that results from interaction between a p^a configuration and a nonpenetrating (nd) series is most evident along an isoelectronic sequence for transitions involving the p^a configuration. Perturbations due to p^a tend to be distributed over several series members, whereas the effects of the series are concentrated on p^a. Examples of f-value trends for s^2p^a-sp^{a+1} transitions representing three different sequences are presented below to illustrate this type of interaction.

A distinction should be noted between the principal quantum numbers involved in the p^a and nd configurations that are interacting in the second period and the third period. Since there is no 2d electron, both $2p^a$ (second period) and $3p^a$ (third period) interact initially with the 3d configuration. The mixing in the third period thus arises from within the $n = 3$ electron shell and is generally observed to be more pronounced than the inter-shell mixing in the second period. The third example below suggests the extent of significant interaction effects along a third-period sequence, and it can be compared with the first two examples from the second period, in which such effects are seen to be more restricted in range. These interactions in the third period exhibit some unique features, and detailed studies of the resulting trends will be discussed in Section 6.3.4.

The B I sequence displays the effects of interaction between the $2s2p^2\ ^2D$ term and the $2s^2nd\ ^2D$ series in a plot of the f-values for the $2s^22p\ ^2P^o-2s2p^2\ ^2D$ transition (see Fig. 45). Weiss (We 69a) has shown that the effects of two interactions are actually superposed here: a uniform reduction in f below the single-configuration values due to ground-state configuration interaction between $2s^22p$ and $2p^3$; and a further loss of oscillator strength resulting from perturbation of the $2s^2nd$ series by $2s2p^2$. (The former interaction was discussed earlier in connection with the $^2P^o-^2P$ transition - see Fig. 31.) More extensive theoretical calculations and numerous experimental measurements, including our values for O IV and Ne VI, have essentially confirmed the trend, indicated by Weiss' SOC calculations, that passes through the early phase-shift result of Lawrence and Savage (La66) at C II. (Notice, however, the factor of 2 discrepancy between Weiss and Nicolaides at B I). The effect of configuration mixing in the ^2D term decreases rapidly for higher series members as the $2s2p^2$ and $2s^23d$ configurations separate.

Just as with the penetrating series, if the p^a perturber lies below the series, the f-value anomaly (strongest mixing) occurs for the sequence member at which the mixing terms are closest together. For both types of series, at this ion there is strong cancellation

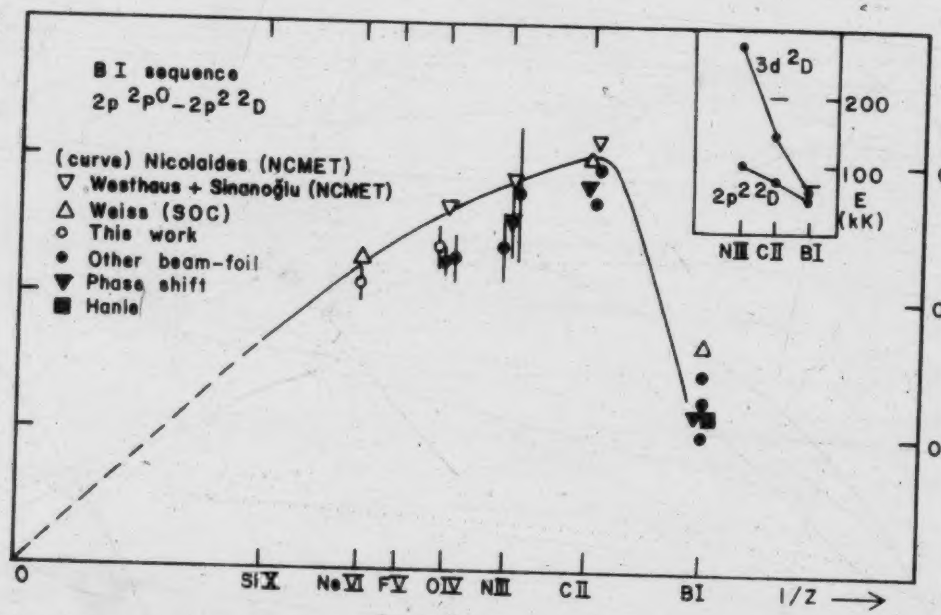

Fig.45. f vs. 1/Z, $2s^2 2p\ ^2P^o - 2s2p^2\ ^2D$ transition, B I sequence. Sources: theory (Ni73a, We69b, We69a); experiment: B I (La66, He68b, An69b, Br71, Be69), C II (La66, Br69, Po73), N III (He67, Du72, Bu72a), O IV (Bi67b, Ma71a).

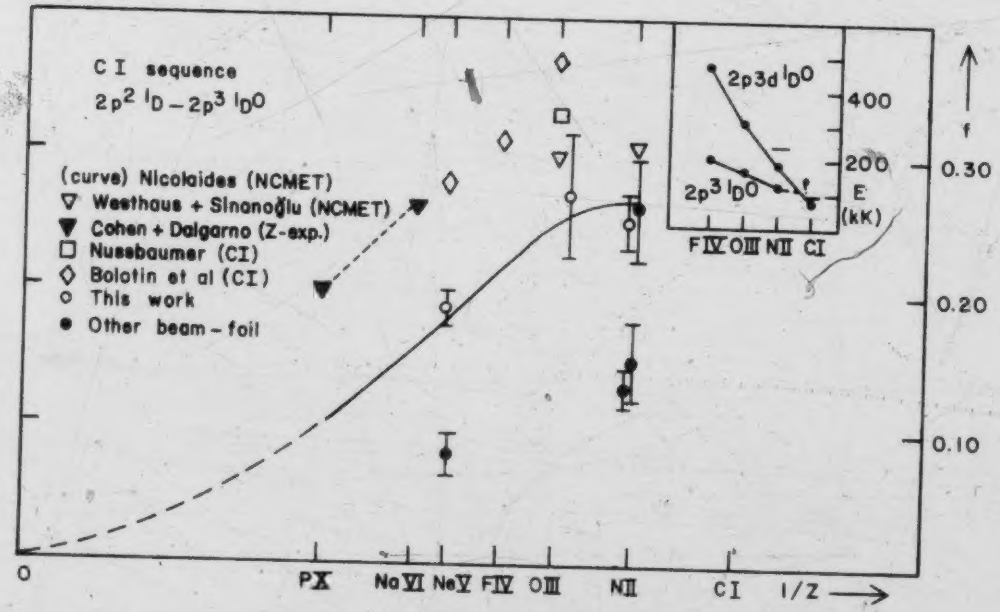

Fig.46. f vs. 1/Z, $2s^2 2p^2\ ^1D - 2s2p^3\ ^1D^o$ transition, C I sequence. Sources: theory (Ni73a, We69b, Co64, Nu69, Bo56); beam-foil (Sm70, Bu72a, Du72, Ke72).

between the two configurations that contribute to the transition moment. For nonpenetrating series, oscillator strength is lost to the series by the perturber, whereas for the penetrating series discussed so far (P-S multiplets), the series loses oscillator strength to the perturber.

A trend very similar to that shown in Fig. 45 appears in the C I sequence, representing the analogous interaction between $2s2p^3\ {}^3D^o$ and $2s^22p3d\ {}^3D^o$ (not shown here; see Smith and Wiese (Sm 71a)). Again, recent extensive calculations by Nicolaides (Ni 73a) and our mean-life measurements in oxygen and neon have confirmed the earlier results for the $2p^2\ {}^3P-2p^2\ {}^3D^o$ transition.

A similar interaction is to be expected between the ${}^1D^o$ terms of these two carbon-like configurations, and Fig. 46 displays f-value results for the $2s^22p^2\ {}^1D-2s2p^3\ {}^1D^o$ transition. Three observations may be made regarding these results: (1) various theoretical calculations indicate similar trends but are displaced vertically from one another; (2) large discrepancies are apparent among the experimental results (all are beam-foil); (3) our results show excellent agreement with the calculations of Nicolaides (Ni 73a).

The spread observed among the theoretical results reflects the differing degrees of configuration interaction that were included in the various treatments.

Cohen and Dalgarno (Co 64) and Bolotin et al (Bo 56) consider only interaction within the same complex, in this case between $2s^22p^2$ and $2p^4$ in the ^1D lower state, showing that the f-values are considerably reduced from the results given by a single-configuration treatment (e.g. f = 0.53 at O III with no configuration interaction - see Westhaus and Sinanoğlu (We 69b)). Nussbaumer (Nu 69) included also the upper level $2s2p^3$, $2s^22p3d$ interaction for O III and predicted a slight additional reduction in f (∿10%). Detailed electron correlation was considered in the many-electron-theory calculations of Westhaus and Sinanoğlu (We 69b) and Nicolaides (Ni 73a), the latter author employing more accurate wavefunctions, and still further reductions of ∿10% and ∿25%, respectively, were obtained. The Nicolaides results are conclusively verified by our lifetime measurements in N II, O III, and Ne V. From the results of Nussbaumer it is evident that the $2s2p^3$, $2s^22p3d$ interaction here is relatively weak. This is reflected in the "turnover" of the f-value trend being more gentle than that for the boron sequence discussed above, and is probably due, in part at least, to the rather wide energy separation of these $^1D^o$ terms in the critical ion (N II).

The three very low beam-foil f-values are somewhat disconcerting, since they represent fairly recent work. The results of Kernahan et al for neon were fully discussed in Ch. V. In N II, the result of Smith et al (Sm 70) could be a consequence of insufficient time resolution in their system. Although they claimed, in principle, to be able to detect a lifetime as short as our result (0.36 ns), they presented no discussion or short-lifetime results to support this claim. The result of Buchet et al (Bu 72a) is difficult to understand. They had better time resolution than Smith et al and reported several lifetimes shorter than 0.3 ns. Their results for nitrogen agree well with ours for about 20 out of 25 comparisons.

The $3s^2 3p^2\ {}^1D - 3s3p^3\ {}^1D^o$ transition in the Si I sequence is homologous to that just discussed in the C I sequence. However, configuration interaction here between $3s3p^3$ and $3s^2 3p3d$ is expected to be more extensive than that between $2s2p^3$ and $2s^2 2p3d$, since the mixing configurations for third-period elements are within the same complex. There is no theoretical work available for this transition, but three beam-foil measurements in S III, Cl IV, and Ar V clearly indicate that the effects of the interaction extend well along the sequence (see Fig. 47). Although these results give no indication of the turnover point, a crude qualitative

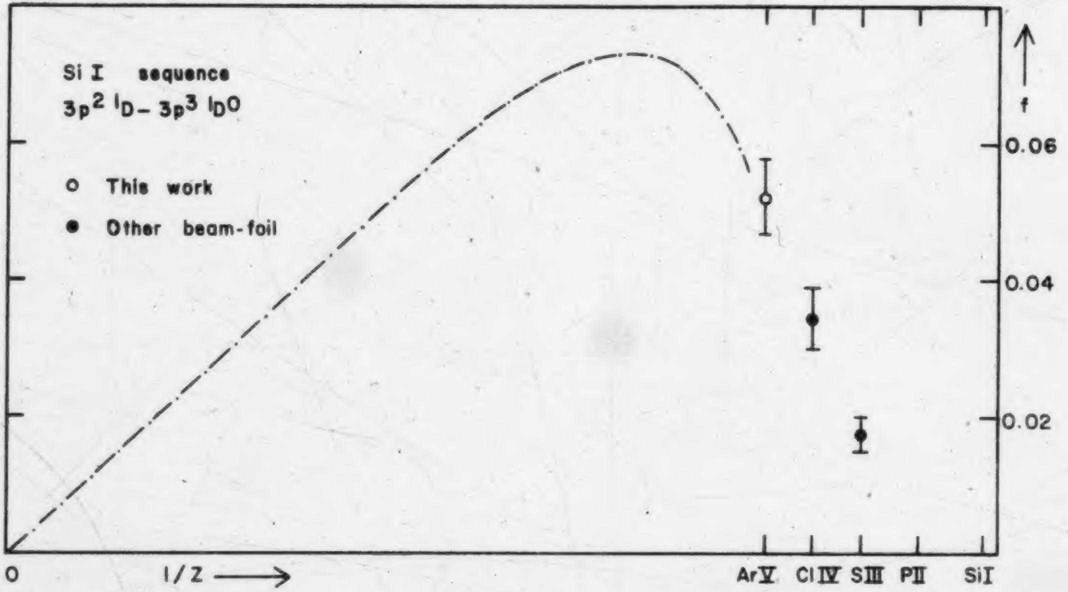

Fig.47. f vs. 1/Z, $3s^23p^2\ {}^1D-3s3p^3\ {}^1D^o$ transition, Si I sequence. Sources: S III (Be70b), Cl IV (Ba71).

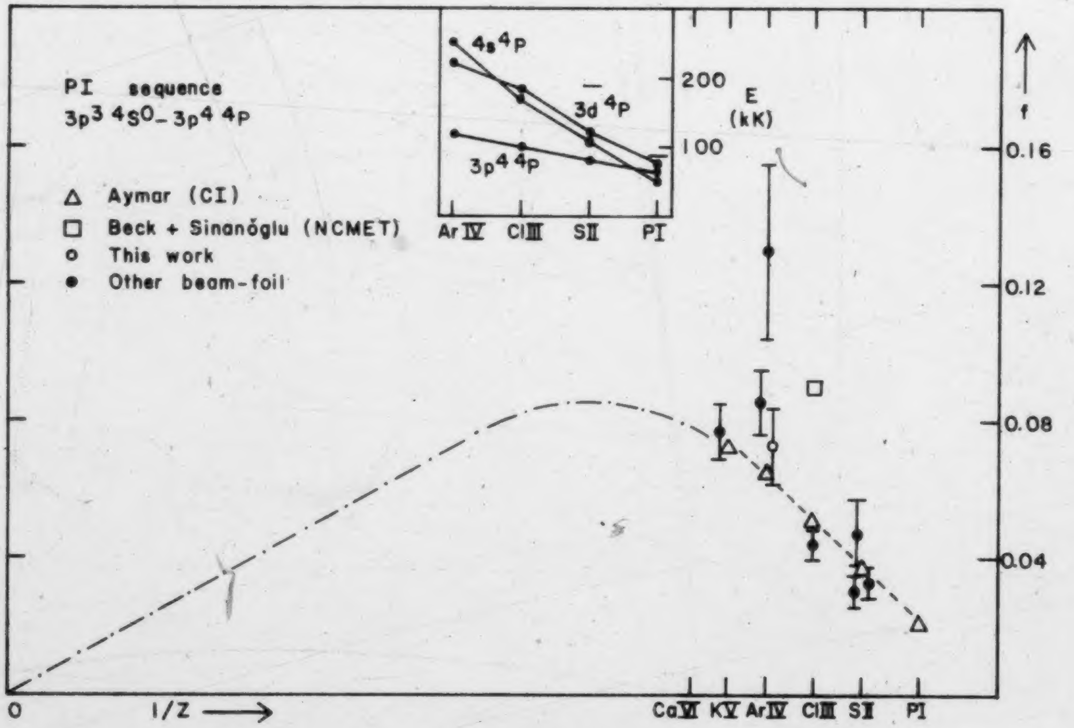

Fig.48. f vs. 1/Z, $3s^23p^3\ {}^4S^o-3s3p^4\ {}^4P$ transition, P I sequence. Sources: theory (Ay73, Be72a); experiment (La68, Sa66, Mu68, Ba71, Pi71, An73).

guess can be made on the basis of more extensively studied third-period sequences (see Section 6.3.4), and this is indicated by the dashed line. Comparison of this trend with the two previous examples reveals that significant configuration mixing of a nonpenetrating series term with a perturbing term is evident much farther along an isoelectronic sequence if the mixing configurations are within the same complex. The resultant f-value anomalies are of comparable magnitude, however. (The transition in Ar V was recently assigned by Ekberg and Svensson (Ek 70)).

The pattern indicated by these three examples for a perturbing term approaching a nonpenetrating series appears to be true in general for such situations. Weiss (We 69c), in considering the particular case of the ^2D series of Al I (which we shall discuss later), has proposed an approximate model for providing a qualitatively reliable description of the term-scheme and oscillator-strength trends that result from such interactions. For strong configuration interaction he offers two conclusions. (1) If the perturber would normally appear below the series in the absence of interaction, the interaction pushes the perturbing state down and transfers oscillator strength from it to the series. This is just what we have seen for the three transitions considered in this section. (2) If the perturber would normally appear embedded in the series or in an autoionizing state above the series, the interaction produces a (higher) autoionizing state which takes up most of the series oscillator strength. The latter characteristic is evident in several third-period sequences to be discussed later. Weaker configuration interaction produces more localized results: repelling of neighboring series states by the perturber and less transfer of oscillator strength. The model is valid only for a nonpenetrating series, where the electron is radially far removed from the rest of the atom. These general characteristics, however, will be useful for helping to specify the dominant interaction when both a penetrating and a nonpenetrating series can interact with the perturber, as will be discussed in Section 6.3.3.

6.3.3 Competing Interactions

In atomic systems where a penetrating series and a nonpenetrating series both produce the same term as a p^a configuration, the effects of mixing from both configurations may be apparent in the f-values of transitions involving the p^a perturber. Of the ns and nd series in the second and third periods, only the 3d configuration in third-period systems belongs to the same electron shell as its perturber. For this reason, the mixing characteristics are expected to be different for the two periods, particularly those involving non-penetrating series, as mentioned earlier (see Section 6.3.2).

This contrast is clearly displayed by the f-value trends for the $s^2p^3\ {}^4S^o$-$sp^4\ {}^4P$ transitions in the homologous N I and P I sequences (see Figs. 48 and 49). Aymar (Ay 73) has recently performed configuration-interaction calculations for the phosphorus-like systems and found the interaction of $3s3p^4$ with $3p^24s$ to be negligible compared to that with $3p^23d$. The interaction thus reverts simply to that for a non-penetrating series. The characteristic turnover of the trend fairly well down the sequence is suggested by both theory and experiment (Fig. 48), with our result for Ar IV providing clarification of the previous disagreement for that ion. (The extrapolation to $Z^{-1} = 0$ above K V is only qualitative.)

In the N I sequence (Fig. 49), consistency among experimental results is excellent for N I, O II, and Ne IV, each of which we have measured. An abrupt turnover of f-value at O II is indicated, very much like that shown by the B I sequence as a result of the analogous $2s2p^2$, $2s^23d$ interaction (see Fig. 45). The extent of the interaction along the sequence is seen to be more limited in the second period than in the

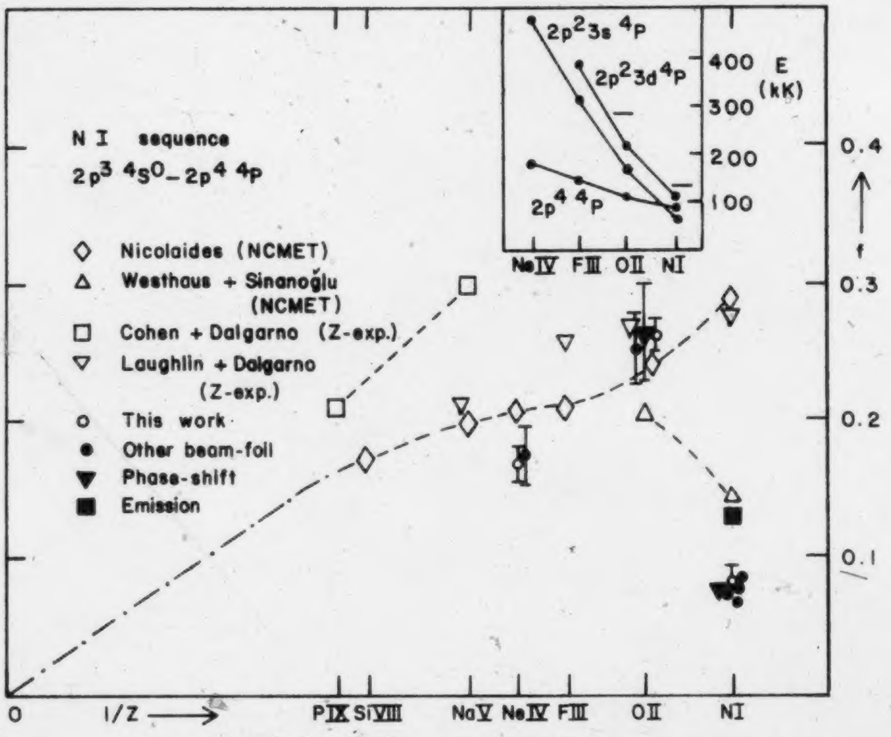

Fig.49. f vs. 1/Z, $2s^2 2p^3\ ^4S^o - 2s2p^4\ ^4P$ transition, N I sequence. Sources: theory (Ni73a, We69b, Co64, La73a); experiment: N I (La66, La65, Du72, Sm70, Be71b, Ba69), O II (La70, Sm71c), Ne IV (Ke72).

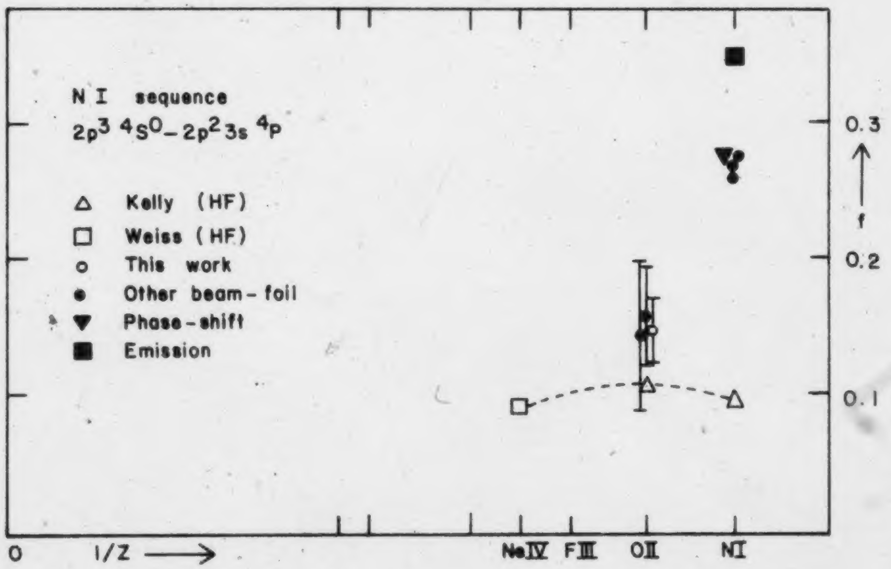

Fig.50. f vs. 1/Z, $2p^3\ ^4S^o - 2p^2 3s\ ^4P$ transition, N I sequence. Sources: theory (Ke64, Wi66); experiment: N I (La65, Be71b, Du72, La68), O II (Ma71a, Li72b).

third period, but large losses of oscillator strength characterize both situations. The anomaly at N I may not be due entirely to perturbation of $2s2p^4$ by $2p^23d$, however. The $2p^23s$ ^4P term could be relatively more influential than its third-period counterpart, for reasons mentioned above. Unfortunately, a simple qualitative model of the results of penetrating series interactions, like that discussed earlier for non-penetrating series, does not seem to be possible.

Various recent theoretical results for this transition are not particularly consistent. Laughlin and Dalgarno (La 73a) have recently improved the Z-expansion technique for terms where zero-order configuration mixing does not occur (i.e. where no common terms exist among configurations involving the same electron shell). Their results are exact to first order in the 1/Z expansion of f, but still do not allow for interactions from other shells, such as from $2p^23s$ or $2p^23d$ here. Consequently, there is improvement over earlier Z-expansion results, but no agreement with experiment except at O II, and this is probably coincidental. The NCMET calculations include these and other correlations, but for N I and O II Nicolaides (Ni 73a) and Westhaus and Sinanoğlu (We 69b) disagree, with the latter authors at least predicting the observed direction of the trend for the low Z members.

The sensitivity of the many-electron theory to detailed correlations in neutral atoms has been pointed out by Nicolaides (Ni 73a) and discussed very recently by Froese Fischer (Fi 74). Attributing discrepancies and trends to individual configurations is not easy from the way NCMET results are presented, however, if indeed there is a single dominant interacting configuration to be identified here.

Inspection of the transition involving $2p^2 3s\ ^4P$ (Fig. 50) again reveals excellent agreement among numerous experimental results. The f-value in N I is anomalously high with respect to the single-configuration value. This probably accounts for much of the oscillator strength lost by the transition involving $2s2p^4\ ^4P$ and indicates that interference between $2p^2 3s$ and $2s2p^4$ is constructive for the transition from the ^4P term of the former and destructive for that of the latter. The effect of $2p^2 3d$ upon $2s2p^4$, though, should produce the same type of turnover in the trend of f for the $2p^3$-$2p^4$ transition, but the relative contributions of the interactions with 3s and with 3d are not known. No experimental results are available for the $2p^3\ ^4S^o$-$2p^2 3d\ ^4P$ transition. Note that the arc emission f-values of Labuhn (La 65) for N I are too high for both transitions (Figs. 49 and 50).

An almost analogous f-value trend exists for ^2D-^2D transitions in this sequence (Figs. 51 and 52). In the $2p^3$-$2p^4$ multiplet, the relative values of the three reliable sets of calculations are very similar to their values in Fig. 49. (There is no known $2p^4\ ^2D$ state in N I - it is probably above the $2p^2(^3P)n\ell$ ionization limit and thus autoionizing.) Again there is reasonably good experimental verification of Nicolaides' results at O II and Ne IV (the higher beam-foil result for Ne IV probably is not reliable - see Ch. V). Our measurement for the $2p^3\ ^2D^o$-$2p^2 3s'\ ^2D$ transition in N I confirms previous experimental indications of a positive discrepancy from the theoretical single-configuration value. The interaction here with $2p^4$ is complicated by its probable autoionizing characteristics. The general resemblance of these trends to those for the $^4S^o$-^4P transitions strongly suggests that configuration interaction effects are qualitatively the same in both cases. The observed "dips" in Nicolaides' calculated trends near F III are difficult to understand and probably are not real. In fact, Fig. 49 in particular suggests that his N I and O II values depart from the indicated turnover in the experimental trend, which implies that his agreements with experiment for O II are no less coincidental than

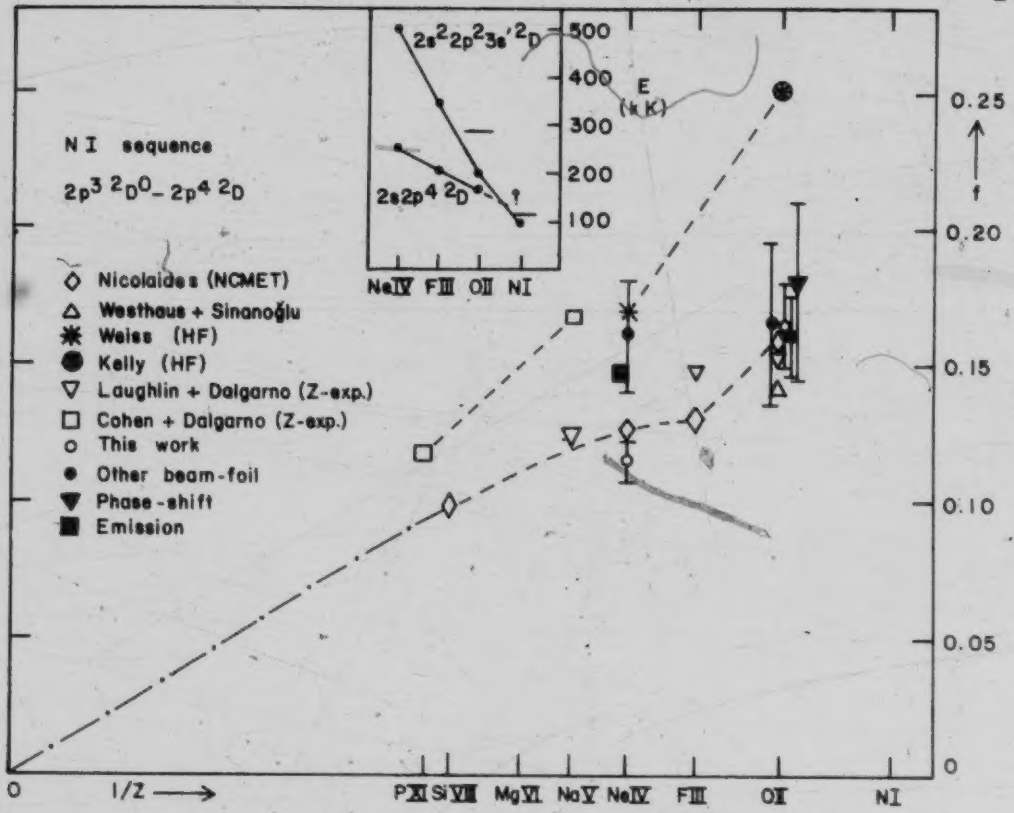

Fig.51. f vs. 1/Z, $2s^2 2p^3\,^2D^o - 2s2p^4\,^2D$ transition, N I sequence. Sources: theory (Ni73a,We69b,Wi66,Ke64,La73a, Co64); experiment: O II(Sm71c,Ma71a,La70),Ne IV(Ke72,Hi66).

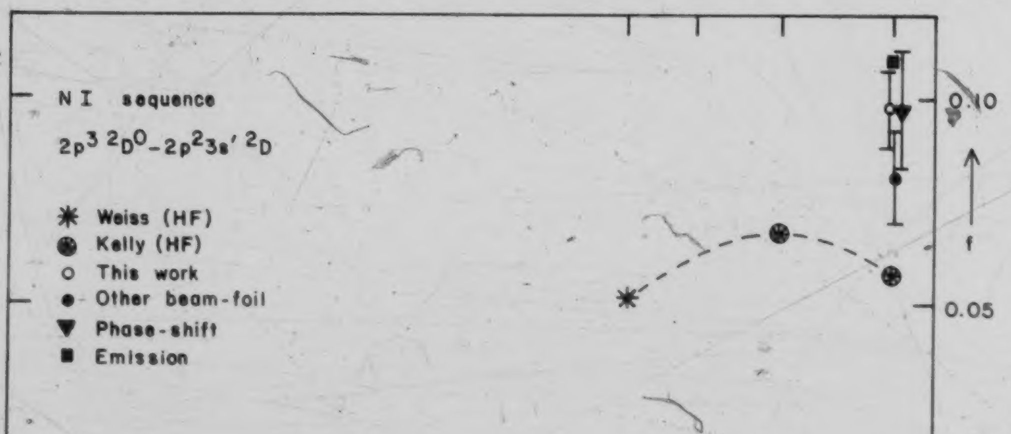

Fig.52. f vs. 1/Z, $2p^3\,^2D^o - 2p^2 3s'\,^2D$ transition, N I sequence. Sources: theory (Ke64, Wi66); experiment (Ba69, La66, La65).

those of Laughlin and Dalgarno for both transitions in this ion.

The O I sequence displays this type of level-crossing as well (see Fig. 53). The $^3P^o$ terms of $2p^33s"$ and $2p^33d'$ cross the $^3P^o$ term of $2s2p^5$ between F II and O I, with all three lying above the $2p^3(^4S^o)n\ell$ limit in O I. For LS coupling, however, these are bound states since autoionization to the continuum is forbidden by the parity-conservation selection rule (i.e. there are no $^3P^o$ states in the $(^4S^o)n\ell$ continuum). Our results in F II and Ne III confirm for the first time the NCMET trend of Nicolaides (Ni 73a) for the $2p^4$-$2p^5$ transition, at least for the ionized sequence members. The reduction of f-value for the neutral end of the sequence appears to be spread over more ions than in the N I sequence examples. A measurement of f for the O I member here (792 Å) would be valuable not only as a test of Nicolaides' result but also as an indication of the importance of weak autoionization in these $^3P^o$ terms due to slight deviations from LS coupling (i.e. mixing with S and D terms that exhibit allowed autoionization). This mixing has been discussed by Lawrence (La 70) for the $2p^23s"$ $^3P^o$ term.

In the C I sequence, once again the analogous crossing of a 3s term by p^a occurs, but this time between the second and third sequence members, with

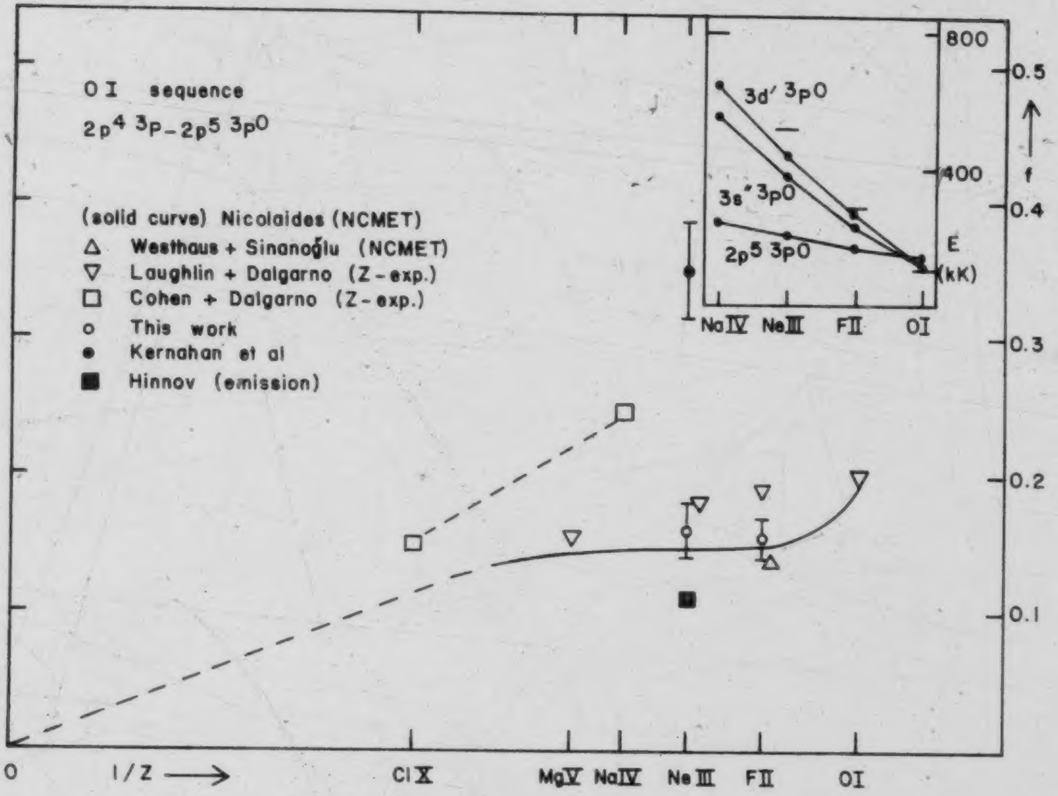

Fig.53. f vs. 1/Z, $2s^22p^4\ ^3P-2s2p^5\ ^3P^o$ transition, O I sequence. Sources: theory (Ni73a, We69b, La73a, Co64); experiment (Ke72, Hi66).

subsequent crossing of the 3d term occurring between N II and C I (see Fig. 54). The $2p^2\ ^1D-2p^3\ ^1P^o$ transition shows the characteristic loss of oscillator strength at N II, where the $2p^3$ perturber is closest to the nonpenetrating 2pnd series. Our lifetime measurement and that of Buchet et al (Bu 72a) are consistent in indicating the NCMET prediction to be again too high, as they were for the analogous case in the N I sequence (see Fig. 49). In O III we find agreement with the NCMET theory, revealing the depth of the anomaly from O III to N II to be greater than was indicated by earlier experimental results. The $2p^3\ ^1P^o$ lifetime in O III is very short (∿0.08 ns) and time-resolution limitations in the earlier experiments could account for the lower f-values that were obtained.

The f-value trend for the transition from the potentially-interacting 2p3s $^1P^o$ level is particularly interesting, and has been discussed by Smith et al (Sm 73). The C I value is fairly well-established by various measurements and the SOC calculations of Weiss (see Fig. 55). For ionized members, though, only one highly uncertain (±50%) lifetime measurement in N II and a limited configuration interaction calculation in O III have been available previously, aside from several single-configuration treatments that are of dubious accuracy. We have measured both the N II and

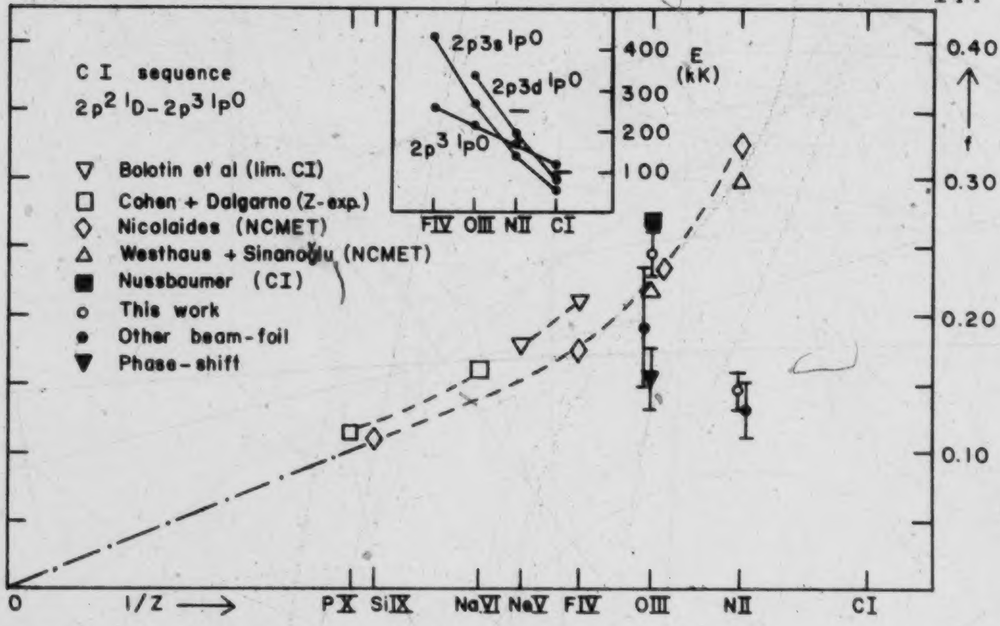

Fig.54. f vs. 1/Z, $2s^2 2p^2\ ^1D-2s2p^3\ ^1P^o$ transition, C I sequence. Sources: theory (Bo56, Co64, Ni73a, We69b, Nu69); experiment: N II (Bu72a), O III (Li72b, He68c).

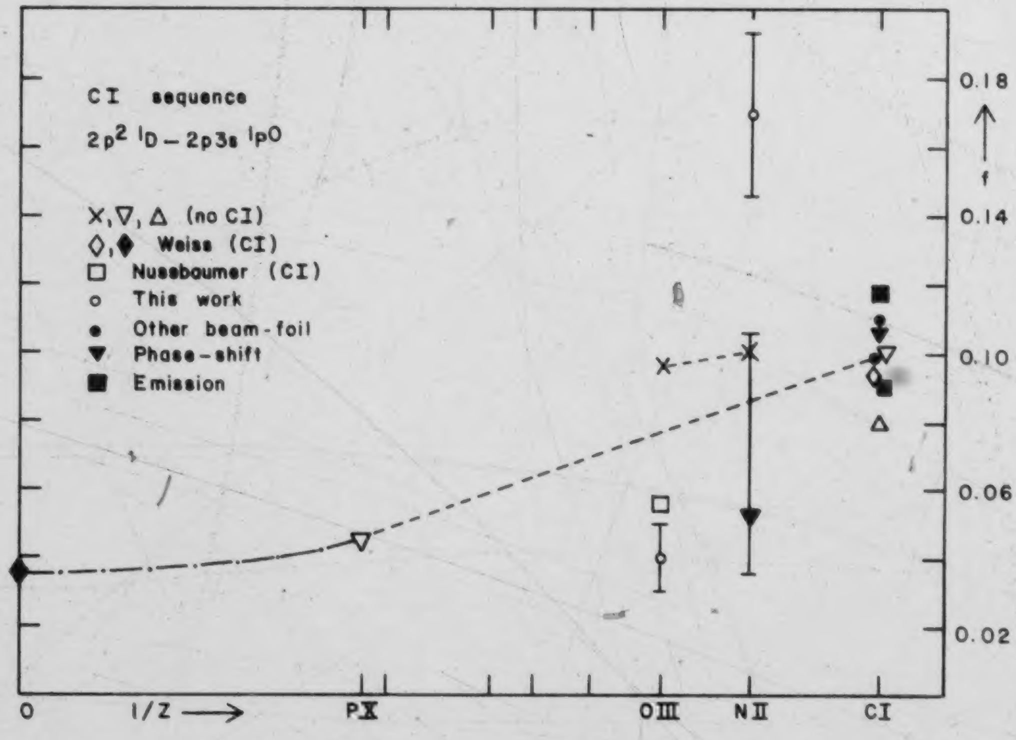

Fig.55. f vs. 1/Z, $2p^2\ ^1D-2p3s\ ^1P^o$ transition, C I sequence. Sources: theory (We67a, Nu69, see Sm73); experiment: C I (Ma72b, see Sm73), N II (He68a).

0 III lifetimes and find fair agreement with Nussbaumer (Nu 69) for 0 III, but a surprisingly high f-value for N II.

In 0 III, our results here and in Fig. 54 show Nussbaumer's values to be slightly high. It appears that he included only the interaction between $2s2p^3$ and 2p3s in both cases and, although this accounts for most of the deviation of f from single-configuration predictions in 0 III, complete agreement with experiment would not be expected. The negative f-value anomaly here, where the perturber lies below the series, indicates that the configuration interaction in this ion causes cancellation in the transition moment of the $2p^2\ ^1D$-$2p3s\ ^1P^o$ transition, just as in the C II $2p\ ^2P^o$-$3s\ ^2S$ transition in the B I sequence discussed earlier (see Fig. 41). This is in contrast to the trend that was shown in Fig. 50 in which f was seen to be slightly higher than the single-configuration prediction in 0 II, where the perturber also lies below the series. Clearly, even the qualitative result of mixing with a penetrating series depends upon the individual multiplet involved, which was seen not to be the case for mixing with a nonpenetrating series (Section 6.3.2).

In N II, the earlier phase-shift measurement by Hesser and Lutz (He 68a) is probably unreliable. Apart from their large and somewhat arbitrarily quoted uncertainty of ±50%, two of the remaining three lifetime results that they report for nitrogen depart from well-established values by more than a factor of two. The positive discrepancy from single-configuration predictions that is indicated by our result is again consistent with the trend shown by the 2p $^2P^o$-3s ^2S transition in the B I sequence (Fig. 41). The magnitude of the anomaly here is much greater, however. The numerous results for the C I sequence member do not reflect this very high value of f, although Weiss reports his SOC value to be slightly higher than his single-configuration result. A detailed calculation of f for N II is called for by these results, which are the first to indicate a significant double anomaly in the f-value trend along an isoelectronic sequence.

Partial support for the existence of this behavior is found in the analogous multiplets of the N I sequence (Figs. 56 and 57). The level crossing characteristics are identical to those described above in the C I sequence and, as before, the f-value of the s^2p^n-sp^{n+1} transition in the singly-ionized member (O II) is below NCMET predictions. Particularly important for our comparison is the fact that in both N I and O II, f is well above the single-configuration predictions for the $2p^3$-$2p^23s$ transition, the departure

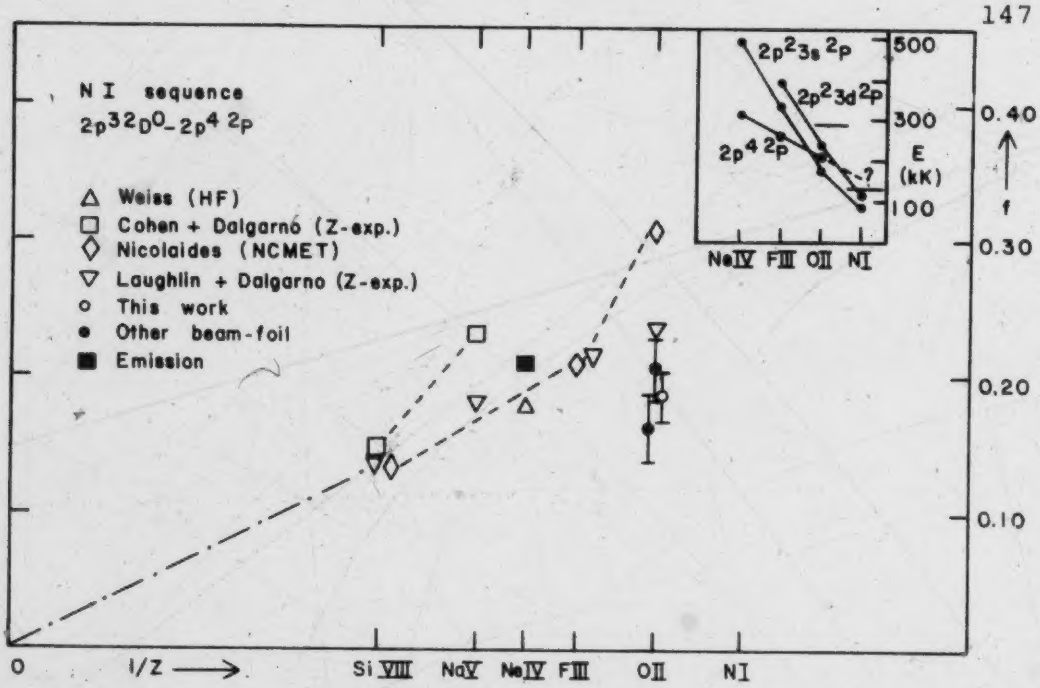

Fig.56. f vs. 1/Z, $2s^2 2p^3\ ^2D^o - 2s2p^4\ ^2P$ transition, N I sequence. Sources: theory (Wi66, Co64, Ni73a, La73a); experiment: O II (Li72b, Ma71a), Ne IV (Hi66).

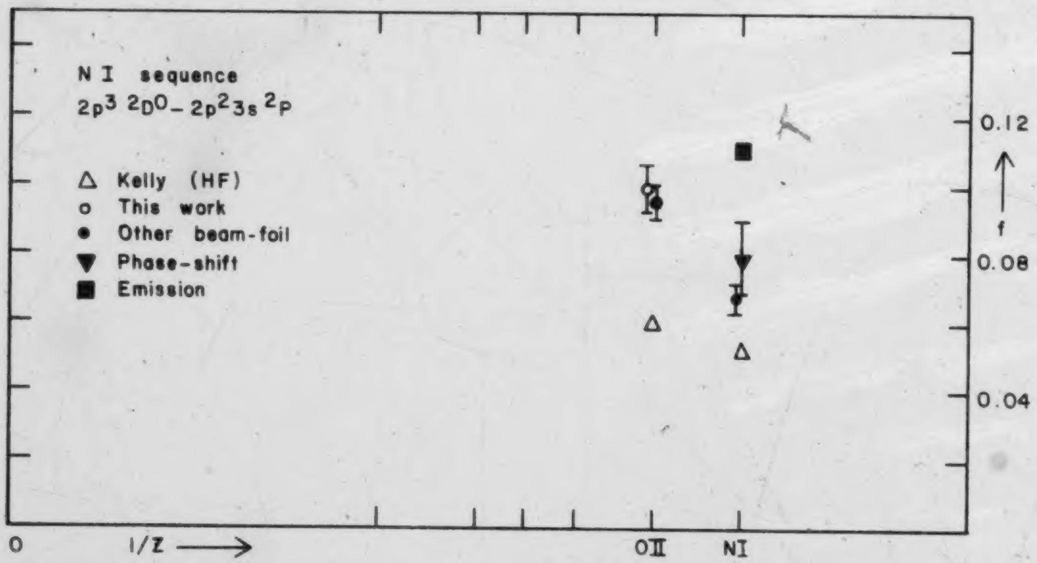

Fig.57. f vs. 1/Z, $2p^3\ ^2D^o - 2p^2 3s\ ^2P$ transition, N I sequence. Sources: theory (Ke64); experiment: N I (Be71b, La65, La66), O II (Li72a).

being greatest at O II. (The arc emission result of Labuhn for N I again appears to be too high - see also Figs. 49 and 50). Unfortunately, no experimental results are available here for more highly-ionized members to further verify that the trend follows that of the C I sequence, and no configuration-interaction calculations have been reported for these transitions.

We note that the upper terms of the transitions in the C I and N I sequences just discussed all have branch transitions (to $2p^2\ ^1S$ and $2p^3\ ^2P^o$, respectively). These complicate the conversion of lifetimes into f-values, particularly when different theoretical calculations yield different branching ratios, so that the experimental f-values remain subject to correction for erroneous theoretical branching ratios. However, the transitions discussed above are all the dominant branches from their respective terms, and reasonable adjustments of branching ratios should have little effect on the experimental results.

6.3.4 Third-Period Nonpenetrating Series

Configuration mixing in third-period isoelectronic sequences is particularly strong between $3p^a$ and $3s3p^{a-2}3d$. These two configurations in each of the Mg I to S I sequences produce the same upper terms, and the interference effects between these terms are evident over a wide range of sequence members. The interaction is so strong near the neutral end of the sequence that unique, dominant-configuration lab~~els~~ for the terms can become meaningless. One example of the f-value trend resulting from such interaction has already been discussed for each of the Si I and P I sequences (Figs. 47 and 48 respectively). Two further examples involving transitions from the $3p^a$ term will now be presented for the S I sequence. Trends from the Mg I, Al I, and Si I sequences, involving transitions from both the mixing terms, will then be discussed with regard to the relative effects of the interference upon each transition. Finally, a transition will be discussed involving higher terms in the Mg I sequence, and somewhat different interacting configurations.

S I sequence

Aymar (Ay 73) has recently reported a theoretical study of limited configuration mixing in the P I and S I sequences. For sulfur-like systems, she found that strong interactions between both the $^1P^o$ and the $^3P^o$ terms of the $3s3p^5$ and $3p^3nd$ configurations result in large cancellation in the transition moments involving $3s3p^5$ terms. For the sequence members from S I to Ca V, reductions of f-value by factors of ∿10-200 from single-configuration results are predicted. The main interaction is attributed to the $3p^3(^2D^o)3d$ configuration (called 3d') in both cases (see Figs. 58 and 59), although weak contributions come from higher series members(4d, 5d, etc.) near the neutral end of the sequence. Mixing between $3s3p^5$ and $3p^3ns$ was found to be always weak in this sequence.

Of particular interest for the singlet transitions (Fig. 58) is her finding that the $^1P^o$ level involved actually receives its major contribution from the $3p^3(^2D^o)3d$ configuration in both Cl II and Ar III, while that from $3s3p^5$ dominates in Ca V, both configurations contributing about equally in K IV. Clearly, single-configuration labels for these upper terms are inappropriate, since no one configuration completely dominates for any ion and the major contributer changes along the sequence. No theoretical result was reported for S I due to an ambiguity in its theoretical assignment.

Experimental comparison with these singlet calculations is available for Cl II and Ar III. (The Cl II result is based upon a measurement by Bashkin and Martinson (Ba 71). They reported a mean life measured at 961 Å, but did not assign the transition, indicating only that it appeared strongest at low ion energy. On the basis of the $3p^4\ ^1D-3p^5\ ^1P^o$ wavelength

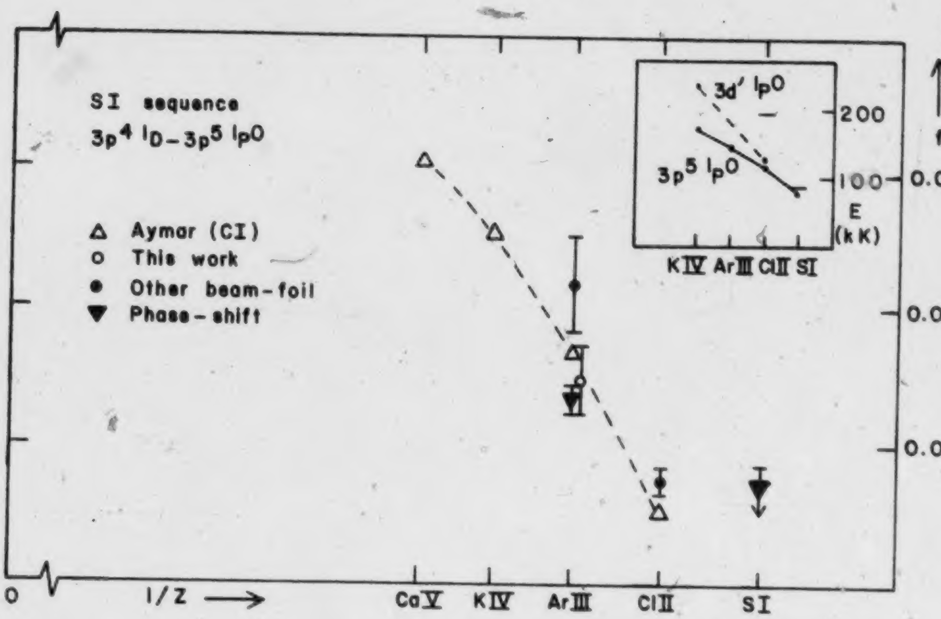

Fig.58. f vs. 1/Z, $3s^23p^4\ ^1D-3s3p^5\ ^1P^o$ transition, S I sequence. Sources: theory (Ay73); experiment: S I (La68), Cl II (Ba71), Ar III (La68, Pi71).

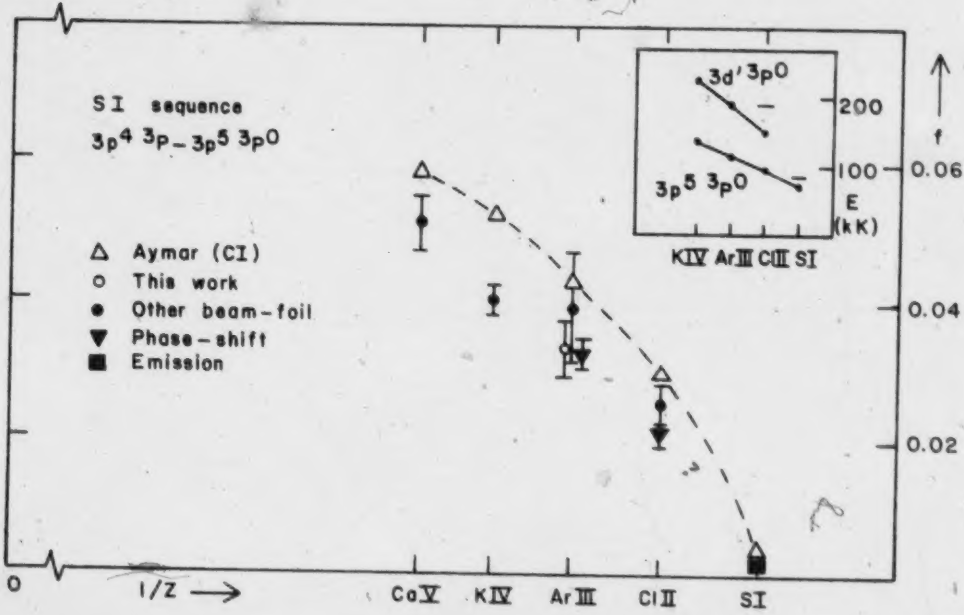

Fig.59. f vs. 1/Z, $3s^23p^4\ ^3P-3s3p^5\ ^3P^o$ transition, S I sequence. Sources: theory (Ay73); experiment (Mu68, Ba71, La68, Pi71, An73).

of 961.5 Å in Kelly (Ke 73), and the f-value derived from the above mean-life result, the present assignment is proposed.) In view of the limited interaction treatment by Aymar and the scatter among measured values, agreement is very good, indicating that mixing of $3s3p^5$ with the $3p^3(^2D^o)nd$ series accounts for essentially all the interaction here. An upper limit to the theoretically unavailable S I f-value is provided by the phase-shift lifetime measurement of Savage and Lawrence (Sa 66). This result should be close to the actual value if branching to $3p^4\ ^1S$ is as weak in S I as Aymar indicates it to be for Cl II to Ca V.

The $^3P-^3P^o$ multiplet for the same configurations displays an almost identical f-value trend (Fig. 59). Aymar finds that mixing is somewhat less pronounced along the sequence, with the $3s3p^5$ configuration dominating in $^3P^o$ for all sequence members. The effect upon the f-value appears to be no less significant than before, however, and the interaction in S I nearly results in complete cancellation in the transition moment. The theoretical trend is verified by experiment from S I to Ca V, with a systematic negative discrepancy being indicated at all sequence members.

Al I sequence

In this sequence configuration interaction arises between the terms $3s3p^2\ ^2D$ and $3s^23d\ ^2D$. The energies of these terms along the Al I sequence are plotted in Fig. 60, along with plots for interacting terms in the Mg I and Si I sequences to be discussed below. The scale has been chosen to yield approximately constant energy at high values of Z. The terms having the same dominant configuration are connected to indicate trends, with broken lines indicating those ions in which mixing is pronounced. The f-value characteristics of the aluminum-like transitions from these ^2D terms to $3s^23p\ ^2P^o$ are the most extensively studied, both theoretically and experimentally, of all such anomalous trends in the third period (see Figs. 61 and 62). Froese Fischer (Fi 68) has studied both transitions between Al I and Fe XIV, assuming limited configuration interaction, and her results show that (1) the $3s3p^2$ and $3s^23d$ configurations are heavily mixed along the entire sequence, with the lower terms forming an isoelectronic sequence and having as dominant component $3s3p^2$ in all members but Al I, where $3s^23d$ dominates; (2) the $3s^23d$ contribution to $3s3p^2$ causes cancellation in the multiplet strength of the $3s^23p\ ^2P^o$-$3s3p^2\ ^2D$ transition and consequently a reduction in the f-value for all members except Al I; (3) the increase in cancellation with decreasing ionization leads to a change

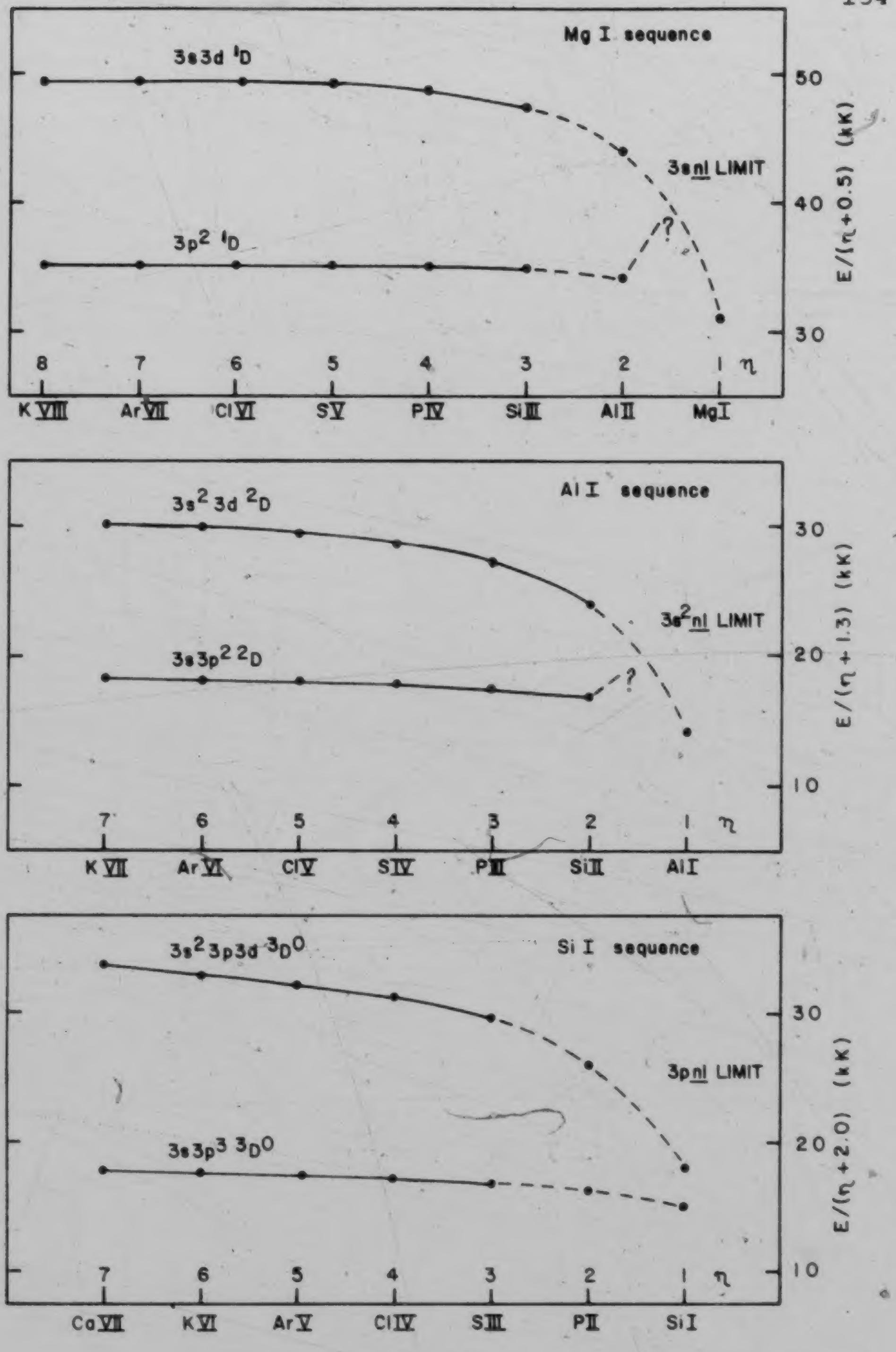

Fig.60. Energies of common terms for interacting configurations along three isoelectronic sequences.

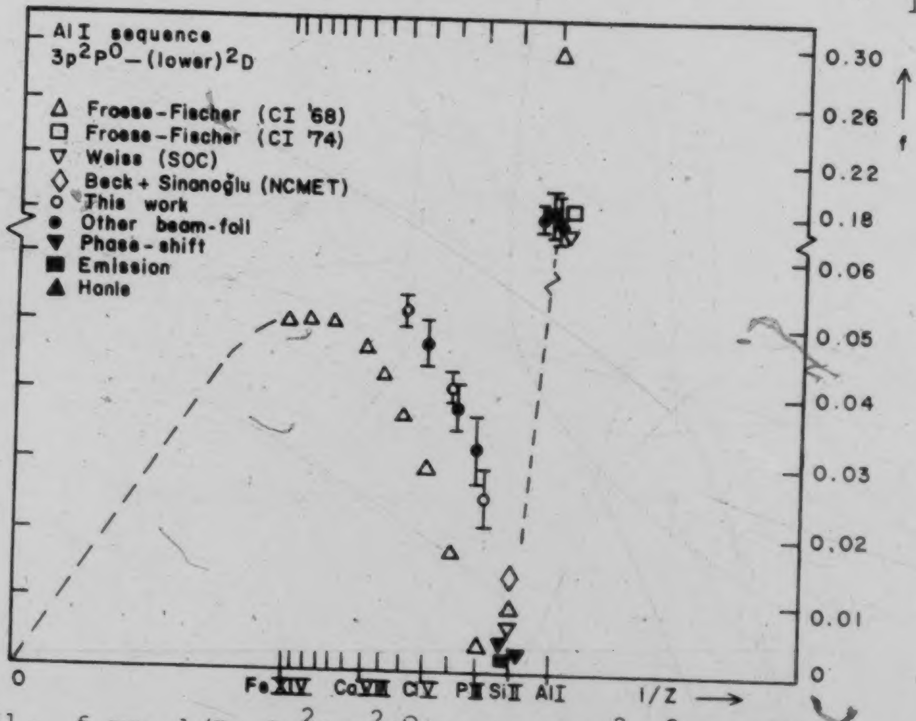

Fig.61. f vs. 1/Z, $3s^2 3p\ ^2P^o$-lower($3s3p^2$) ^2D transition, Al I sequence. Sources: theory (Fi68, Wi69, We69c, Be72a); experiment: Al I (An69a, Sm71b, Bu66), Si II (Sa66, Ho69, Cu74), P III (Cu71b), S IV (Be70b), Cl V (Ba71).

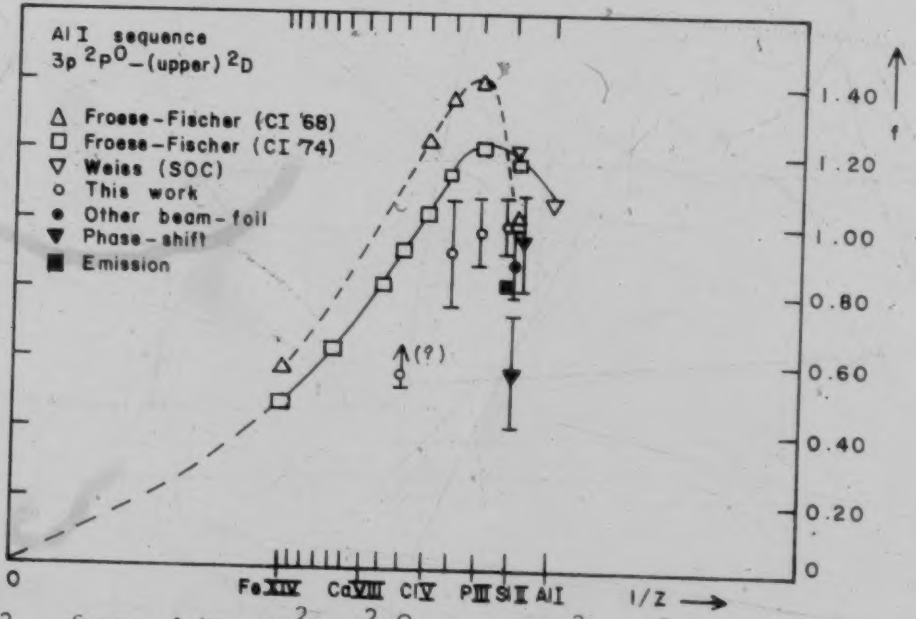

Fig.62. f vs. 1/Z, $3s^2 3p\ ^2P^o$-upper($3s^2 3d$) ^2D transition, Al I sequence. Sources: theory (Fi68, Wi69, We69c); experiment (Sa66, Ho69, Be71a, Cu74).

of sign in the trend of the transition moment between P III and Si II.

Conclusion (2) is consistent with the model of Weiss (We 69c) that was described earlier (see Section 6.3.2). Conclusion (1) points out that the presence of strong configuration mixing precludes the use of a single-configuration label to connect, along a sequence, terms that truly exhibit similar isoelectronic properties. The configuration label becomes somewhat artificial, and more detailed characteristics (such as the relative phases of mixing coefficients, as suggested by Froese Fischer) appropriately identify the terms, and hence the transitions, that form a sequence. This procedure has been adopted here in that the results for Al I in Fig. 61 represent what is usually labelled the 3p $^2P^o$-3d ^2D transition, whereas the results for all other members represent the 3p $^2P^o$-$3p^2$ ^2D transition. Conclusion (3) implies the existence of a node in the oscillator strength trend at the zero crossing and hence very low f-value in nearby ions, resulting from the almost exact cancellation in the multiplet strength. Note that the zero occurs near P III whereas the "crossover" in dominant configuration for ^2D is found between Si II and Al I. This is to be expected in general since, even for an idealized mixing of only two competing configurations, their contributions to the multiplet strength are weighted by their individual multiplet strengths, which are normally not equal.

Experimental agreement with the predicted trends is very good, although systematic discrepancies are evident for both transitions. In particular, for the lower ^2D transition (Fig. 61) our results are consistent with other measurements in suggesting that the zero in f is closer to Si II than P III. The discrepancy is not surprising, however, since the exact zero position is very sensitive to mixing coefficients. Thus, contributions which are relatively small become important due to mutual cancellation of the major components, and these smaller contributions are largely omitted in a limited-configuration approach. More extensive interactions have been considered in Al I and Si II by Weiss (Wi 69, We 69c) and better agreement with experiment has resulted. The upper ^2D transition (Fig. 62) has been measured less thoroughly. Previous results are available only for Si II, and our value for that ion is consistent with the other beam-foil result (Be 71a) as well as with a very recent phase-shift measurement (Cu 74). Our measurements in P, S, and Ar represent the only experimental results for higher ions and indicate the early Froese Fischer results to be high. (The argon result may be only a lower limit due to possible time resolution limitations of our apparatus). Froese Fischer has recently recalculated these f-values employing more interacting configurations (private communication, 1974). The improved values are consistent with that of Weiss (Wi 69) for Si II and significantly reduce the discrepancy from our results shown by her earlier calculations.

Mg I sequence (a)

A very similar situation exists in this sequence for the transitions to 3s3p $^1P^o$ from the ^1D levels involving the heavily-mixed $3p^2$ and 3s3d configurations (Fig. 60). This sequence perhaps represents the classic example of configuration interaction in the third period, with Bacher (Ba 33) first proposing the $3p^2$, 3s3d interaction to account for a term inversion in Mg I. Detailed studies of mixing along the sequence have been reported by Zare (Za 67) and Weiss (We 67b). Their results are presented in Figs. 63 and 64 along with available experimental results (all beam-foil data). The calculations of Zare (Za 67) are particularly instructive here since he lists the numerical contributions from ten different configurations to the total wavefunctions of the two ^1D levels. Again a zero in the multiplet strength is found (near Al II) where the competing contributions to the transition

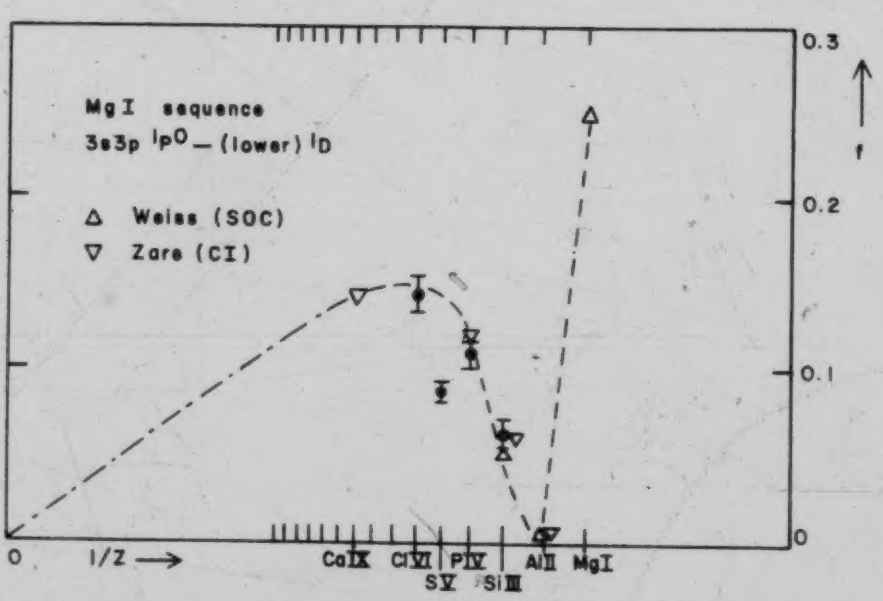

Fig.63. f vs. 1/Z, 3s3p $^1P^o$-lower($3p^2$) ^1D transition, Mg I sequence. Sources: theory (We67b, Za67); beam-foil: Si III (Be71a), P IV (Cu71b), S V (Be70b), Cl VI (Ba71).

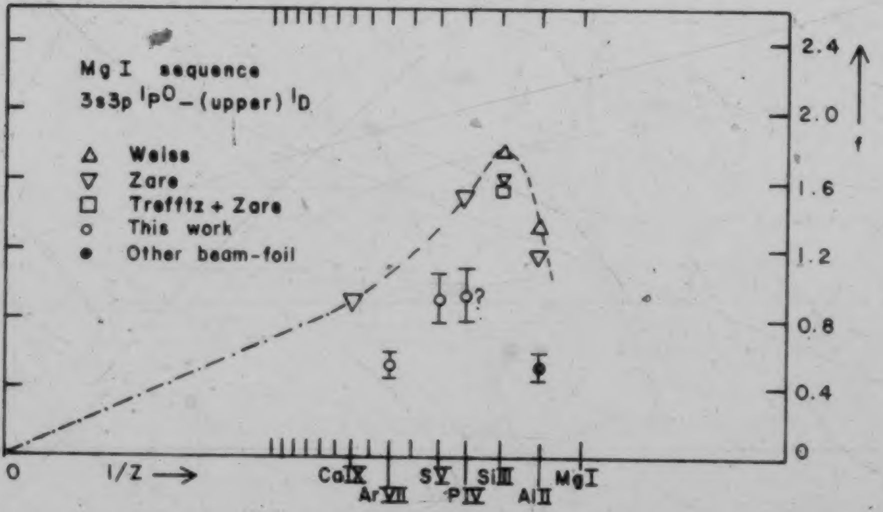

Fig.64. f vs. 1/Z, 3s3p $^1P^o$-upper(3s3d) ^1D transition, Mg I sequence. Sources: theory (We67b, Za67, Tr69); beam-foil (An69a).

involving the lower ^1D level exactly cancel. Also, the 3s3d configuration dominates in Al I for this lower level, with the $3p^2$ configuration providing the largest contribution for all ionized sequence members. The mixing is somewhat more severe than in the Al I sequence, however. There Froese Fischer (Fi 68) indicated that neither ^2D state contains less than 60% of its dominant configuration, whereas Zare finds in Al II the dominant contributions for the lower and upper ^1D states to be 54% $3s3p^2$ and 44% 3s3d, respectively. Clearly, single-configuration labels are inappropriate to describe these states and, as Zare states, their use is

> "a fiction, sanctioned by tradition
> but devoid of much significance."

As before, we follow Froese Fischer's convention of defining an isoelectronic sequence by requiring uniform relative phases of the dominant mixing coefficients, and include the transition involving the lower Mg I ^1D level in Fig. 63.

Beam-foil lifetime results for the lower ^1D level verify the theory quite well (see Fig. 63), except in S V where the measured lifetime appears to be too long. No measurements have been made for Mg I or Al II. The Mg I transition is in the infra-red region (8807 Å), and the Al II lifetime is probably very long (theoretically ~200 ns) and consequently the transition intensity low. No results for these transitions were obtained during this project, and the trend is presented for completeness. Experimental work for transitions involving the upper ^1D level has previously been limited to the single result of Andersen et al (An 69a) in Al II, where a significant negative discrepancy from theory was found (Fig. 64). In Mg I this level is not known and is probably autoionizing, while in Si III the transition coincides in wavelength with the Si III resonance transition and is difficult to isolate. The transitions for P IV to Ar VII have only very recently been assigned (see Ch. V), those in phosphorus and argon during this project. We have measured lifetimes in P, S, and Ar and find consistency with the form of theoretical trend, but systematic discrepancies in the absolute values occur, similar to that found for Al II. The overall picture is not unlike that in Fig. 62 for the Al I sequence. In both the Mg I and Al I sequences it appears that extensive configuration interaction treatments are more successful in predicting f-values involving the lower D-states than the higher ones.

Si I sequence

Analogous configuration mixing occurs between $3s3p^3$ and $3p3d$ in the two lowest $^3D^o$ terms of the Si I sequence (see Fig. 60). Beam-foil and phase-shift lifetime measurements have shown the screened hydrogenic calculations of Varsavsky (Va 61) to be much too high for the $3s^23p^2\ {}^3P-3s3p^3\ {}^3D^o$ transitions in lower sequence members (see Fig. 65 and 66). Only very recently have many-electron-theory calculations been performed by Sinanoğlu and Beck (Si 74) to provide theoretical agreement with these results. The zero in oscillator strength occurs near P II, where again the calculations show mixing to be so strong that single-configuration labels are meaningless. Fig. 65 displays results for the transitions involving the lower ${}^3D^o$ term of each system, for which the dominant configuration is $3s3p^3$, except possibly in P II and Si I.

There are no calculations available for transitions from the upper ${}^3D^o$ term. Hofmann (Ho 69) has reported a very low f-value for Si I (Fig. 66), the upper term being a bound state in the neutral member here, in contrast to the previous two sequences. Our mean-life results present the only f-values known for ionized members. Both the trend and approximate magnitude of f for these results are consistent with their counterparts shown previously in Figs. 62 and 64. (The trend joining the data points has been drawn to aid the eye; the extrapolation to the hydrogenic limit

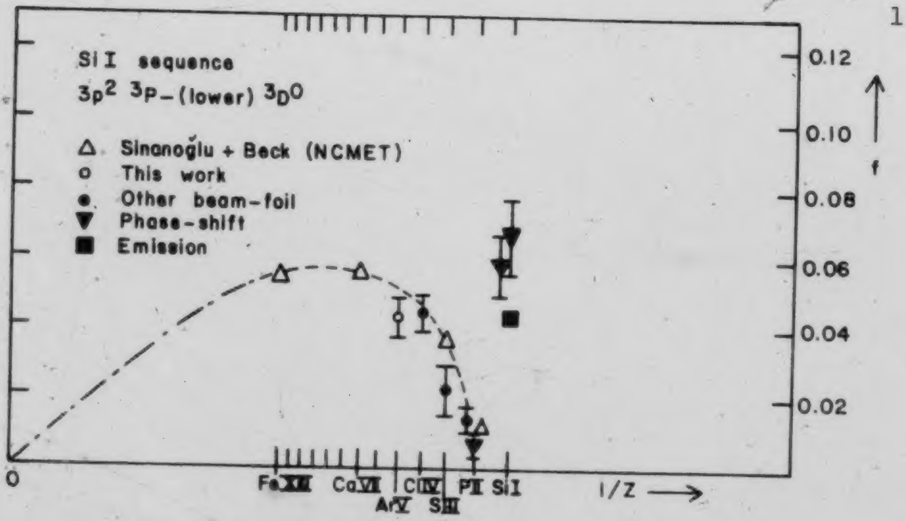

Fig.65. f vs. 1/Z, 3s^{2}3p^2 ^{3}P-lower(3s3p^3) ^{3}D^o transition, Si I sequence. Sources: theory (Si74); experiment: Si I (Sa66, Ho69, Cu74), P II (Sa66, Cu71b), S III (Be70b), Ci IV (Ba71).

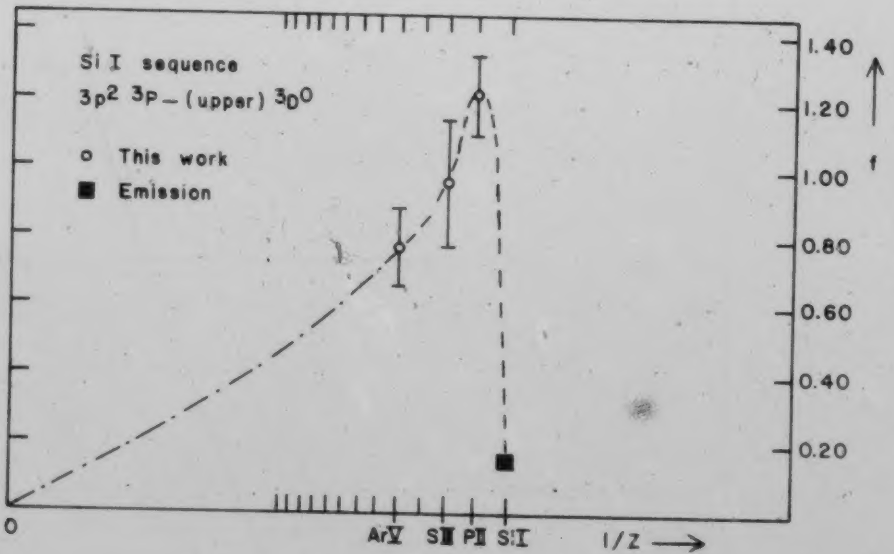

Fig.66. f vs. 1/Z, 3s^{2}3p^2 ^{3}P-upper(3s^{2}3p3d) ^{3}D^o transition, Si I sequence. Sources: emission (Ho69).

is only qualitative). Oscillator strength calculations for both transitions in Si I would be useful for ascertaining the mixing characteristics of the two $^3D^o$ terms.

Mg I sequence (b)

Perturbations between members of two high-lying series are less frequently encountered than are those between p^a and a series. One example is the interaction between 3snf and 3pnd, both of which produce $^3F^o$ terms in magnesium-like systems. The dominant interaction involves the lowest series members, 3s4f and 3p3d, except in Al II where the 3p3d $^3F^o$ term penetrates the 3snf $^3F^o$ series and perturbs higher series members as well (see inset in Fig. 67). The Al II case has been discussed by Edlén (Ed 64) and by Weiss (We 70), the latter having performed configuration interaction calculations to obtain the f-values for this ion. Limited-configuration-interaction results have also been reported by Trefftz and Zare for Si III (Tr 69) and by Trefftz for Mg I (Tr 50).

For the 3s3d ^3D-3p3d $^3F^o$ transition (Fig. 67), Weiss' results indicate that perturbation of 3p3d $^3F^o$ by the 3snf series reduces the f-value by about 25% from the single-configuration prediction, in good

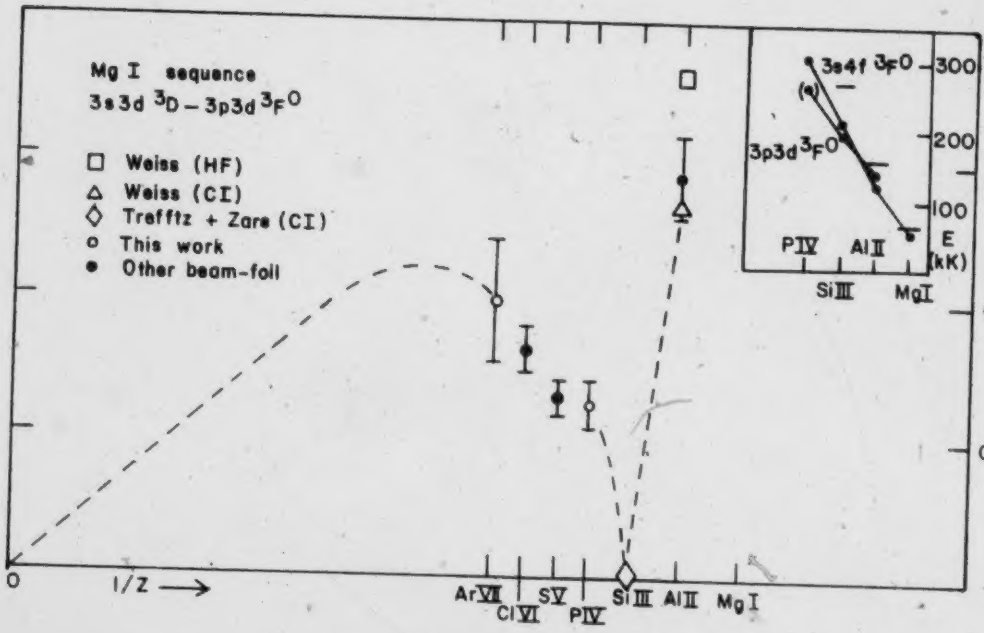

Fig.67. f vs. 1/Z, 3s3d ^3D-3p3d $^3F^O$ transition, Mg I sequence. Sources: theory (We70,see An71, Tr69, Tr50); beam-foil: Al II (An71), S V (Be70b, see Ba73b), Cl VI (Ba71, see Ba73b).

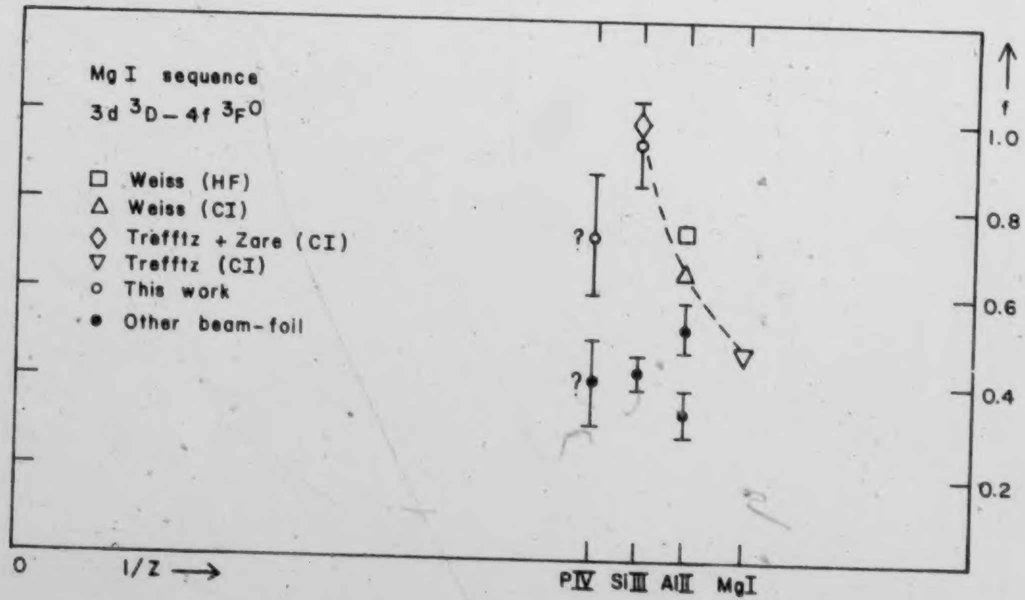

Fig.68. f vs. 1/Z, 3s3d ^3D-3s4f $^3F^O$ transition, Mg I sequence. Sources: theory (We70, see An71, Tr69, Tr50); beam-foil: Al II (An 69a, An71), Si III (Be71a), P IV (Cu71b).

agreement with the beam-foil result of Andersen et al (An 71). (The results of Weiss here are unpublished, revised values quoted by Andersen et al, and replace his earlier results (We 70) for this transition.) Trefftz and Zare, however, indicate that cancellation in the multiplet strength is almost complete in Si III, where the 3p3d perturber lies just below the series. The trend indicated by beam-foil measurements in the next 4 ions tends to support this result. The perturber appears to be losing oscillator strength to the 3snf series in the same way that a p^a term loses oscillator strength as it approaches a non-penetrating series. It should be noted that all four beam-foil results here represent newly-assigned transitions. Those for S V and Cl VI were recently reported by Bashkin et al (Ba 73b), using results of earlier investigations of these elements. The P IV and Ar VII classifications are proposed in the present work (see Ch. V). The relatively large uncertainty in the Ar VII f-value reflects severe line blending in our spectra for this multiplet. The dashed line drawn above argon indicates a qualitative extrapolation to the hydrogenic value for this $\Delta n = 0$ transition.

The situation for the 3d ^3D-4f $^3F^o$ transition is less clear (Fig. 68). The increase in f-value indicated by theory from Mg I to Si III is not supported by previous beam-foil results. However, our measurement in Si III indicates a higher f-value, in agreement with theory. In view of the oscillator strength lost by the transition to 3p3d in this ion, a maximum in f-value near Si III for the 3d-4f transition seems to be more appropriate. There is some doubt about the assignment of the P IV transition (877 Å) in beam-foil work (see Ch. V). The P IV transition 3s3p $^1P^o$-3s3d ^1D is expected to appear near this wavelength, and our lifetime measurement for this feature yields a result that is not inconsistent with either assignment. We have plotted the derived f-values for both possible assignments (Figs. 64 and 68). The earlier result of Curtis et al (Cu 71b) for P IV is not consistent with either of our oscillator strength trends.

6.4 Fourth-Period Sequences

There has been very little work done on the measurement of lifetimes or oscillator strengths for elements of the fourth period, excepting the iron-group elements. The only systematic studies for both ionized and neutral atoms are those by Andersen et al (An 73) and Sørensen (So 73), involving four transitions in the Cu I and Zn I sequences and several transitions in As I and As III. The investigations of spectra and lifetimes of Kr I-VIII in the vacuum ultraviolet during the present project represent the most extensive studies for any fourth-period element in this wavelength region. Comparison with the results of Andersen et al can be made for three isoelectronic sequences (see Fig. 69).

In the Cu I sequence our measurement in Kr VIII approximately confirms their trend for the 4s-4p transition, indicating a uniform fall-off in f-value toward higher Z. This trend is typical of the results found for such simple systems (i.e. one electron outside an argon-like core in this case) where configuration interaction effects are normally small (see Figs. 35 and 36).

In the Zn I sequence, however, we find an f-value in Kr VII for the $4s^2\ ^1S$-$4s4p\ ^1P^o$ transition that is significantly higher than the trend of the earlier results would suggest. A similar discrepancy is indicated by our Kr VI result for the $4p\ ^2P^o$-$4d\ ^2D$ transition in the Ga I sequence, where a fall-off in f-value toward higher Z is also expected, although Andersen et al report only the As III result for this sequence. It may be significant to note that this As III result and the two lowest f-values in the Zn I sequence represent the shortest lifetimes ($\sim$0.3 ns) from the results of Andersen et al and Sørensen shown

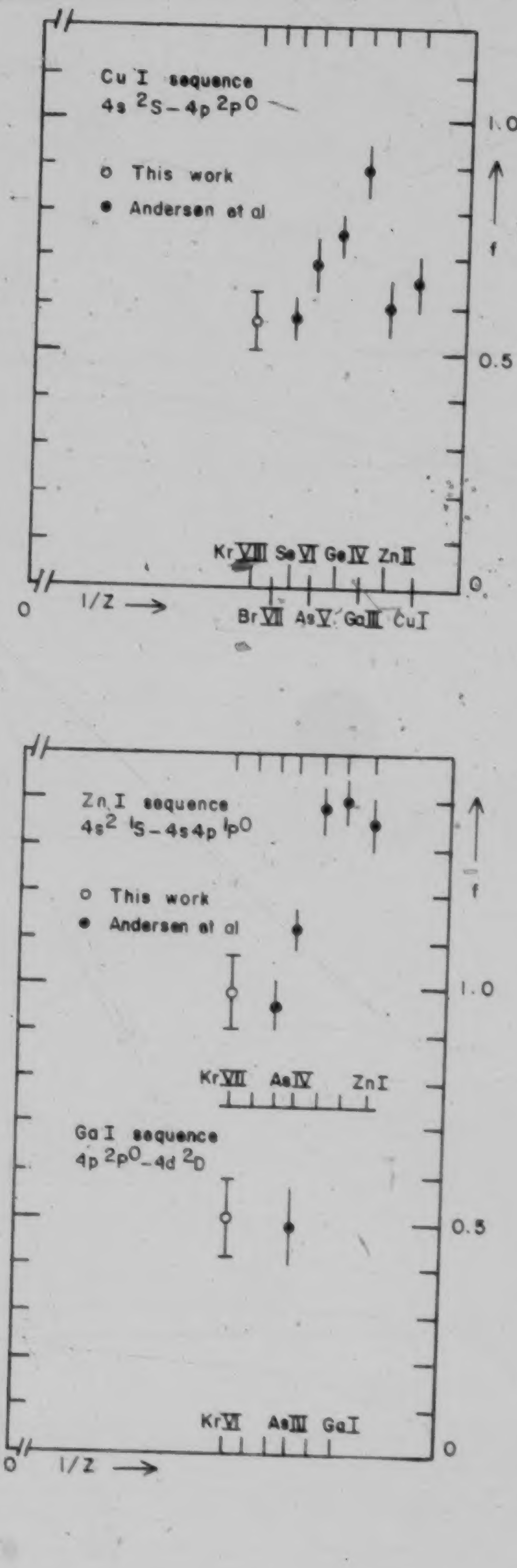

Fig.69. f vs. 1/Z, Cu I, Zn I, Ga I sequences. Sources (So73, An73).

in Fig. 69. This could reflect insufficient time resolution in their experimental system to detect very short decay components in the presence of the observed cascading. The ion speeds available for those experiments were about one-half the speeds that we employed to obtain our krypton results.

Sørensen (So 73) points out that there seems to be "a general trend for the f-values in the Cu I and Zn I sequences to decrease much more rapidly with increasing ionic charge than in the (homologous) Na I and Mg I sequences". The transitions shown earlier in Figs. 35 to 38 correspond to those he has investigated. Comparison of the homologous trends indicates very little difference for three of the four transitions. The Cu I 4p-4d trend is the only one that is noticeably steeper than its third period counterpart (Na I 3p-3d). However, short lifetimes are again involved for these fourth-period transitions and, in view of the comments above, this difference may not be real. Unfortunately, the 4p-4d transition in Kr VIII (491 Å) was too weak in our spectra for a lifetime measurement to be made.

CHAPTER VII

SUMMARY

A program for the improvement of experimental and analytic techniques in beam-foil spectroscopy, coupled with systematic studies of spectra and mean lives for ions representing a variety of elements, has been undertaken during this project. A large number of atomic transitions with important applications to atomic structure studies and astrophysical calculations has been investigated. The measurement of reliable mean lives has allowed detailed comparison to be made with existing theoretical oscillator strength calculations and has provided useful guidance for further calculations in such complicated systems as the third-period elements. The technique of studying systematic trends along isoelectronic sequences has been employed extensively for these comparisons.

Several subjects that merit further investigation are suggested by the results of this work:

(1) Among elements with $Z \leq 18$, only fluorine has not been studied in detail by the beam-foil method. Investigation of fluorine mean lives in the vacuum-ultraviolet region would supply the missing link in a number of f-value trends for second-period elements, and would provide further tests for recent detailed

calculations for certain transitions.* The extension of systematic observations into the XUV region for several elements would also yield useful information on the spectra and mean lives of highly-ionized systems.

(2) The effects of configuration interaction are fairly common in atomic systems within the second and third periods. Beam-foil results from this work have indicated some transitions for which detailed calculations are needed to identify the type of interaction that is present, as well as cases where improvements in the existing theory are required.

(3) The energy-level structures of multiply-ionized atoms are not well known for most elements. In particular, this work has revealed a large number of unassigned transitions in the higher ionization stages of the inert-gas elements neon, argon, and krypton. Preliminary analysis has yielded more than a dozen proposed classifications, and further work on the data should provide additional information on these level schemes.

---

* A beam-foil study of fluorine has, in fact, been undertaken at the University of Alberta following the writing of this thesis.

(4) This systematic study of a variety of transitions, ions, and elements has clearly demonstrated the existence of various types of trends among atomic properties. In several instances, oscillator-strength trends for different transitions show very similar behavior, i.e. there exist "trends in the trends". Furthermore, it is often apparent that only one or two reliable measurements along an isoelectronic sequence may be needed to determine the trend for the entire sequence. Even anomalous trends can sometimes be established by only a few measurements. This suggests that most future work involving the measurement of lifetimes and oscillator strengths should concentrate on selected transitions for specific ions that are crucial either to the establishment of trends or for the direct application to particular problems, such as astrophysical calculations.

BIBLIOGRAPHY

(An 69a) T. Andersen, K.A. Jessen, and G. Sørensen, J. Opt. Soc. Am. 59, 1197 (1969).

(An 69b) T. Andersen, K.A. Jessen, and G. Sørensen, Phys. Rev. 188, 76 (1969).

(An 70a) T. Andersen, J. Desesquelles, K.A. Jessen, and G. Sørensen, J. Quant. Spectrosc. Radiat. Transfer 10, 1143 (1970).

(An 70b) T. Andersen, J. Desesquelles, K.A. Jessen, and G. Sørensen, J. Opt. Soc. Am. 60, 1199 (1970).

(An 71) T. Andersen, J.R. Roberts, and G. Sørensen, Physica Scripta 4, 52 (1971).

(An 72) T. Andersen, O.H. Madsen, and G. Sørensen, Physica Scripta 6, 125 (1972).

(An 73) T. Andersen, S.W. Jørgensen, and G. Sørensen, Abstracts for the Fifth E.G.A.S. Meeting, Lund, Sweden, July 1973 (unpublished).

(Ay 70) M. Aymar, S. Feneuille, and M. Klapisch, Nucl. Instr. and Meth. 90, 137 (1970).

(Ay 73) M. Aymar, Nucl. Instr. and Meth. 110, 211 (1973).

(Ba 33) R.F. Bacher, Phys. Rev. 43, 264 (1933).

(Ba 64) S. Bashkin, and A. Meinel, Astrophys. J. 139, 413 (1964).

(Ba 68) S. Bashkin, Appl. Optics 7, 2341 (1968).

(Ba 69) S. Bashkin, H.G. Berry, W.S. Bickel, and J. Desesquelles, C.R. Acad. Sci. 268B, 234 (1969).

(Ba 71) S. Bashkin, and I. Martinson, J. Opt. Soc. Am. 61, 1686 (1971).

(Ba 73a) S. Bashkin, ed., "Beam-Foil Spectroscopy" (Nucl. Instr. and Meth. 110 (1973)).

(Ba 73b) S. Bashkin, J. Bromander, J.A. Leavitt, and I. Martinson, Physica Scripta 8, 285 (1973).

(Be 69) I. Bergström, J. Bromander, R. Buchta, L. Lundin, and I. Martinson, Phys. Lett. 28A, 721 (1969).

(Be 70a) H.G. Berry, J. Bromander, and R. Buchta, Physica Scripta 1, 181 (1970).

(Be 70b) H.G. Berry, R.M. Schectman, I. Martinson, W.S. Bickel, and S. Bashkin, J. Opt. Soc. Am. 60, 335 (1970).

(Be 71a) H.G. Berry, J. Bromander, L.J. Curtis, and R. Buchta, Physica Scripta 3, 125 (1971).

(Be 71b) H.G. Berry, W.S. Bickel, S. Bashkin, J. Desesquelles, and R.M. Schectman, J. Opt. Soc. Am. 61, 947 (1971).

(Be 72a) D.R. Beck and O. Sinanoğlu, Phys. Rev. Lett. 28, 945 (1972).

(Be 72b) G. Beauchemin, J.A. Kernahan, E. Krystautas, D.J.G. Irwin, and R. Drouin, Phys. Lett. 40A, 194 (1972).

(Be 73) L.M. Bayer, W.E. Maddox, and L.B. Bridwell, J. Opt. Soc. Am. 63, 365 (1973).

(Bi 67a) W.S. Bickel, Appl. Optics 6, 1309 (1967).

(Bi 67b) W.S. Bickel, Phys. Rev. 162, 7 (1967).

(Bo 56) A.B. Bolotin, I.B. Levinson, and L.I. Levin, Sov. Phys. - JETP 2, 391 (1956).

(Br 69) J. Bromander, R. Buchta, and L. Lundin, Phys. Lett. 29A, 523 (1969).

(Br 70) L. Bridwell, L.M. Beyer, W.E. Maddox, and R.C. Etherton, Nucl. Instr. and Meth. 90, 187 (1970).

(Br 71) J. Bromander, Physica Scripta 4, 61 (1971).

(Bu 66) B. Budick, Bull. Am. Phys. Soc. 11, 456 (1966).

(Bu 72a) J.P. Buchet, M.C. Poulizac, and M. Carré, J. Opt. Soc. Am. 62, 623 (1972).

(Bu 72b) J.P. Buchet, M. Dufay, and M.C. Poulizac, Phys. Lett. 40A, 127 (1972).

(Co 64) M. Cohen, and A. Dalgarno, Proc. Roy. Soc. Lond. A280, 258 (1964).

(Co 71) C.L. Cocke, B. Curnutte, and J.H. Brand, Astron. Astrophys. 15, 299 (1971).

(Cr 65) R.J.S. Crossley, and A. Dalgarno, Proc. Roy. Soc. Lond. A286, 510 (1965).

(Cu 70a) L.J. Curtis, H.G. Berry, and J. Bromander, Physica Scripta 2, 216 (1970).

(Cu 70b) L.J. Curtis, R.M. Schectman, J.L. Kohl, D.A. Chojnacki, and D.R. Shoffstall, Nucl. Instr. and Meth. 90, 207 (1970).

(Cu 71a) L.J. Curtis, H.G. Berry, and J. Bromander, Phys. Lett. 34A, 169 (1971).

(Cu 71b) L.J. Curtis, I. Martinson, and R. Buchta, Physica Scripta 3, 197 (1971).

(Cu 74) L.J. Curtis, and W.H. Smith (to be published in Phys. Rev. A, 1974).

(Da 73) A. Dalgarno, Nucl. Instr. and Meth. 110, 183 (1973).

(De 62) W. Demtröder, Z. Physik 166, 42 (1962).

(De 68) A. Denis, J. Desesquelles, M. Dufay, and M.C. Poulizac, Beam-Foil Spectroscopy , S. Bashkin, ed. (Gordon and Breach, New York, 1968), p. 362.

(Du 72) P.D. Dumont, Physica 62, 104 (1972).

(Ed 64) B. Edlén, "Encyclopedia of Physics", vol. 27, p. 80 (ed. S. Flügge, Springer, Berlin, 1964).

(Ek 70) J.O. Ekberg and L.A. Svensson, Physica Scripta 2, 283 (1970).

(Ek 71) J.O. Ekberg, Physica Scripta 4, 101 (1971).

(Fi 68) C. Froese Fischer, J. Quant. Spectrosc. Radiat. Transfer 8, 755 (1968), and private communication, 1974.

(Fi 74) C. Froese Fisher, J. Phys. B7, L91 (1974).

(Fr 64) C. Froese, Astrophys. J. 140, 361 (1964).

(Gr 66) P.F. Gruzdev, and V.K. Prokofev, Opt. Spectrosc. 21, 151 (1966).

(Gr 71) P.F. Gruzdev, Opt. Spectrosc. 30, 319 (1971).

(He 67) L. Heroux, Phys. Rev. 153, 156 (1967).

(He 68a) J.E. Hesser, and B.L. Lutz, J. Opt. Soc. Am. 58, 1513 (1968).

(He 68b) A. Hese, and H.P. Weise, Zeit. Phys. 215, 95 (1968).

(He 68c) L. Heroux, in Beam-Foil Spectroscopy (ed. S. Bashkin, Gordon and Breach, New York, 1968), p. 205.

(He 69) L. Heroux, Phys. Rev. 180, 1 (1969).

(Hi 66) E. Hinnov, J. Opt. Soc. Am. 56, 1179 (1966).

(Ho 69) W. Hofmann, Z. Naturforsch. 24A, 990 (1969).

(Ho 72) S. Hontzeas, I. Martinson, P. Erman, and R. Buchta, Physica Scripta 6, 55 (1972).

(Ir 73a) D.J.G. Irwin, and A.E. Livingston, Can. J. Phys. 51, 848 (1973).

(Ir 73b) D.J.G. Irwin, A.E. Livingston, and J.A. Kernahan, Can. J. Phys. 51, 1948 (1973).

(Ir 73c) D.J.G. Irwin, A.E. Livingston, and J.A. Kernahan, Nucl. Instr. and Meth. 110, 105 (1973).

(Ir 73d) D.J.G. Irwin, A.E. Livingston, and J.A. Kernahan, Nucl. Instr. and Meth. 110, 111 (1973).

(Ir 74a) D.J.G. Irwin, and A.E. Livingston (to be submitted for publication).

(Ir 74b) D.J.G. Irwin, and A.E. Livingston (to be published in Comput. Phys. Comm., 1974).

(Ka 63) L. Kay, Phys. Lett. 5, 36 (1963).

(Ke 64) P.S. Kelly, Astrophys. J. 140, 1247 (1964).

(Ke 72) J.A. Kernahan, A. Denis, and R. Drouin, Physica Scripta 4, 49 (1972).

(Ke 73) R.L. Kelly, and L.J. Palumbo, "Atomic and Ionic Emission Lines below 2000 Angstroms - Hydrogen Through Krypton", NRL Report 7599 (U.S. Govt. Printing Office, Washington, D.C., 1973).

(Ke 74) J.A. Kernahan, A.E. Livingston, and E.H. Pinnington (submitted for publication, 1974).

(Ku 71) H.J. Kunze and R.U. Datla, Astrophys. J. 169, 425 (1971).

(La 65) F. Labuhn, Z. Naturforsch. 20A, 998 (1965).

(La 66) G.M. Lawrence, and B.D. Savage, Phys. Rev. 141, 67 (1966).

(La 68) G.M. Lawrence, Phys. Rev. 179, 134 (1968).

(La 70) G.M. Lawrence, Phys. Rev. A2, 397 (1970).

(La 73a) C. Laughlin, and A. Dalgarno, Phys. Rev. A8, 39 (1973).

(La 73b) C. Laughlin, M.N. Lewis, and Z. Horak, J. Opt. Soc. Am. 63, 736 (1973).

(Le 56) I.B. Levinson, A.B. Bolotin, and L.I. Levin, Trudy Vil'nyusskogo Univ. 5, 49 (1956).

(Li 71) C.C. Lin, "Beam-Foil Studies of the Oxygen Spectrum", Ph.D. Thesis, University of Alberta (1971).

(Li 72a) A.E. Livingston, D.J.G. Irwin, and E.H. Pinnington, J. Opt. Soc. Am. 62, 1303 (1972).

(Li 72b) C.C. Lin, D.J.G. Irwin, J.A. Kernahan, A.E. Livingston, and E.H. Pinnington, Can. J. Phys. 50, 2496 (1972).

(Li 74) A.E. Livingston, J.A. Kernahan, D.J.G. Irwin, and E.H. Pinnington (to be submitted for publication).

(Lu 73) L. Lundin, B. Engman, J. Hilke, and I. Martinson, Physica Scripta 8, 274 (1973).

(Ma 70a) I. Martinson, J. Bromander, and H.G. Berry, eds., "Beam-Foil Spectroscopy" (Nucl. Instr. and Meth. 90 (1970)).

(Ma 70b) I. Martinson, W.S. Bickel, and A. Ölme, J. Opt. Soc. Am. 60, 1213 (1970).

(Ma 70c) I. Martinson, and W.S. Bickel, Phys. Lett. 31A, 25 (1970).

(Ma 71a) I. Martinson, H.G. Berry, W.S. Bickel, and H. Oona, J. Opt. Soc. Am. 61, 519 (1971).

(Ma 71b) I. Martinson, Proceedings, Second European Conference on Beam-Foil Spectroscopy, Lyon, July, 1971.

(Ma 72a) R. Marrus, and R.W. Schmieder, Phys. Rev. A5, 1160 (1972).

(Ma 72b) J.V. Mallow, and J. Burns, J. Quant. Spectrosc. Radiative Transfer 12, 1081 (1972).

(Ma 73) J. Marek, and J. Richter, Astron. & Astrophys. 26, 155 (1973).

(Mo 49) C.E. Moore, "Atomic Energy Levels", vol. 1, NBS Circular 467 (U.S. Govt. Printing Office, Washington, D.C., 1949).

(Mü 68) D. Müller, Z. Natur. 23A, 1707 (1968).

(Ni 73a) C.A. Nicolaides, Chem. Phys. Lett. 21, 242 (1973), and private communication, 1972.

(Ni 73b) C.A. Nicolaides, and D.R. Beck, J. Phys. B6, 535 (1973).

(No 70) L.C. Northcliffe, and R.F. Schilling, Nucl. Data Tables A7, 233 (1970).

(Nu 69) H. Nussbaumer, Astrophys. Lett. 4, 183 (1969).

(Nu 72) H. Nussbaumer, Astron. Astrophys. 16, 77 (1972).

(Pi 69) E.H. Pinnington, and C.C. Lin, J. Opt. Soc. Am., 59, 780 (1969).

(Pi 70) E.H. Pinnington, Nucl. Instr. and Meth. 90, 93 (1970).

(Pi 71) E.H. Pinnington, B. Curnutte, and M. Dufay, J. Opt. Soc. Am. 61, 978 (1971).

(Po 71) M.C. Poulizac, and J.P. Buchet, Physica Scripta 4, 191 (1971).

(Po 73) M.C. Poulizac, and J.P. Buchet, Physica Scripta 8, 40 (1973).

(Sa 66) B.D. Savage, and G.M. Lawrence, Astrophys. J. 146, 940 (1966).

(Si 73) J.S. Sims, and R.C. Whitten, Phys. Rev. A8, 2220 (1973).

(Si 74) O. Sinanoǧlu, and D.R. Beck, Chem. Phys. Lett. 24, 20 (1974).

(Sm 69) P.L. Smith, and W. Whaling, Phys. Rev. 188, 36 (1969).

(Sm 70) W.H. Smith, J. Bromander, L.J. Curtis, and R. Buchta, Physica Scripta 2, 211 (1970).

(Sm 71a) M.W. Smith, and W.L. Wiese, Astrophys. J. Suppl. Ser. 23, 103 (1971).

(Sm 71b) W.H. Smith, and H.S. Liszt, J. Opt. Soc. Am. 61, 938 (1971). (see also W.H. Smith, Nucl. Instr. and Meth. 90, 115 (1970)).

(Sm 71c) W.H. Smith, J. Bromander, L.J. Curtis, H.G. Berry, and R. Buchta, Astrophys. J. 165, 217 (1971).

(Sm 73) M.W. Smith, G.A. Martin, and W.L. Wiese, Nucl. Instr. and Meth. 110, 219 (1973).

(So 73) G. Sørensen, Phys. Rev. A7, 85 (1973), which also quotes unpublished results of Andersen and Sørensen.

(St 71) J.O. Stoner, Jr., and J.A. Leavitt, Appl. Phys. Lett. 18, 477 (1971).

(Tr 50) E. Trefftz, Z. Astrophys. 28, 67 (1950).

(Tr 69) E. Trefftz, and R.N. Zare, J. Quant. Spectrosc. Radiat. Transfer 9, 643 (1969).

(Va 61) C.M. Varsavsky, Astrophys. J. Suppl. Ser. 6, 75 (1961).

(Vi 73) G.A. Victor, and C. Laughlin, Nucl. Instr. and Meth. 110, 189 (1973).

(We 67a) A.W. Weiss, Phys. Rev. 162, 71 (1967).

(We 67b) A.W. Weiss, J. Chem. Phys. 47, 3573 (1967).

(We 69a) A.W. Weiss, Phys. Rev. 188, 119 (1969).

(We 69b) P. Westhaus, and O. Sinanoğlu, Phys. Rev. 183, 56 (1969).

(We 69c) A.W. Weiss, Phys. Rev. 178, 82 (1969).

(We 70) A.W. Weiss, Nucl. Instr. and Meth. 90, 121 (1970).

(We 72) A.W. Weiss, Phys. Rev. A6, 1261 (1972).

(Wh 70) W. Whaling, M. Martinez-Garcia, D.L. Mickey, and G.M. Lawrence, Nucl. Instr. and Meth. 90, 363 (1970).

(Wi 66) W.L. Wiese, M.W. Smith, and B.M. Glennon, "Atomic Transition Probabilities" Vol. I, NSRDS-NBS 4 (U.S. Govt. Printing Office, Washington, D.C., 1966).

(Wi 68a) W.L. Wiese, and A.W. Weiss, Phys. Rev. 175, 50 (1968).

(Wi 68b) W.L. Wiese, Appl. Optics 7, 2361 (1968).

(Wi 69) W.L. Wiese, M.W. Smith, and B.M. Miles, "Atomic Transition Probabilities" Vol. II, NSRDS-NBS 22 (U.S. Govt. Printing Office, Washington, D.C., 1969).

(Wi 70) W.L. Wiese, Nucl. Instr. and Meth. 90, 25 (1970).

(Za 67) R.N. Zare, J. Chem. Phys. 47, 3561 (1967).

APPENDIX I

REPORTS AND PUBLICATIONS OF RESULTS OBTAINED DURING THIS RESEARCH PROJECT

(A) Reports

(1) "Mean-Life Measurements for Argon and Oxygen..." D.J.G. Irwin, J.A. Kernahan, C.C. Lin, A.E. Livingston, E.H. Pinnington*. Third EGAS Conference on Atomic Spectroscopy, Reading, U.K., July 1971.

(2) "Recent Results at Edmonton" E.H. Pinnington*. Second European Conference on Beam-Foil Spectroscopy, Lyon, France, July 1971.

(3) "Lifetime Results for Oxygen, Fluorine, and Neon in the Vacuum Ultraviolet" D.J.G. Irwin*, A.E. Livingston, J.A. Kernahan. Third International Conference on Beam-Foil Spectroscopy, Tucson, U.S.A., October 1972.

(4) "Beam-Foil Lifetimes for Silicon, Sulfur, and Argon in the Vacuum Ultraviolet" D.J.G. Irwin, A.E. Livingston*, J.A. Kernahan. Third International Conference on Beam-Foil Spectroscopy, Tucson, U.S.A., October 1972.

(5) "Beam-Foil Studies of Oxygen in the Vacuum U.V." J.A. Kernahan*, E.H. Pinnington, A.E. Livingston, D.J.G. Irwin. CAP Atomic and Molecular Physics Division Meeting, Windsor, Canada, April 1973.

(6) "Mean-Life Measurements using the Beam-Foil Technique" E.H. Pinnington*, A.E. Livingston, J.A. Kernahan, D.J.G. Irwin. Canadian Astronomical Society Meeting, Edmonton, Canada, May 1973.

(7) "Beam-Foil Spectroscopy in the Vacuum U.V. for Elements of the Third Period" A.E. Livingston*, E.H. Pinnington, J.A. Kernahan, D.J.G. Irwin. Fifth EGAS Conference on Atomic Spectroscopy, Lund, Sweden, July 1973.

(8) "f-values for Transitions in the Al I Isoelectronic Sequence" E.H. Pinnington*, A.E. Livingston, J.A. Kernahan. CAP Spectroscopy Division Meeting, Vancouver, Canada, February 1974.

* Presented the Report.

(B) Publications

(1) "Lifetime Measurements in Ar II- Ar VIII", A.E. Livingston, D.J.G. Irwin, and E.H. Pinnington, J. Opt. Soc. Am. 62, 1303 (1972).

(2) "Beam-Foil Studies of Oxygen below 2000 Å", C.C. Lin, D.J.G. Irwin, J.A. Kernahan, A.E. Livingston, and E.H. Pinnington, Can. J. Phys. 50, 2496 (1972).

(3) "Recent Lifetime Measurements for Oxygen, Fluorine, and Neon in the Vacuum Ultraviolet", D.J.G. Irwin, A.E. Livingston, and J.A. Kernahan, Nucl. Instr. and Meth. 110, 105 (1973).

(4) "Beam-Foil Lifetimes in the Third Period Elements Silicon, Sulfur, and Argon in the Vacuum Ultraviolet", D.J.G. Irwin, A.E. Livingston, and J.A. Kernahan, Nucl. Instr. and Meth. 110, 111 (1973).

(5) "Lifetime Measurements in Fluorine and Silicon in the Vacuum Ultraviolet", D.J.G. Irwin and A.E. Livingston, Can. J. Phys. 51, 848 (1973).

(6) "Radiative Mean-Life Measurements in Neon below 1000 Å", D.J.G. Irwin, A.E. Livingston, and J.A. Kernahan, Can. J. Phys. 51, 1948 (1973).

(7) "Comment on the Reliability of Experimental Atomic Mean Lives obtained with the Beam-Foil Technique", E.H. Pinnington, A.E. Livingston, and J.A. Kernahan, Phys. Rev. A 9, 1004 (1974).

(8) "HOMER: A Program for the Extraction of Radiative Lifetimes from Experimental Beam-Foil Data", D.J.G. Irwin, and A.E. Livingston, Comput. Phys. Comm. 7, 95 (1974).

(9) "Mean-Life Measurements for some Energy Levels of O I - O VI", E.H. Pinnington, D.J.G. Irwin, A.E. Livingston, and J.A. Kernahan (submitted to Can. J. Phys., April 1974).

(10) "Beam-Foil Mean-Life Measurements of Levels in N I - N V", J.A. Kernahan, A.E. Livingston, and E.H. Pinnington (to be published in Can. J. Phys., Sept., 1974).

(11) "Lifetime Measurements in S III - S VI", D.J.G. Irwin, and A.E. Livingston (to be submitted for publication, 1974).

(12) "Lifetime Measurements in P I - P V", A.E. Livingston, J.A. Kernahan, D.J.G. Irwin, and E.H. Pinnington (to be submitted for publication, 1974).

APPENDIX II

Mean-life values obtained during this project, from which the oscillator strength results in Ch. VI have been derived*.

Fig.	Ion	λ(Å)	τ(ns)	f
30	B I	1465	0.50±0.05	0.21
	N III	772	0.24±0.02	0.125
	O IV	626	0.20±0.02	0.098
	Ne VI	453	0.13±0.02	0.079
31	B I	1378	0.45±0.05	0.63
	O IV	554	0.16±0.02	0.29
	Ne VI	402	0.13±0.01	0.186

---

* The absorption oscillator strength (f_{ik}) for a transition involving upper level k and lower level i is related to the mean life of level k (τ_k) by the following expression, assuming the level decays via a single branch:

$$f_{ik} = 0.15 \times 10^{-6} \frac{g_k}{g_i} \frac{\lambda_{ik}^2}{\tau_k} ,$$

where λ is in Ångstroms, τ is in nanoseconds, and g is the statistical weight (2J + 1) of a level.

Fig.	Ion	λ(Å)	τ(ns)	f
32	O II	644	0.20±0.01	0.104
	Ne IV	422	0.13±0.01	0.068
33	F I	955	1.4 ±0.2	0.098
	Ne II	446	0.24±0.02	0.124
34	B II	1362	1.0 ±0.1	0.83
	N IV	765	0.44±0.04	0.60
	O V	630	0.38±0.03	0.47
	Ne VII	465	0.23±0.04	0.42
35	Si IV	1397	1.4 ±0.1	0.63
	P V	1121	0.95±0.05	0.59
	S VI	937	0.70±0.07	0.56
	Ar VIII	705	0.50±0.04	0.45
36	Si IV	1126	0.48±0.04	0.66
	P V	869	0.31±0.02	0.60
	S VI	711	0.25±0.04	0.51
	Ar VIII	524	0.15±0.02	0.47
37	Si III	1207	0.41±0.06	1.60
	P IV	951	0.35±0.04	1.16
	S V	786	0.26±0.02	1.06
	Ar VII	586	0.18±0.02	0.86

Fig.	Ion	λ(Å)	τ(ns)	f
38	Si III	1299	0.59±0.06	0.43
	P IV	1030	0.36±0.03	0.44
	S V	855	0.32±0.03	0.35
	Ar VII	637	0.20±0.02	0.30
39	Si III	1112	0.42±0.06	0.75
	P IV	826	0.24±0.03	0.68
	S V	663	0.17±0.02	0.64
	Ar VII	477	0.13±0.02	0.44
40	Si II	1251	0.34±0.04	0.23
	S IV	800	0.15±0.02	0.21
	Ar VI	590	0.14±0.02	0.13
41	N III	452	0.44±0.05	0.023
	O IV	279	0.11±0.03	0.035
42	O IV	608	0.29±0.02	0.063
	Ne VI	435	0.22±0.02	0.043
44	S IV	813	0.22±0.03	0.15
	Ar VI	592	0.15±0.02	0.12
45	O IV	789	1.6 ±0.1	0.097
	Ne VI	562	0.96±0.04	0.082
46	N II	776	0.36±0.03	0.25
	O III	599	0.20±0.04	0.27
	Ne V	416	0.14±0.01	0.185

Fig.	Ion	λ(Å)	τ(ns)	f
47	Ar V	725	1.55±0.20	0.051
48	Ar IV	844	4.5 ±0.7	0.071
49	N I	1134	6.8 ±0.6	0.085
	O II	834	1.2 ±0.1	0.26
	Ne IV	542	0.79±0.05	0.167
50	O II	539	0.9 ±0.1	0.145
51	O II	718	0.44±0.04	0.16[a]
	Ne IV	470	0.25±0.02	0.11[a]
52	N I	1243	2.3 ±0.2	0.098
53	F II	607	0.36±0.02	0.15
	Ne III	490	0.22±0.02	0.16
54	N II	660	0.22±0.02	0.15[a]
	O III	526	0.087±0.008	0.24[a]
55	N II	747	0.28±0.04	0.18[b]
	O III	396	0.29±0.05	0.035[c]
56	O II	538	0.14±0.02	0.19[a]
57	O II	617	0.25±0.02	0.10[d]
58	Ar III	769	1.8 ±0.3	0.030
59	Ar III	878	3.5 ±0.4	0.033

Fig.	Ion	λ(Å)	τ(ns)	f
61	P III	1340	18±3	0.025
	S IV	1068	7.0±0.3	0.041
	Ar VI	760	2.8±0.2	0.052
62	Si II	1265	0.40±0.03	0.99
	P III	858	0.19±0.02	0.97
	S IV	660	0.12±0.02	0.91
	Ar VI	462	0.095±0.010	0.56
64	P IV	877	0.22±0.03	0.87
	S V	696	0.13±0.02	0.93
	Ar VII	501	0.12±0.02	0.52
65	Ar V	827	4.0±0.4	0.043
66	P II	964	0.19±0.03	1.22
	S III	680	0.12±0.03	0.96
	Ar V	448	0.06±0.01	0.84
67	P IV	1370	3.1±0.3	0.127
	Ar VII	825	0.7±0.2	0.20
68	Si III	1501	0.54±0.05	0.88
	P IV	877	0.22±0.03	0.73
69	Kr VIII	670	0.35±0.06	0.57
	Kr VII	585	0.16±0.02	0.96
	Kr VI	450	0.10±0.02	0.51

Branching ratios employed:

a Nicolaides (Ni 73a)

b No branching correction used

c Nussbaumer (Nu 69)

d Kelly (Ke 64)